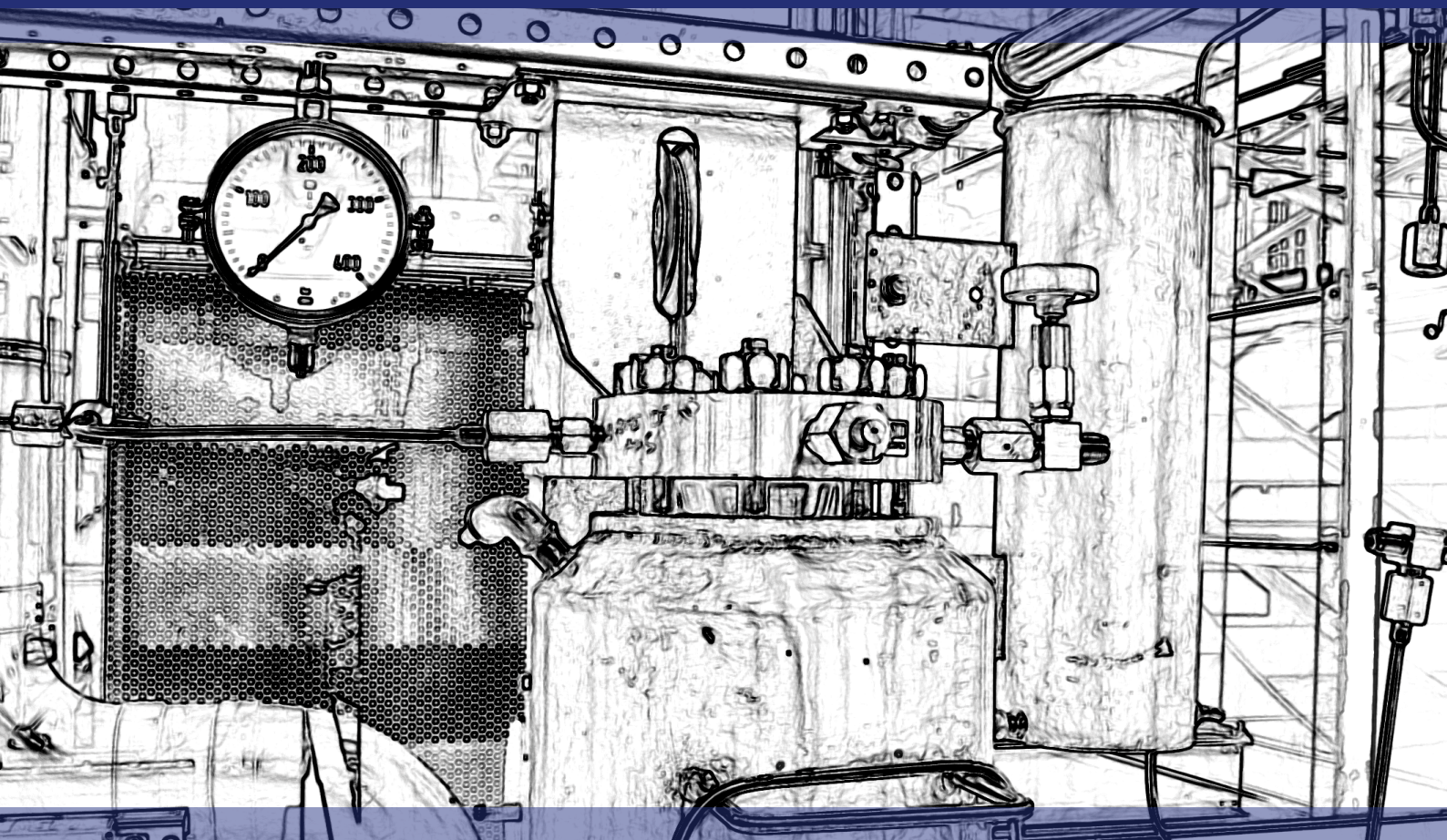Thomas Gamse (editor)

Book of Abstracts

ERASMUS+ BIP ESS-HPT 2024

The European Summer School in
High Pressure Technology

7.7. – 20.7.2024

TU Graz
Graz University of Technology

Erasmus+

EFCE
European Federation of Chemical Engineering
Europäische Föderation für Chemie-Ingenieur-Wesen
Fédération Européenne de Génie Chimique

Imprint

Preface

The European Summer School in High Pressure Technology (ESS-HPT) is the continuation of many years of high pressure intensive courses. The history of this very successful series of courses started in 1995, when the first intensive course took place in Monselice, Italy. Most of these Intensive Courses were supported by SOCRATES and later Life Long Learning, as shown in following overview:

SOCRATES IP "Current Trends in High Pressure Technology and Chemical
Engineering"
        1995 Monselice / Italy
        1996 Nancy / France
        1997 Erlangen / Germany

SOCRATES IP "High Pressure Technology in Process and Chemical Engineering"
        1999 Abano Terme / Italy
        2000 Valladolid / Spain
        2001 Maribor / Slovenia and Graz / Austria

SOCRATES IP "High Pressure Chemical Engineering Processes: Basics and
Applications"
        2002 Graz / Austria and Maribor / Slovenia
        2003 Budapest / Hungary
        2004 Barcelona / Spain

SOCRATES IP "Basics, Developments, Research and Industrial Applications in High
Pressure Chemical Engineering Processes"
        2005 Prague / Czech Republic
        2006 Lisbon / Portugal
        2007 Albi / France

Life Long Learning IP "SCF- GSCE: Supercritical Fluids – Green Solvents in
Chemical Engineering"
        2008 Thessaloniki / Greece
        2009 Istanbul / Turkey
        2010 Budapest / Hungary

EFCE Intensive Course "High Pressure Technology - From Basics to Industrial
Applications"
        2011 Belgrade / Serbia

Life Long Learning IP "PIHPT: Process Intensification by High Pressure
Technologies – Actual Strategies for Energy and Resources
Conservation"
        2012 Maribor / Slovenia and Graz / Austria
        2013 Darmstadt / Germany
        2014 Glasgow / Great Britain

Unfortunately, the financial support for these Intensive Programmes was cancelled within ERASMUS+. The EFCE Working Party "High Pressure Technology" decided in September 2014 to go on with this course in the form of a Summer School. The ESS-HPT takes place every year within the first 2 weeks of July at University of Maribor, Slovenia and Graz University of Technology, Austria.

EFCE ESS-HPT "The European Summer School in High Pressure Technology"

ESS-HPT 2015	Maribor / Slovenia and Graz / Austria
ESS-HPT 2016	Maribor / Slovenia and Graz / Austria
ESS-HPT 2017	Maribor / Slovenia and Graz / Austria
ESS-HPT 2018	Maribor / Slovenia and Graz / Austria
ESS-HPT 2019	Maribor / Slovenia and Graz / Austria
ESS-HPT 2021	Online Course, Graz / Austria
GEHPT and ESS-HPT 2022	Maribor / Slovenia and Graz / Austria

Since 2023 ESS-HPT is organised again as an ERASMUS+ Blended Intensive Programme (BIP). Unfortunately, there is no possibility to organise this summer school in two countries. So the whole intensive programme takes place at Graz University of Technology.

ESS-HPT 2023   Graz / Austria

This year ESS-HPT 2024 will take place at Graz University of Technology in the period 7.7.2024 till 20.7.2024.

All participants have to give an oral presentation and the abstracts of these presentations, which are peer-reviewed by the EFCE WP Members, are published in this book of abstracts.

The editor

Thomas Gamse
Organiser of ERASMUS+ BIP ESS-HPT 2024

Many thanks to our sponsors,

NATEX Prozesstechnologie GesmbH,

INNOWELD-Metallverarbeitung GmbH

and Tourismusverband Stadt Graz.

Time Schedule
Oral Presentations Participants

	Monday, 8 July 2024		
1	9:25 - 9:40	**A. Weber**, M. Busch Modeling the Kinetics of the High Pressure Copolymerization of Ethene and Acrylic Acid	1
2	9:40 - 9:55	**N. Zachmann**, B. Ebin Towards the Stepwise Extraction of Electrolyte Solvents from LiB Waste Material Using Supercritical CO_2	5
3	9:55 - 10:10	**E. González Cortés** Thermophysical Characterization of Fluids of Interest for the Energy Transition	12

	Wednesday, 10 July 2024		
4	17:00 - 17:15	**M. Irgolič**, M. Čolnik, M. Škerget Decomposition of Polycarbonate in Subcritical Water	19
5	17:15 - 17:30	**L. Dietrich**, M. Busch Polymerization of Ethene and Acrylic Acid under High-Pressure Conditions	24
6	17:30 - 17:45	**I. Magdaleno de la Fuente**, A. Fernández, D. Cantero Hydrothermal Liquefaction of Residual Biomass for Sustainable Aviation Fuel Precursors Production	29
7	17:45 - 18:00	**B. Mihajlović** Extraction of Oil from Waste Tomato Seeds and Waxes from Waste Tomato Peel Using Supercritical Carbon Dioxide	33
8	18:00 - 18:15	N. Krusberská, **I. Troppová**, L. Matějová Valorisation of Beef Bones to Value-Added Natural Products by Using Green Solvents - Process Optimization	36
9	18:15 - 18:30	**M. Altinisik,** M. Sauceau, R. D'Elia, R. Sescousse, F. Baillon, G. Michona Numerical Modelling of Thermoplastic Foaming by Supercritical CO2 Assisted Extrusion: Exploring the Process-Microstructure Relationship	39
10	18:30 - 18:45	**Z. Maghazeh** Characterization of Mass Transport of Pure Gases and Mixtures in Bio-Based Polymeric Membranes for Carbon Capture Applications	45

	Friday, 12 July 2024		
11	17:00 - 17:15	**T. Skarlovnik**, U. Bren, G. Hostnik Influence of Hop (Humulus lupulus) and its Components (α-Acids and β- Acids) on Micellization	50
12	17:15 - 17:30	**C. Weigel**, M. Busch Implementation of a Multi-Zone Autoclave in the High-Pressure Polymerization Process	55
13	17:30 - 17:45	**S. Pahino Villardón** Formulation of Rutin to Improve its Bioavailability	60
14	17:45 - 18:00	**A. Leluc,** S. De Paiva Lacerda, J.-J. Letourneau, F. Espitalier Development of a Supercritical CO_2 Assisted Process Combining Simultaneous Extraction and Encapsulation of a Bioactive Component Derived from Agricultural Waste: Enhancing Stability and Bioavailability	69
15	18:00 - 18:15	**M. Gilardi, F. Bisotti** HS3, An Innovative Solvent for CO_2 Capture	74
16	18:15 - 18:30	**M. Štosel**, R. Nadányi, A. Ház Extraction of Phenolic Compounds from Spruce Bark by Supercritical CO_2 Extraction with Ethanol and Ethyl Acetate Co-Solvents	80

	Monday, 15 July 2024		
17	17:00 - 17:15	**A. Arribas Sanchidrián** Continuous Hydrothermal Fractionation of Carrot Waste using Subcritical and Supercritical Water, Purification and Application to Produce Bio-Based Films	85
18	17:15 - 17:30	**N. Atelšek Hozjana**, G. Horvata, Z. Novak Production of Bioaerogels for Biomedical Applications Using Supercritical CO_2	92
19	17:30 - 17:45	**P. Weigmann**, M. Busch Mini-Plant Scaled Semi-Batch Experiments for Kinetic Investigations of Metallocene Catalyzed Solution Polymerizations	98
20	17:45 - 18:00	**F. Caballero Rojo** Catalytic Carbon Dioxide Reduction	102
21	18:00 - 18:15	**D. Terhorst** Investigation of the Pressure and Power Characteristics of Planetary Roller Extruders	108
22	18:15 - 18:30	**R. Di Carlo** Investigating CO_2 Transport Properties in High-Pressure Conditions for Applications in the CCUS Supply Chain Through Experimental and Modelling Methods	112

	Wednesday, 17 July 2024		
23	8:30 - 8:45	**F. Caballero Rojo** Catalytic Carbon Dioxide Reduction	118
24	8:45 - 9:00	**R. Lysowski**, E. Ksepko Development of Oxygen Carriers for Chemical Looping Combustion Process	124
25	9:00 - 9:15	**V. Sliesarenko**, U. Bren, A. Lobnik Photonic Nanosensor Receptors Based on Functionalized SiO_2-Nanoparticles for Detection of Stress Biomarkers	128
26	9:25 - 9:40	**P. Sewruk**, M. Busch Sampling Device for High-Pressure Polymerization Systems	133
27	9:40 - 9:55	**A. Bajramova** Sustainable Supercritical Fluid Processing of Vegetable Oils	138
28	9:55 - 10:10	**R. Sahraeian** Synthesis and Characterization of PVDF Aerogels	143
	Thursday, 18 July 2024		

HIGH-PRESSURE VESSELS

HIGH PRESSURE VESSELS FOR VARIOUS APPLICATIONS UP TO 3.000 BAR CAN BE DESIGNED, CALCULATED, FABRICATED AND TESTED BY INNOWELD. THE POSSIBILITIES OF USING A HIGH-PRESSURE VESSEL IS NUMBERLESS. CARRYING OUT REACTIONS, SEPARATING MEDIUMS AND STORING CHEMICALS ARE ONLY A FEW OF IT. FOR INNOWELD, THE INTEREST INCREASES PROPORTIONAL TO THE PRESSURE AND THE TEMPERATURE.

With our experience from engineering and welding pressure vessels with wall thicknesses up to nearly 250mm and combining them with weld overlays out of materials like nickel, nickel chromium alloys and stainless steels, we are always looking for individual solutions for our partners with individual requirements. The core business of Innoweld starts, whenever high temperature, high pressures and dangerous acids come together.

Beside this individual solutions, we are also manufacturing high pressure and high temperature vessels according to exact specifications from our clients. With best delivery times and our high flexibility during the execution of the project, we make sure that the high pressure vessel with the best quality is ready for installation during the next scheduled shutdown.

Furthermore, our focus is also on the economical side of the project. With our weight saving designs, we make sure that the vessels is not only from the technical, but also from the financial point of view

www.innoweld.at

Modeling the Kinetics of the High-Pressure Copolymerization of Ethene and Acrylic Acid

Alina Weber, Markus Busch*

Ernst-Berl-Institute of Technical and Macromolecular Chemistry, Technical University of Darmstadt, 64287 Darmstadt/Germany. *email: markus.busch@pre.tu-darmstadt.de

Introduction

Low density polyethylene (LDPE) can be synthesized under high-pressure in a stirred autoclave at 1300-2500 bar and 230-280 °C or in a tubular reactor (2000-3000 bar, 130-330 °C)[1]. To customize LDPE, comonomers such as acrylic acid (AA) may be added to form poly(ethylene-co-acrylic acid) also called EAA. By adding AA the polarity of the otherwise non-polar LDPE is increased, which improves the adhesion towards polar substances[2]. EAA has a high thermal stability, environmental stress crack resistance and can act as a barrier towards moisture and gasses[3]. This enables the usage of EAA in various applications requiring a precise calibration of the properties, which are mainly influenced by the micro structure of the copolymers. Knowledge of the kinetic network sets the basis for a successful synthesis of a copolymer. Hereby, simulations can be a useful tool for the optimization of the reaction process whilst reducing the risks of experiments, which may come carrying high costs and efforts. Copolymerizations are composed of a complex system of elementary reactions, that have an influence on the molecular weight distribution (MWD) as well as the number of long- and short-chain branches. A mathematical model based on kinetics derived from experimental data of a copolymerization can be used for predicting these properties.[4] In this work the kinetic rate coefficients describing the propagation and the reactivity ratios of an EAA copolymerization under high-pressure conditions are derived from literature and experimental data to set up a deterministic simulation using the software Predici®.

Modeling

To model a polymerization, kinetic rate coefficients for every elementary reaction step are required. The temperature and pressure dependency of these coefficients is described using an Arrhenius expression.

At first, available literature data on the propagation rate coefficient of the homopolymerization of AA was collected and evaluated using the approach of covariance ellipses to determine its reliability[5]. In case of the propagation rate coefficient of acrylic acid, density functional fluid theory (DFT) [6] calculations served as a good estimate for the activation energy, while the pre-exponential factor was fitted to conversions of different experiments by assuming a similar initiator efficiency as for ethene homopolymerizations. Special consideration was given to modeling the cross propagation reactions, which requires a set of reactivity ratios. They are estimated via the non-linear fit equation of Mayo[7] using experiments of varying AA content at different temperatures. As the reactivity ratios of AA and ethene are both not equal to one the concentration inside the reactor changes with conversion. Therefore, only experiments at a conversion lower than 10% were used for fitting. Reactivity ratios at 220 °C - 250 °C were determined.

The occurrence of the transfer to monomer reaction rates were modeled by fitting the maximum of the experimentally determined MWD of low conversion EAA-samples. First the homo reaction rate coefficients were taken from literature[8,9] and in case of the AA homo coefficient, altered to fit into the modeled temperature range. The cross transfer to monomer was derived on basis of the homo transfer by assuming them to be proportional to one another. This led to the introduction of a proportionality factor, which was fitted for different temperatures and estimated with an Arrhenius expression.

To reduce future experimental efforts the number and accuracy of experiments required for the determination of the transfer to polymer reaction rate coefficients were determined. During a transfer to polymer reaction mid chain radicals are formed, that can either propagate to form a long chain branch (LCB) or undergo a β-scission reaction (Figure 1). Both reaction routes are correlated to one another and cannot be viewed separately.
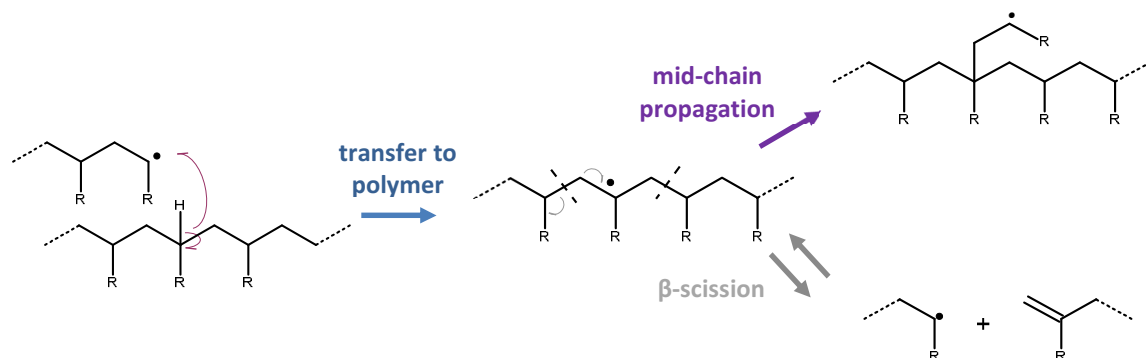

Figure 1: Reaction scheme showing the formation and the subsequent reaction routes of a mid-chain radical.

For analysis, high conversion samples are needed (conversion higher than 5 %). First, a sensitivity study was conducted, investigating the influence of the transfer to polymer and the β-scission reaction of AA and the corresponding cross reactions with ethene on the number of LCBs. It was assumed, that a cross transfer to polymer of an AA-unit onto an ethene-unit is unlikely to occur, as a secondary ethene radical instead of a tertiary AA-radical would be formed. The latter has a higher stability, and the formation of an AA-mid chain radical is therefore preferred. To model the respective cross transfer to polymer reaction a proportionality factor (Fac_{12}) is introduced linking the cross and the homo transfer reactions. To find Arrhenius expressions for the remaining reaction coefficients VAN BOXTEL[10] developed an experimental strategy for estimating the factor Fac_{12} on the number of LCBs per 1000C atoms. For this, experiments are needed, that vary in conversion, while temperature, pressure and AA content are kept constant. This keeps the ratio between ethene and AA constant, causing the probability for the occurrence of a cross transfer reaction to remain constant. To minimize future experimental efforts, a series of simulations were performed, determining the necessary number of samples and their accuracy to apply the parameter estimation tool in Predici®. Hereby, 10 fictive experiments according to the stated conditions were calculated. Possible error sources in the experimental data could be fluctuations in the concentration of the reaction mixture due to the preferred incorporation of AA into the copolymer, leading to a wrong assumption of the molar content of AA within the monomer which is used to calculate the proportion of AA in the copolymer. However, a constant AA content is the basis for the correct determination of the kinetic coefficients. The influence of this error on the number of experiments necessary for a valid parameter estimation was investigated.

Summary

In this work a kinetic network was set up for modeling the copolymerization of ethene with acrylic acid. This was done by gathering the available literature data on the respective homo reaction rate coefficients. For estimating the cross reactions experimental data of DIETRICH[11] was considered. Finally, a sensitivity analysis was conducted to reduce future experimental efforts when investigating the cross transfer to polymer and the β-scission reaction.

References

[1] G. Luft, *Chemie in unserer Zeit* 2000, *34*, 190–199.

[2] A. Castello, *Journal of Plastic Film & Sheeting* **1985**, *1*, 124–133.

[3] E. Otocka, T. Kwei, *Macromolecules* **1968**, *1*, 244–249.

[4] N. Wulkow, R. Telgmann, K.-D. Hungenberg, C. Schütte, M. Wulkow, *Macromolecular Theory and Simulations* **2021**, *30*, 2100017.

[5] A. M. van Herk, *Journal of Chemical Education* **1995**, *72*, 138.

[6] P. Deglmann, I. Müller, F. Becker, A. Schäfer, K.-D. Hungenberg, H. Weiß, *Macromolecular Reaction Engineering* **2009**, *3*, 496–515.

[7] F. R. Mayo, F. M. Lewis, *Journal of the American Chemical Society* **1944**, *66*, 1594-1601.

[8] M. Busch, Macromolecular Theory and Simulations, 2001, 10, 408–429

[9] N. F. G. Wittenberg, C. Preusser, H. Kattner, M. Stach, I. Lacík, R. A. Hutchinson, M. Buback, *Macromolecular*

[10] Hendricus C.M. van Boxtel, Dissertation, Georg-August-Universität Göttingen,**2000**.

[11] L. Dietrich, Masterthesis, Technische Universität Darmstadt, **2023**.

Towards the Stepwise Extraction of Electrolyte Solvents from LiB Waste Material Using Supercritical CO$_2$

N. Zachmann*, B. Ebin

Department of Chemistry and Chemical Engineering, Chalmers University of Technology, *zachmann@chalmers.se

Introduction

The Li-ion battery (LiB) demand is forecasted to steadily increase in the upcoming years[1]. For electricial vehicle the lifetime is about 10-15 years[2]. Thus, a tremendous accumulation of spent LiBs is to be expected in the future. Recycling of the spent LiBs will not be only crucial for the valorisation of the (critical) raw materials (i.e., Li, Mn, Ni, Co, and graphite) processed in the LiBs but also to minimize risks accompanied by the handling of the end-of-life LiBs[2,3]. Spent LiBs are classified by EU legislation as hazardous waste and burden a high risk of fire[4–6]. A major risk factor is attributed to the state-of-the-art non-aqueous electrolyte. The complex mixture contains a conductive salt dissolved in a combination of different organic solvents and additives[7]. Most of the components are flammable, (highly) volatile and classified to be toxic[8]. An uncontrolled release of these components can have a serious impact on the environment and the health of the workers in a recycling plant. Moreover, LiB waste side streams containing electrolyte residues entail a financial burden for the recycling industry as they are still classified as hazardous waste[6]. Once successfully recovered, extensive purification of the collected products is required to be saleable for reuse in the battery manufacturing process, or repurpose in other industries[9]. Thus, the recovery of the electrolyte is a necessary step for the development of a safe recycling process.

In the state-of-the-art recycling process the LiBs are pre-treated using several steps such as dismantling, sorting, crushing, shredding, grinding and/or milling to produce a black mass which is a mixture of anode and cathode material. Additionally, a (vacuum) vaporization pre-treatment step is often added to separate the remaining electrolyte from the LiB waste material[2,9]. Thereby, the commonly used conductive salt, lithium hexafluorophosphate (LiPF$_6$), is prone to decompose to gaseous HF and other toxic organo-fluorophosphates[10,11]. Moreover, the complete removal and recovery of the electrolyte remains a major challenge for recycling companies.

An alternative option to (vacuum) vaporization is supercritical carbon dioxide extraction[12]. The easily adjustable $ScCO_2$ properties and excellent mass-transfer characteristics can be potentially used to selectively extract the electrolyte components from the LiB waste to achieve purified extraction products. In our previous research, it was shown that the non-polar electrolyte solvents dimethyl carbonate (DMC) and ethyl methyl carbonate (EMC) can be fully extracted at 80 bar and 29°C[13]. However, under the studied conditions the polar electrolyte solvent ethylene carbonate (EC) remained as a residue in the LiB waste. Thus, further research is required to retrieve thermodynamic and kinetic data for extraction purpose.

Experimental

LiB black mass obtained by pre-treatment of vehicle battery waste was received from an industrial partner. The remaining electrolyte content in terms of composition and amount was characterized using thermal gravimetric analysis (TGA) and gas chromatography coupled with mass spectrometer (GC-MS). The TGA results showed that the LiB black mass still contained 5.7±0.5 wt% of electrolyte. To determine the electrolyte composition, 6 g of LiB waste material was mixed in 5 ml of acetonitrile. After shaking by hand for 5 minutes, the liquid was filtered out and analysed using (GC-MS).

In total 31 components were observed in the chromatograph. Among these, commonly used electrolyte solvents such as dimethyl carbonate (DMC), ethyl methyl carbonate (EMC), ethylene carbonate (EC), polypropylene carbonate (PC), and biphenyl were identified. The remaining peaks were assigned to additives and degradation products which evolved during the cycling of the LiB or the pre-treatment process of the LiB waste material of the industrial partner.
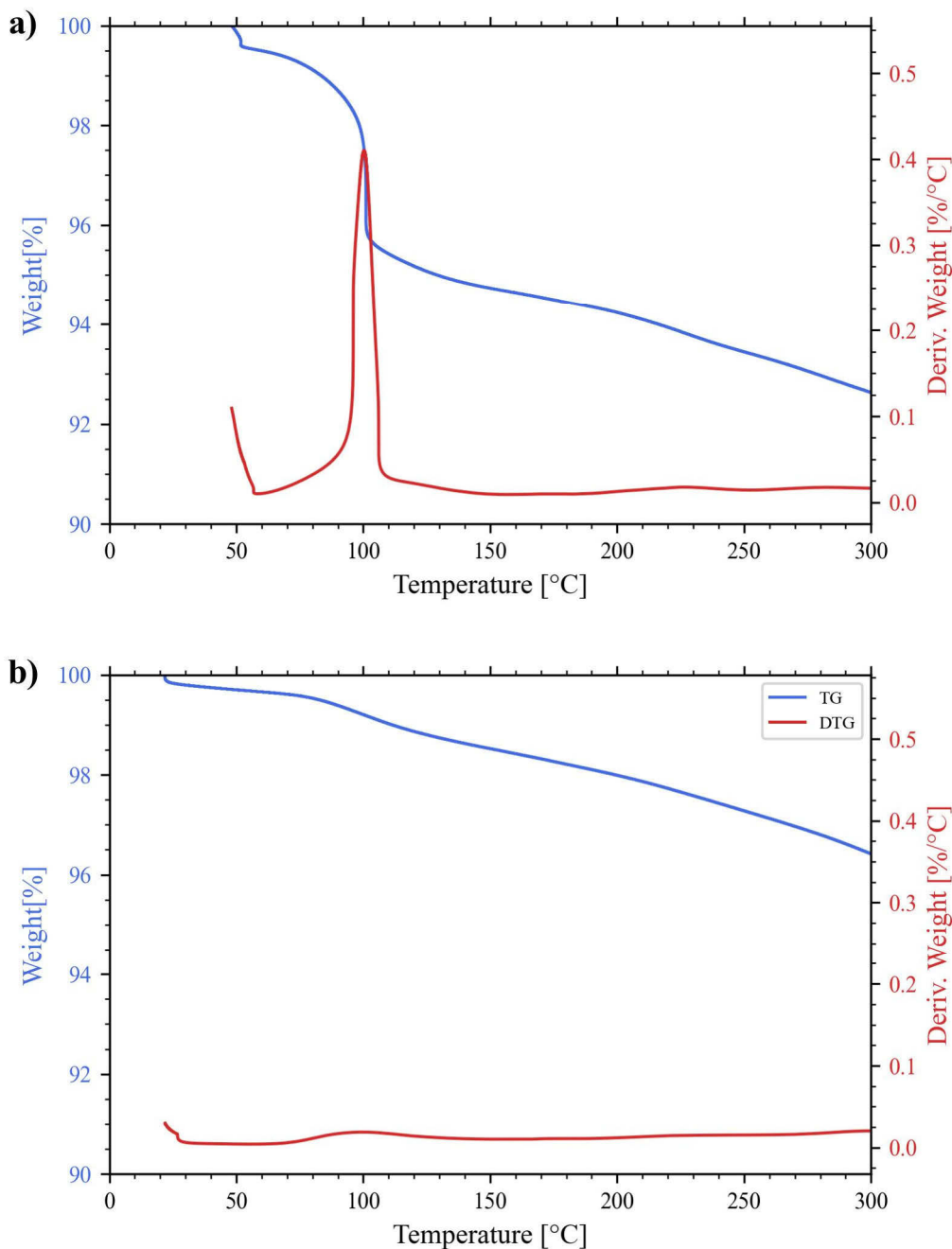
Fig. 1.: Thermogravimetric (TG, blue) and differentiate thermogravimetric (DTG, red) curves of the LiB waste material a) before and b) after the extraction process.

Besides, the full removal of the electrolyte from the LiB waste material, the aim of this study was to selectively extract the electrolyte solvents using a gradually change of the supercritical carbon dioxide extraction conditions pressure, and temperature. Based on the binary liquid-vapour equilibrium (LVE) phase diagrams in the literature a set of conditions (see Table 1.) were selected to target the selective extraction of EC, PC, and

biphenyl. However, it must be pointed out that an LVE phase diagram for EC could not be found in the literature.

Tab. 1.: Selected conditions for the three consecutive extraction steps.

Step 1	60 bar	25°C	30 minutes
Step 2	80 bar	25°C	30 minutes
Step 3	140 bar	40°C	30 minutes

The LiB black mass (6g) was inserted as received into the extraction chamber and dynamic extraction was performed using the desired pressure and temperature conditions. After the desired extraction time, the collected extract was sampled, and the conditions were adjusted for the upcoming extraction step. Finally, the collected extract was quantitatively analyzed using GC-MS. After the last extraction step, the LiB waste material was collected and characterized by TGA.

The TGA results presented in Figure 1 showed that with the studied conditions and extraction time, most of the remaining electrolyte solvents were successfully extracted. The remaining product (1.4wt%) could be attributed to the conductive salt residues, but further verification analysis is still ongoing. The analysis of the collected extract presented in Figure 2 showed the potential to selectively extract the electrolyte by gradually increasing the pressure and temperature conditions. However, a high co-extraction of the electrolyte solvents is obvious. It must be highlighted that in this study, the extraction time was kept the same for all steps. By retrieving thermodynamic and kinetic data for the different solvents the extraction process can be potentially fined-tuned and the co-extraction of the solvents minimized in the future.
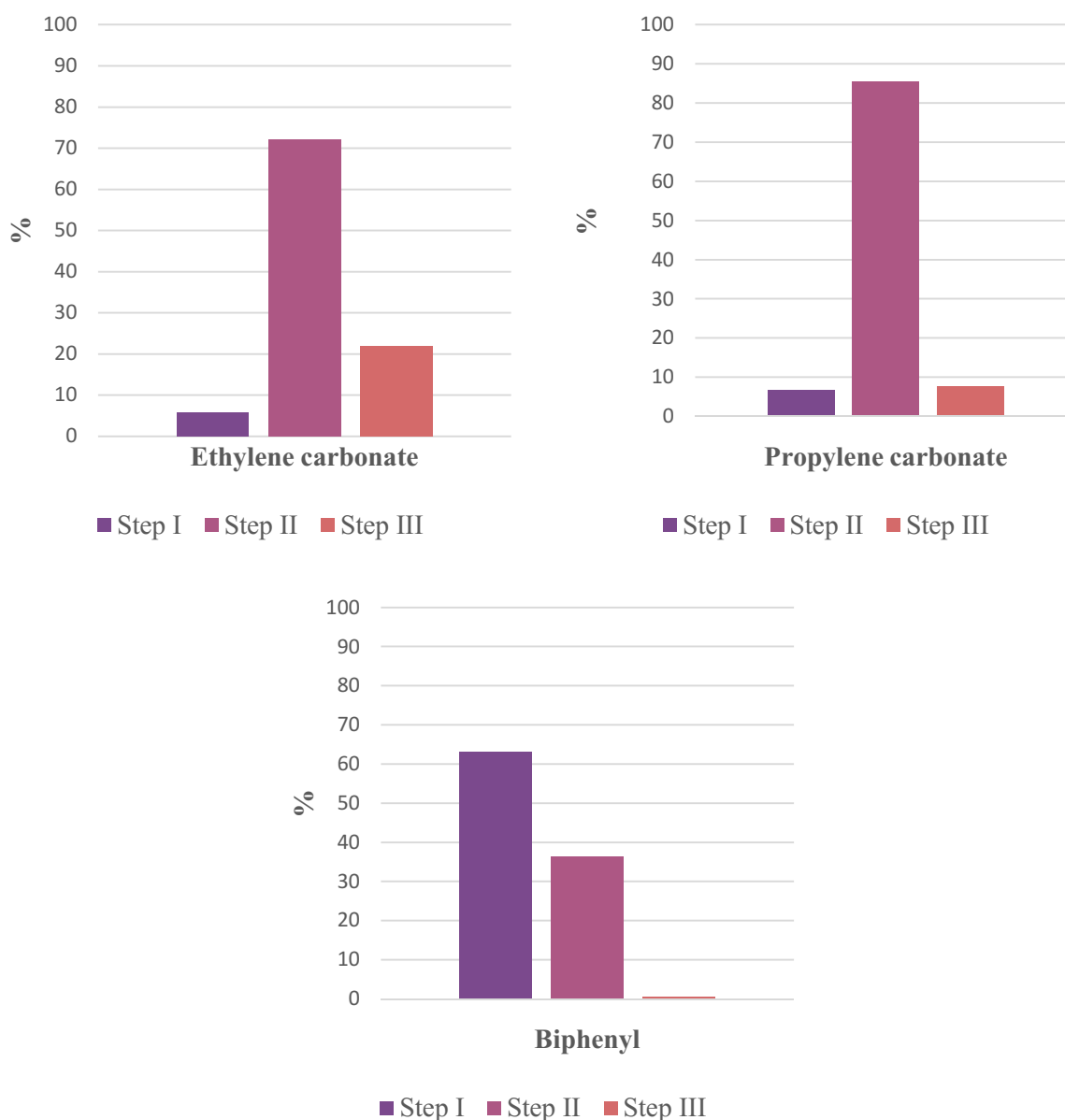
Fig. 2.: Share of detected amount for each step of the total extracted a) ethylene carbonate, b) propylene carbonate, and c) biphenyl

Summary & Outlook

In a previous study, it was shown that non-polar electrolyte solvents such as DMC and EMC can be selectively extracted using low density CO_2 conditions [13]. However, the polar electrolyte solvents such as EC remained in the LiB waste sample after the studied extraction process. The presented initial results showed that by gradually increasing the pressure and temperature conditions, the more polar electrolyte components EC and PC can be successfully extracted. However, the co-extraction of the solvents was rather high. Thus, thermodynamical, and kinetic data is required to optimize the extraction process.

Based on the models of the extraction behaviour, the extraction process can be potentially designed in such a way as to retrieve a higher purity of the solvents. The high purity of the solvents enables the recycling industry to re-sell the solvents for another purpose or even reuse them for battery production.

Acknowledgment

References

1. Agency, I. E. Global EV Outlook 2024. (2024) doi:https://www.iea.org/reports/global-ev-outlook-2024.
2. Neumann, J. *et al.* Recycling of Lithium-Ion Batteries — Current State of the Art , Circular Economy , and Next Generation Recycling. **2102917**, (2022).
3. Sobianowska-Turek, A., Urbańska, W., Janicka, A., Zawiślak, M. & Matla, J. The Necessity of Recycling of Waste Li-Ion Batteries Used in Electric Vehicles as Objects Posing a Threat to Human Health and the Environment. *Recycling* **6**, 35 (2021).
4. Bertilsson, S., Larsson, F., Furlani, M., Albinsson, I. & Mellander, B. E. Lithium-ion battery electrolyte emissions analyzed by coupled thermogravimetric/Fourier-transform infrared spectroscopy. *J. Power Sources* **365**, 446–455 (2017).
5. Nedjalkov, A. *et al.* Toxic Gas Emissions from Damaged Lithium Ion Batteries—Analysis and Safety Enhancement Solution. *Batteries* **2**, 5 (2016).
6. Marshall, J. *et al.* Disassembly of Li Ion Cells—Characterization and Safety Considerations of a Recycling Scheme. *Metals (Basel).* **10**, 773 (2020).
7. Xu, K. Nonaqueous liquid electrolytes for lithium-based rechargeable batteries. *Chem. Rev.* **104**, 4303–4417 (2004).
8. Lebedeva, N. P. & Boon-Brett, L. Considerations on the Chemical Toxicity of Contemporary Li-Ion Battery Electrolytes and Their Components. *J. Electrochem. Soc.* **163**, A821–A830 (2016).
9. Harper, G. *et al.* Roadmap for a sustainable circular economy in lithium-ion and future battery technologies. *J. Phys. Energy* **5**, 021501 (2022).
10. Zachmann, N., Petranikova, M. & Ebin, B. Electrolyte recovery from spent Lithium-Ion batteries using a low temperature thermal treatment process. *J. Ind. Eng. Chem.* **118**, 351–361 (2022).
11. Diaz, F., Wang, Y., Weyhe, R. & Friedrich, B. Gas generation measurement and

evaluation during mechanical processing and thermal treatment of spent Li-ion batteries. *Waste Manag.* **84**, 102–111 (2019).

12. Nowak, S. & Winter, M. The role of sub- and supercritical CO2 as 'processing solvent' for the recycling and sample preparation of lithium ion battery electrolytes. *Molecules* **22**, 403 (2017).

13. Zachmann, N., Fox, R. V., Petranikova, M. & Ebin, B. Implementation of a sub-and supercritical carbon dioxide process for the selective recycling of the electrolyte from spent Li-ion battery. *J. CO2 Util.* **81**, 102703 (2024).

Thermophysical Characterization of Fluids of Interest for the Energy Transition

Elizabeth González Cortés

School of Industrial Engineering, Department of Energy Engineering and Fluid Mechanics, University of Valladolid,

elizabeth.gonzalez22@uva.es

1. Introduction

The European Union is committed to ending its contribution to global warming, achieving net-zero greenhouse gas emissions by 2050 [1]. Achieving this goal requires significant changes in the current energy system, using clean energy sources and increasing energy efficiency. The low capacity and intermittency of current renewable energies make it necessary to search for new solutions for energy storage. In this context, green hydrogen production offers an ideal solution for energy storage in an integrated system that combines not only harmless energy production, but also high gravimetric energy density. However, hydrogen has the lowest volumetric energy density, so to satisfy energy demands like those of other fuels, larger volumes of hydrogen must be moved [2]. Consequently, the most important current challenges to overcome are to achieve practical storage that combines its high gravimetric energy density with an efficient volumetric energy density.

One way is hydrogen store in a stable and non-toxic compound such us chemical absorption in ionic liquids (IL). According to various studies reported in the literature [3-4], ILs containing imidazolium cation offers an effective solution for this purpose. This ILs family deserves to be researched, it allows an optimal hydrogen storage capacity [5]. ILs are a promising candidate because of its good chemical and thermal stability, low vapor pressure, neglectable volatile and have a good capacity to act as a dehydrogenation promoting agent; allowing lower temperatures for faster dehydrogenation [6].

On the other hand, stable hydrogen storage under ambient conditions can be achieved by binding atomic hydrogen to hydrogen-poor molecules in liquid phase; an example of those compounds is called liquid organic hydrogen carriers (LOHC). LOHCs have a high capacity to store hydrogen without losses even in the long term, they undergo completely reversible hydrogenation/dehydrogenation cycles, hydrogen-poor compound usually has a high boiling point, so pure hydrogen can be separated easily from liquid molecules through a condensation process, making this hydrogen storage approach economically

and technologically attractive for implementation in real applications [7-8]. N-ethyl carbazole (NEC) has been identified as the best LOHC in their extensive heterocycle series; this can store 5.8 wt % hydrogen with an energy density of 1.9 kWh/kg [9].

2. Experimental

2.1 Materials

The design and optimization of hydrogen storage requires the knowledge of key properties such as density (ρ), viscosity (η) and solubility. These properties will be measured for each pure compounds, as well as for the LOHC pairs, in the entire molar range. Experimental measurements will be carried out at temperature range: (273.15-393.15) K and pressures from atmospheric up to 70 MPa. Table 1 shows the substances of interest according to literature review. [3-6; 7-9]

Table 1. Fluids of interest for hydrogen storage.

IL	LOHC
1,3-Diethylimidazolium ethyl sulfate 98%	N-ethylcarbazole/Perhydro-N-ethylcarbazole
1,3-Diethylimidazolium methyl sulfate 98%	Dibenzyltoluene/Perhydro-Dibenzyltoluene
1-Butyl-3-methylimidazolium methyl sulfate 98%	Methylcyclohexane/Toluene
1-Ethyl-3-methylimidazolium ethyl sulfate 98%	
1-Ethyl-3-methylimidazolium methyl sulfate 98%	

The ILs were purchased at Iolitec, Methylcyclohexane 99% was purchased at Thermo Scientific, Toluene 99,8% from Sigma Aldrich, 9-Ethyl-9H-carbazole 99% and Dibenzyltoluene 99,9% from Cymit. Perhydro-N-ethylcarbazole and Perhydro-Dibenzyltoluene will be produced in our laboratory through catalytic hydrogenation of N-ethylcarbazole and Dibenzyltoluene, using Pt/Al_2O_3 5% as a catalyst.

2.2 Equipment and procedures

A vibrating tube densimeter (Anton Paar DMA HPM) was used to measure density. Its operating principle is based on the laws that govern simple harmonic motion and consists of measuring the natural period (T) of vibration of a U-shaped tube, which is electromagnetically excited and contains inside the liquid whose density is wanted to know. That technique is able to measures densities from (0 to 3000) kg·m^{-3}, with a resolution of 10^{-2} kg·m^{-3} and uncertainties better than 0,1% with coverage factor (k=2).

This vibrating tube densimeter has a working range in temperature: (263.15-473.15) K and pressure: (0-140) MPa.

The densimeter was calibrated using water and vacuum over the entire working temperature and pressure range. The vibration period (T) and densities are related following equation (1) proposed by [10].

$$\rho(T,p) = A(T)\tau^2(T,p) - B(T,p) \tag{1}$$

where A(T) and B(T,p) are two characteristic parameters of the device that can be determined through calibration at each temperature and pressure.

To obtain experimental dynamic viscosity data, a vibrating wire viscometer was used, which works up to 35 mPa·s in the temperature and pressure range: (288.15-423.15) K and (0-140) MPa respectively. Its operating principle is based on a tungsten wire of length L=50mm and nominal radius R_w=75 μm tensioned and held at both ends. The sensor is housed in a pressure vessel, properly centred and oriented in a constant magnetic field generated by a magnet, which combined with an alternating current flow through the wire establishes a transverse oscillation. The pressure vessel is immersed in a thermostatic bath. The temperature is measured using two platinum resistance thermometers (PTR) and pressure is obtained using a Druck DPI 104 transducer. Relative uncertainty of viscosity measurements is estimated better than 1.5% with a coverage factor k=2. With this technique it is only necessary knowing the density of the liquid, density and radius of the vibrating wire, as well as the resonance frequency and the bandwidth of the resonance curve, as described by equation (2) proposed by [11].

$$\eta(mPa \cdot s) = \frac{\pi f_r R_w^2 \rho}{6}\left(\frac{f_r}{f_b}\right)^2\left(1+\frac{\rho_s}{\rho}\right)^2 \tag{2}$$

where f_r: is the resonance frequency; f_b: is the bandwidth; ρ: is the fluid density; ρ_s: wire density.

The vibrating wire viscometer is an absolute viscometer, that means it does not require calibration. However, the radius of the wire cannot be established with sufficient precision by independent methods. Toluene was used as a reference fluid to calibrate wire radius, carrying out the measurements at a certain T and p with its reference values of η and ρ reported in REFPROP. Finally, the technique is validated by measuring toluene or other reference fluid in a wide range of T and p.

Solubility measurements are performed in an isothermal total pressure cell based on the design of Van Ness et al. [12]. It is also used to measure and can be used to measure

VLE of binary or ternary systems. This cell is a cylindrical piece of stainless steel with a volume of 180 ml with a magnetic stirrer, which is submerged in a thermostatic bath whose temperature is measured using a Pt-100. The system consists of an ISCO pump, which inject know quantities of hydrogen into the cell, at a constant pressure and temperature. Pressure is monitored with two Druck pressure gauges, one for pressures between (0-2) bar and another for pressures up to 130 bar. Before carrying out the measurements, a calibration of the total volume of the cell is carried out by progressively filling with water. As the quantity of water injected in the cell is known, pressure and temperature inside the cell is controlled total volume as function of temperature can be carried out.

The IL in question must be previously degassed in the cell through a series of solidification-melting cycles, these cycles are repeated until the vapor pressure of the compound is the same in two consecutive cycles. Once the IL has been degassed, and the vapor pressure is stable, hydrogen is then injected. When equilibrium is reached, the total pressure of the cell is taken using the appropriate pressure gauge according to the working pressure range. Solubility is calculated based on knowledge of H_2 mass in the vapor phase, with previous calculation of the partial pressure of H_2 and its volume in the vapor phase.

2.3 Results

Experimental result of density measurement of pure species (toluene and methylcyclohexane) is shown in Fig. 1 and Fig. 2 for the isotherms (273.15-393.15) K in the pressure range of (0-70) MPa.
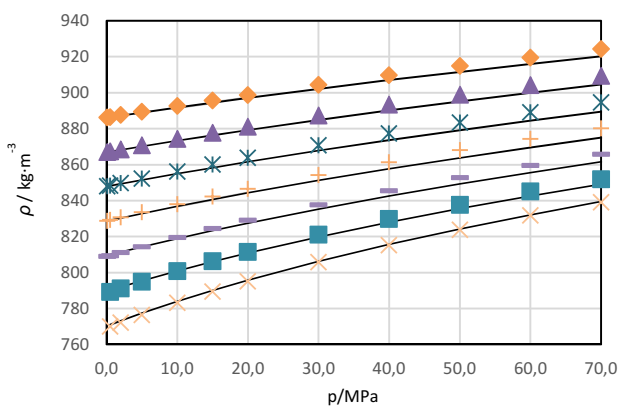

Fig. 1: Experimental density data of toluene (♦ 273.15 K; ▲ 293.15 K; ✳ 313.15 K; + 333.15 K; - 353.15 K; ■ 373.15 K; x 393.15K; — ρ/Tamman-Tait).
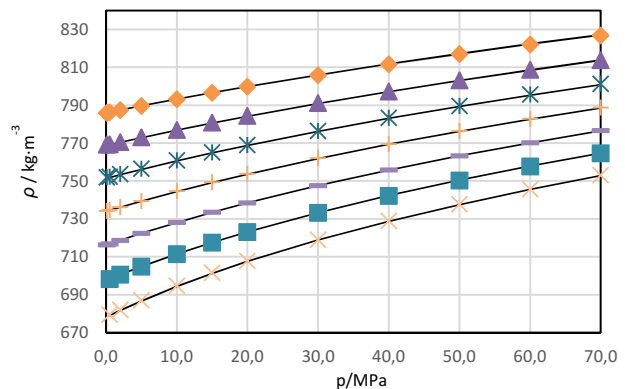
Fig. 2: Experimental density data of methylcyclohexane (♦ 273.15 K; ▲ 293.15 K; ✳ 313.15 K; + 333.15 K; - 353.15 K; ■ 373.15 K; x 393.15K; — ρ/Tamman-Tait).

In Fig. 3 and Fig. 4, density versus pressure for pure toluene, equimolar mixture, and pure methylcyclohexane are shown for the temperatures 273.15 K and 393.15 K.
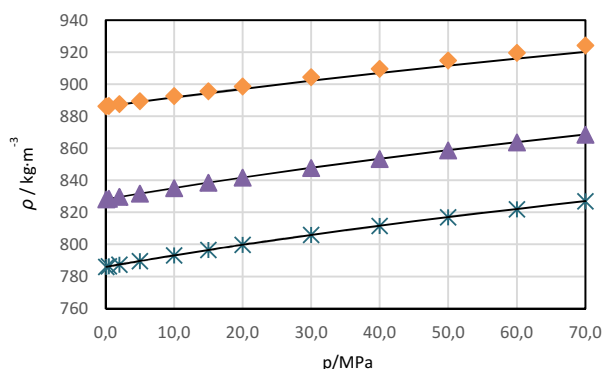

Fig. 3: Experimental density data for 273.15 K (♦ 1% mol toluene; ▲ equimolar mixture; ✳ 1% mol methylcyclohexane).
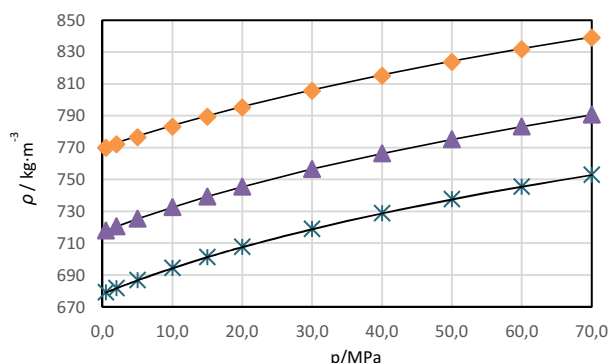
Fig. 4: Experimental density data for 393.15 K (♦ 1% mol toluene; ▲ equimolar mixture; ✳ 1% mol methylcyclohexane).

Density data have been obtained for the pure compounds of the Toluene/Methylcyclohexane pair at the working temperatures and pressures described in section 2.1. These data have been correlated with a modified Tammann-Tait, represented in equation (3) proposed by [13].

$$\rho(T,p) = \frac{\rho(T, \rho_{ref})}{1 - C ln\left[\frac{B(T) + p}{B(T) + \rho_{ref}}\right]} \qquad (3)$$

Table 2 presents the statistical data analysis of experimental data correlated with Tammann-Tait equation; mean absolute relative average (ADD) and the maximum absolute relative deviation (MAD).

Table 2. Statistical parameters of the measurements for the compounds.

Compound	MAD%	AAD%
Toluene	0,5938	0,1981
Equimolar composition	0,0407	0,0190
Methylcyclohexane	0,0438	0,0214

Summary

The densities of toluene and methylcyclohexane have been measured in a wide range of temperature, pressure and compositions. For this purpose, a vibrating tube densimeter with an expanded relative uncertainty of 0.1 % (k = 2) was used. The density data of the

pure components show a similar behavior in terms of the effect of pressure and temperature; the density shows an increasing behavior when pressure rise and decreasing with temperature. The results of the pure components densities in comparison with the equimolar mixture, at a given temperature, the density increases with increasing toluene mole fraction and pressure. The results of the modified Tamman-Tait equation proved to be suitable for correlating experimental density data that depend on temperature and pressure. This model achieved good absolute average relative deviations compared with the experimental density.

Acknowledgment

References

[1]-European Commission. Long-term low greenhouse gas emission development strategy of the European Union and its Member States (2020).

[2]-Ren, J et al. S. Current research trends and perspectives on materials-based hydrogen storage solutions: A critical review. Int. J. Hydrogen Energy, 42, 289–311 (2017).

[3]-Migowski, P., Lozano, P., & Dupont, J. Imidazolium based ionic liquid-phase green catalytic reactions. *Green Chemistry*, *25*(4), 1237-1260 (2023).

[4]-HG Prechtl, M., & Sahler, S. Hydrogen storage using ionic liquid media. *Current Organic Chemistry*, *17*(3), 220-228 (2013).

[5]-Liu, Y., Cui, J., Wang, H., Wang, K., Tian, Y., Xue, X., ... & Zhang, S. Ionic liquids as a new cornerstone to support hydrogen energy. *Green Chemistry*, *25*(13), 4981-4994 (2023).

[6]-Sahler, S. et al. The role of ionic liquids in hydrogen storage. Chem. - A Eur. J. 20, 8934–8941 (2014).

[7]-Crabtree R.H. Nitrogen-containing liquid organic hydrogen carriers: progress and prospects. ACS Sustainable Chem. Eng. 5, 6, 4491–4498 (2017).

[8]-Hurskainen M. et al. Tecno-economic feasibility of road transport of hydrogen using liquid organic hydrogen carriers. Int. J. Hydrogen Energy 45, 32098–32112 (2020).

[9] Hurskainen M. et al. Tecno-economic feasibility of road transport of hydrogen using liquid organic hydrogen carriers. Int. J. Hydrogen Energy 45, 32098–32112 (2020).

[10]-B. Lagourette, C. Boned, H. Saint-Guirons, P. Xans, H. Zhout, Densimeter calibration method versus temperature and pressure, Meas. Sci. Technol 3, 699–703 (1992).

[11]-Assael M.J., Dymond J.H., Papadaki M., Patterson P.M., Correlation and prediction of dense fluid transport coefficients. I. *n*-Alkanes. Int. J. Thermophys 13(2), 269-281 (1992).

[12]-R.E. Gibbs, H.C. Van Ness, Ind. Eng. Chem. Fund. 11 (1972) 410e413.

[13]-J.H. Dymond, R. Malhotra, The Tait Equation: 100 Years On, Int J Thermophys 9 (1988).

Decomposition of Polycarbonate in Subcritical Water

Mihael Irgolič, Maja Čolnik, Mojca Škerget*

Faculty of Chemistry and Chemical Engineering, University of Maribor, Slovenia

*mojca.skerget@um.si

Introduction

In recent years, the chemical recycling of waste polymers has attracted greater attention as a means of recovering valuable products from plastic waste [1]. Polycarbonate (PC), an engineering thermoplastic, is increasingly being used in various applications. Its use, especially in outdoor applications, is increasing due to its favourable properties such as good transparency, low density, and high mechanical strength, making it one of the most widely used engineering thermoplastics [2]. There are two main ways for recycling PC: physical recycling and chemical recycling. Physical recycling, where the chemical composition of the material is not changed, cannot provide a comprehensive solution to the dilemma of environmental pollution. Even though physical recycling can extend the lifespan of PC, the purity of the material deteriorates with each cycle of reuse, while it continues to take up space in the form of residual waste [3]. Chemical recycling is therefore preferred, as plastics can be converted into their monomers, which are then reused as raw materials for polymer production [4]. In the case of PC, the monomeric unit is bisphenol A (BPA). Water in a subcritical state is a medium that could provide optimal conditions for various chemical reactions, including the degradation of various plastics [5].

In this study, the decomposition of virgin PC was carried out in subcritical water in order to determine the optimum reaction conditions (temperature, time). The composition of the oil phase was determined in order to facilitate the comparison of the results obtained with the selected process parameters and to determine the possible degradation pathway.

Experimental

The hydrothermal decomposition of PC was carried out in a high-temperature, high-pressure batch reactor (Parr Instruments, Moline, IL, USA). The temperature range was between 250 °C and 350 °C, and the reaction time was between 5 min and 120 min. Initially, the appropriate amount of material and deionised water was added to the reactor to obtain a material to water ratio of 1:5 (g:mL). The reactor was purged three times with nitrogen through the valve system before heating. After the desired reaction time was reached, the reactor was quenched in cold water to lower the temperature as quickly as possible. Once the reactor reached room temperature, the water-oil mixture was subjected

to vacuum filtration to isolate the solid phase, and the reactor and filter paper were washed with diethyl ether (DEE) to avoid losses. The filter paper was then dried overnight at 70°C. The aqueous and oil phases were separated in a separatory funnel, followed by removal of the DEE from the oil phase in a rotary evaporator under vacuum. The oil, solid and aqueous phase yields were determined gravimetrically, while the gas yield was calculated based on the mass balance.

The composition of the oil phase was determined using a Shimadzu GC-2010 gas chromatograph equipped with flame ionization detector (FID). The compounds of the oil phase were separated using an HP-5MS capillary column with helium as the carrier gas and DEE as solvent. The identification and quantification of the compounds was based on an external calibration for BPA, 4-isopropylphenol (4-IPPH) and phenol. The composition of the oil phase is expressed as mass of component w (%) per mass of oil.

Results

Fig. 1 shows the recovery of oil ($\gamma(o)$), solid ($\gamma(s)$), aqueous ($\gamma(aq)$), and gas ($\gamma(g)$) phases after hydrothermal degradation at different reaction conditions. At a reaction temperature of 250 °C and a reaction time of 60 min, the degradation of PC only started and a lot of undegraded material remained, which is reflected in a high yield of the solid phase (94.5 %). When the reaction time was increased to 120 min the degree of degradation increased, but the amount of remaining undegraded material was still high (59.7 %). When the reaction temperature was increased to 300 °C, the time of 5 min was still too short for degradation. When the time was increased to 15 min, almost all the material was degraded and a high yield of the oil phase was observed (94.9 %). Similar results were reported by Y. Huang et al. [3], where 100 % depolymerization was achieved at 300 °C after 45 min. The difference in the reaction time to achieve 100 % depolymerisation could be due to the influence of the heating rate and the type of reactor. The maximum yield of the oil phase at 300 °C was achieved after a reaction time of 30 min and was 95.1 %. With further increasing the reaction time, the yield of the oil phases started to decrease, while the yield of the gas phase started to increase, reaching 9.9 % after a reaction time of 120 min. Increasing the reaction temperature to 350 °C resulted in faster degradation and the yield of the oil phase was 96.7 % after only 5 min. The maximum oil yield (97.7 %) was achieved at 350 °C and a reaction time of 15 min. At a temperature of 350 °C, the gasification process was also significantly faster, and the yield of the gas phase increased from 0.4 % to 24.0 % when the reaction time increased from 5 min to 120 min. The decrease in the yield of the oil phase with increasing reaction time was also reported by Seshasayee and

Savage [6], who increased the reaction time from 30 to 60 min at a reaction temperature of 350 °C. The yield of aqueous phase was low at all reaction conditions and did not exceed 1.1 %.
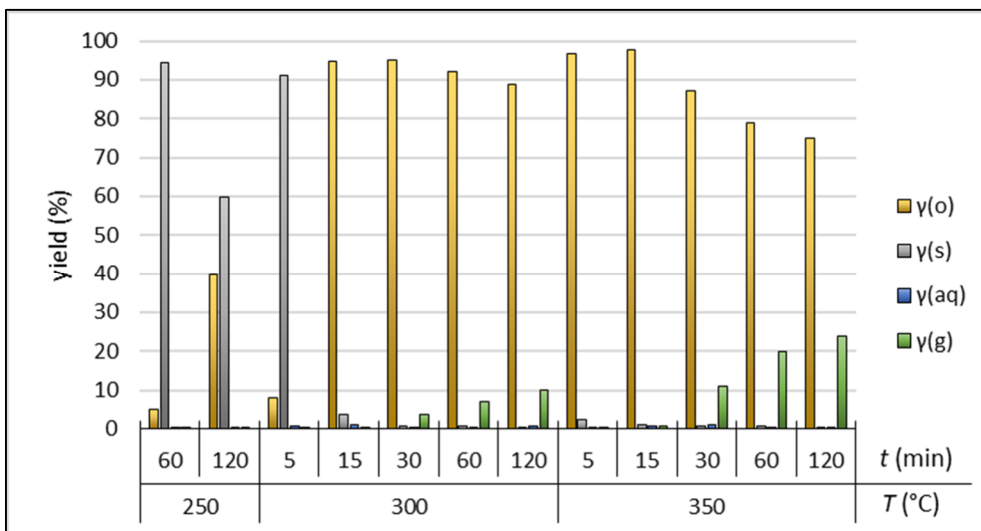
Fig. 1. Yield of oil ($\gamma(o)$), solid ($\gamma(s)$), aqueous ($\gamma(aq)$) and gas ($\gamma(g)$) phase after hydrothermal degradation of PC.

In the oil phase, the three most important products (BPA, 4-IPPH and phenol), which were formed during the degradation of PC, were determined and the composition of the oil phase is shown in Fig. 2.
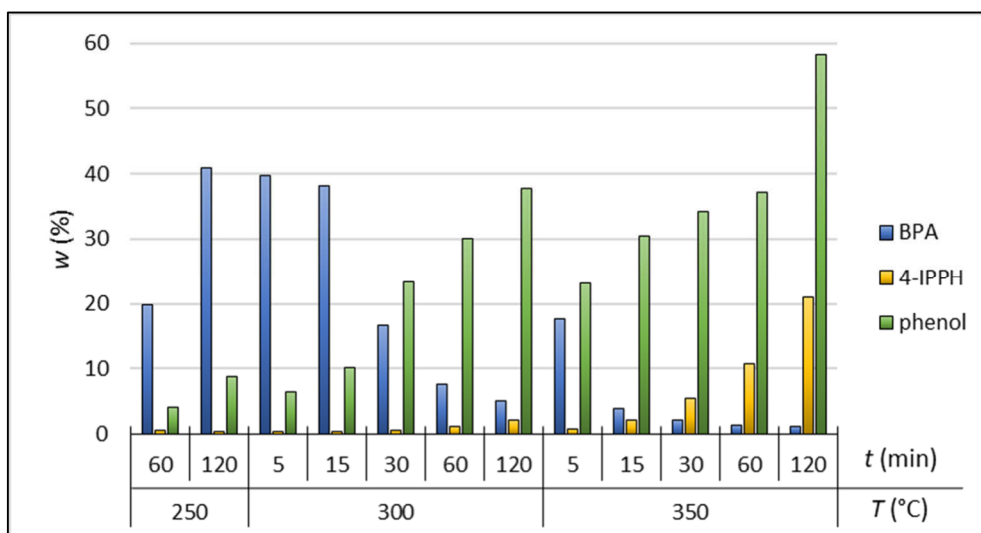
Fig. 2. Composition of the oil phase after hydrothermal degradation of PC by weight fraction w (%) of the component in the oil phase. BPA – bisphenol A, 4-IPPH – 4-isoprophylphenol.

At 250 °C, the BPA content in the oil phase increased from 19.9 % to 40.9 % with increasing reaction time. Similarly, the phenol content increased from 4.0 % to 8.9 %, indicating the subsequent decomposition of BPA. At 300 °C, the BPA content is high at

short reaction times (5 min, 15 min), but since decomposition is not yet complete, the times after 15 min were relevant. The content of BPA decreased from 38.2 % to 7.7 % when the time increased from 15 min to 120 min, and the content of phenol increased from 10.1 % to 37.7 % in the same period. In the study by Y. Huang et al. [3], the maximum yield of BPA at 300 °C was observed after 30 min of reaction time and was about 40 %, which is similar to our results after 15 min of reaction time at the same temperature. The difference may be due to the different equipment and heating rate used for decomposition. Rapid decomposition of BPA was observed at 350 °C, with only 3.8 % of the BPA remaining in the oil phase after 15 min. With increasing reaction time, the amount of 4-IPPH increased steadily from 0.6 % to 21.0 %. Since 4-IPPH is a degradation product of BPA [5], the increase in 4-IPPH content was expected. Similar to the lower degradation temperatures, an increase in phenol content was also observed at 350°C, but it was more pronounced (from 23.1 % to 58.2 %). Based on the results obtained, the degradation pathway was constructed (Fig. 3).
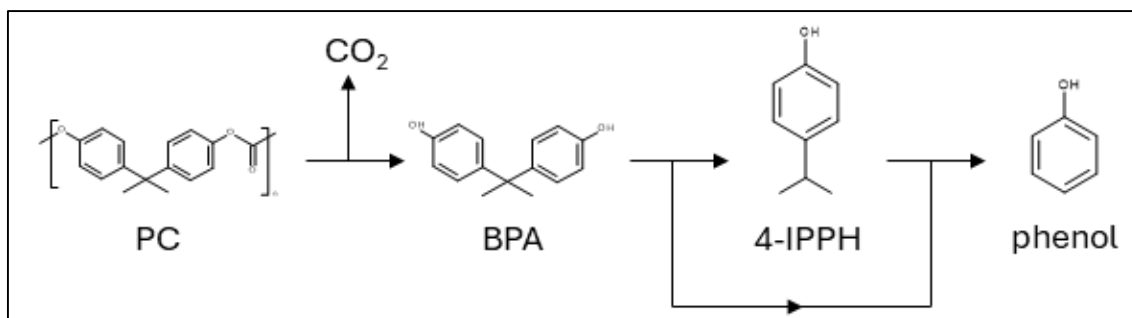
Fig. 3. Degradation pathway of polycarbonate in subcritical water.

Summary

The decomposition of PC to valuable products such as BPA monomer, 4-IPPH and phenol was successfully carried out in subcritical water. An investigation of the influence of the process parameters (temperature and time) showed the maximum yield of the oil phase (97.7 %) at a reaction temperature of 350 °C and a reaction time of 15 min. Poor stability of the BPA monomer was observed in subcritical water, which rapidly degrades to valuable chemicals such as 4-IPPH and phenol at higher reaction temperatures (300°C and 350 °C) and longer reaction times. Further studies could include investigating the degradation of different PC waste materials and analysing additional process parameters such as the material-to-water ratio.

Acknowledgment

References

[1] T. Helmer Pedersen, F. Conti, Improving the circular economy via hydrothermal processing of high-density waste plastics, Waste Manag. 68 (2017) 24–31. https://doi.org/10.1016/j.wasman.2017.06.002.

[2] G. Weibin, H. Shimin, Y. Minjiao, J. Long, D. Yi, The effects of hydrothermal aging on properties and structure of bisphenol A polycarbonate, Polym. Degrad. Stab. 94 (2009) 13–17. https://doi.org/10.1016/j.polymdegradstab.2008.10.015.

[3] Y. Huang, S. Liu, Z. Pan, Effects of plastic additives on depolymerization of polycarbonate in sub-critical water, Polym. Degrad. Stab. 96 (2011) 1405–1410. https://doi.org/10.1016/j.polymdegradstab.2011.05.017.

[4] E.V. Antonakou, D.S. Achilias, Recent Advances in Polycarbonate Recycling: A Review of Degradation Methods and Their Mechanisms, Waste Biomass Valorization 4 (2013) 9–21. https://doi.org/10.1007/s12649-012-9159-x.

[5] A. Ikeda, K. Katoh, H. Tagaya, Monomer recovery of waste plastics by liquid phase decomposition and polymer synthesis, J. Mater. Sci. 43 (2008) 2437–2441. https://doi.org/10.1007/s10853-007-2030-y.

[6] M.S. Seshasayee, P.E. Savage, Oil from plastic via hydrothermal liquefaction: Production and characterization, Appl. Energy 278 (2020) 115673. https://doi.org/10.1016/j.apenergy.2020.115673.

Polymerization of Ethene and Acrylic Acid under High-Pressure Conditions

Laura Dietrich, Markus Busch*

Ernst-Berl-Institute of Technical and Macromolecular Chemistry, Technical University of Darmstadt, 64287 Darmstadt/Germany, *e-mail: markus.busch@pre.tu-darmstadt.de

Introduction

Low-density polyethene (LDPE), which is synthesized under high-pressure conditions, is one of the most important polymers due to its versatility. By adding polar comonomers, such as acrylic acid (AA), the range of properties of the polymer can be extended. The variation of the type and content of the comonomer allows to increase for example the flexibility of the polymer compared to LDPE. Copolymers of ethene and acrylic acid (EAA) have very good adhesive properties on metal, paper or plastics as well as good sealing properties. In addition, these copolymers are particularly hard and flexible. This results in a wide range of applications. Ethene-acrylic acid copolymers can be used in special packaging films for food products or in cable seals.[1,2]

To understand the synthesis of copolymers such as EAA, it is necessary to know the relation between comonomer content in the reaction mixture and polymer. For this purpose, the system can be described by reactivity ratios. Knowledge of the reactivity ratios is essential for better process control and for the development of new polymer grades. By increasing the AA content, the data range of the copolymerization diagram can be expanded, which reduces inaccuracies.[2,3]

Experimental

Reactivity ratios of a copolymerization can be described with the ratio of the rate coefficients of the homo-polymerization step to the cross-polymerization step. This relationship is shown in equation 1 and describes the incorporation behavior of a comonomer in the polymer.[4]

$$r_1 = \frac{k_{11}}{k_{12}} \qquad\qquad r_2 = \frac{k_{22}}{k_{21}} \qquad\qquad (1)$$

Different methods are available for determining reactivity ratios. Nowadays, the nonlinear least square method is used. This method is based on the MAYO-LEWIS[5] copolymer equation (equation 2). A useful tool for determining reactivity ratios using the nonlinear

parameter estimation was developed by REISCHKE[6]. It enables the consideration of a dependent error structure in F and f, when determining the corresponding values for r_1 and r_2.

$$\frac{F_1}{F_2} = \frac{f_1(r_1 f_1 + f_2)}{f_2(r_2 f_2 + f_1)}$$

(2)

To determine reactivity ratios of the EAA-system, continuous experiments were carried out in a corrosion-resistant autoclave R-1 between 220 °C and 250 °C at 2000 bar. The autoclave has a volume of 60 mL and is designed for a maximum pressure/ temperature of 3000 bar/ 300 °C. For the continuous high-pressure polymerization, ethene is compressed to 2000 bar with a three-stage membrane compressor C-1. The comonomer AA can either be fed with a membrane pump MP-1 directly into the reactor or with the high-pressure metering pump KP-1 via the third compressor stage in the reactor. The MP-1 can feed large flows between 80 g h^{-1} and 2000 g h^{-1}, while the KP-1 can feed 2 mL min^{-1}. Moreover, the initiator solution can be fed with the syringe pump SP-1. Via a mixer, the compressed ethene is mixed with the feed substances and afterwards fed into the reactor. Figure 1 shows a flow diagram of the used mini-plant.
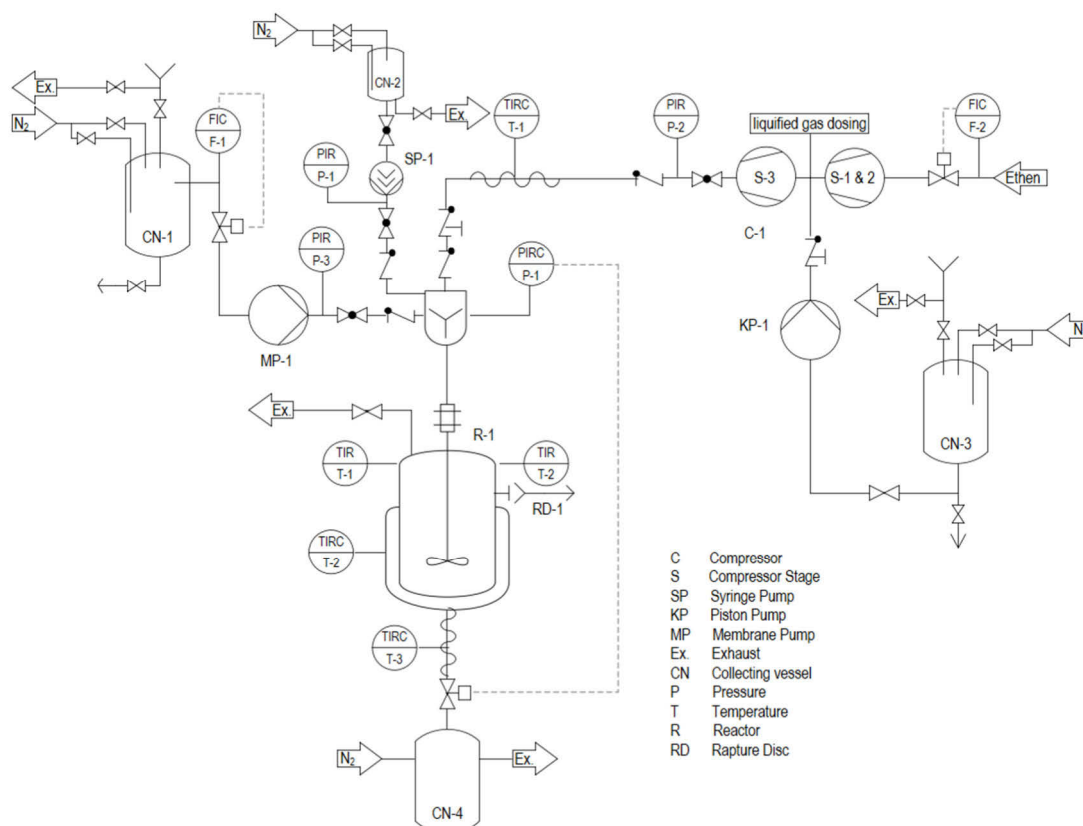
Fig. 1.: Flow diagram of the experimental setup of the continuous high-pressure mini-plant.

In order to estimate the reactivity ratios from the received EAA polymer, the AA content within the copolymer F_{AA} and within the monomer mixture f_{AA} must be determined. The former is measured using ^{1}H-NMR and ATR-IR spectroscopy. To calculate the composition of the monomer mixture, the mass feed of the monomers at the reactor inlet as well as the polymer yield per time unit are required. The existing calibration for higher AA contents in the copolymer could be extended up to 45 wt. % by using the two analytical methods and by changing the ^{1}H-NMR solvent from TCE to the polar one DMSO (see figure 2).
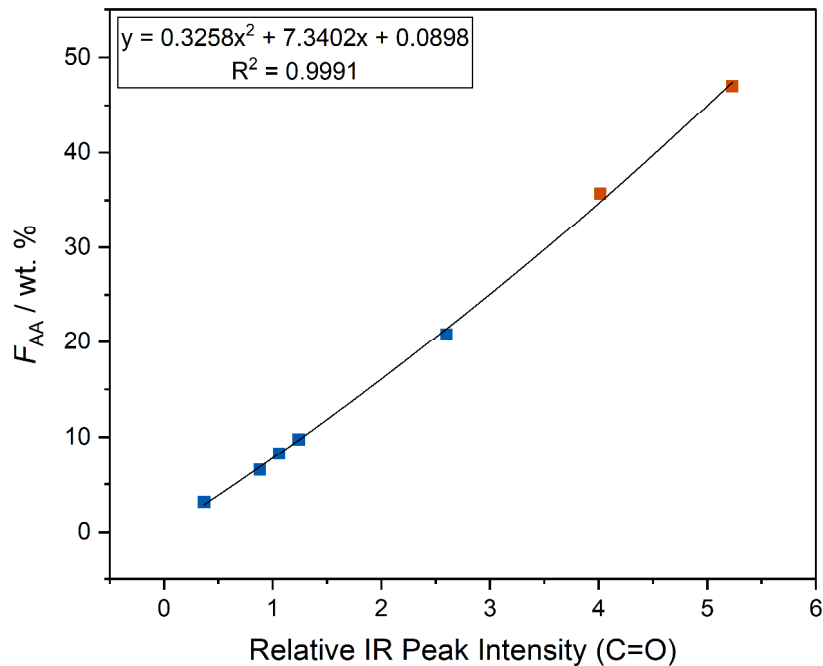
Fig. 2.: Calibration curve for the determination of the AA content in the copolymer. The orange data points represent the added values, expanding the validity range to 45 wt. %.

The most data points for the copolymerization diagram are available at 240 °C, which can be seen in figure 3. The highest experimental AA content achieved is 25.98 mol % (47 wt. %). This is a significant increase in the AA content in the copolymer compared to the literature (6.98 mol %). Furthermore, the determined reactivity ratios are in the same order of magnitude as those of WITTKOWSKI[2] (r_E = 0.05 ± 0.005 and r_{AA} = 8 ± 2) and MÄHLING[3] (r_E = 0.043 ± 25 % and r_{AA} = 7.8) for the same condition (240 °C and 2000 bar). Thus, AA is preferentially incorporated in copolymerization with ethene. The reactivity ratios compared to those in literature are smaller for r_{AA} and slightly higher for r_E. This leads to a lower AA incorporation than expected.
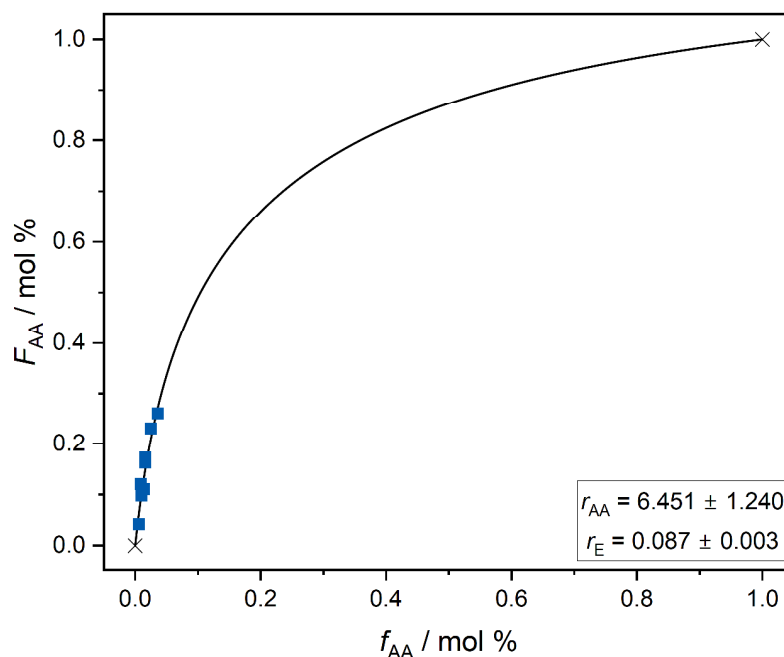
Fig. 3.: Copolymerization plot of the EAA system at 240 °C and 2000 bar.

Summary

It can be summarized that it was possible to increase the AA content in the copolymer and thereby expand the data range in the copolymerization diagram for 240 °C at 2000 bar. With ^{1}H-NMR and ATR-IR it was also possible to extend the calibration curve for higher AA contents. Additionally, the phase behavior of EAA copolymer with increasing AA contents must be investigated and the homogeneity of the samples verified, because this is an important prerequisite for determining kinetic parameters like reactivity ratios.

References

[1]   nbspolymers, "Ethen Acrylsäure Copolymer (EAA)", can be found under: *https://nsb-polymers.de/eaa-ethyle-acrylsaure-copolymer/,* last visited on the **25.07.2023**.

[2]   L. Wittkowski, *Experimentelles Studium und Modellierung der radikalischen Hochdruck-Copolymerisation von Ethen und (Meth)Acrylsäure*, Cuvillier, Göttingen, **1999**.

[3]   F.-O. Mähling, *Thermische und Excimerlaser-induzierte Hochdruck-Copolymerisationen von Ethen mit polaren Comonomeren,* 1. Aufl., Cuvillier, Göttingen, **1995**.

[4]   F. R. Mayo, C. Walling, *Chem. Rev.* **1950**, *46*, 191.

[5]   F. R. Mayo, F. M. Lewis, *J. Am. Chem. Soc.* **1944**, *66*, 1594.

[6]   R. Reischke, *Macromol. Theory Simul.* **2023**, *32*.

Hydrothermal Liquefaction of Residual Biomass for Sustainable Aviation Fuel Precursors Production

Irene Magdaleno de la Fuente[1, 2], Ana Fernández[1, 2], Danilo Cantero[1, 2]

1 BioEcoUVa, Research Institute on Bioeconomy, PressTech Group, University of Valladolid, Spain

2 Dpt. Of Chemical Engineering and Environmental Technology, School of Industrial Engineering, University of Valladolid, Spain, irene.magdaleno@uva.es

Introduction

Over the last 20 years, the industry of transport has been the second largest contributor to global greenhouse gas and CO_2 emissions [1]. In particular, aviation is responsible for approximately 2.1% of global CO_2 emissions [2]. Since alternative energy resources, such as hydrogen or electricity, are not the best fit for large aircrafts, one of the most promising options is the use of Sustainable Aviation Fuel (SAF). SAF will reduce the industry's carbon while also reducing the dependence on the petroleum industry. SAF can be produced from lignocellulosic waste biomass through different processes, one of the most interesting being hydrothermal liquefaction (HTL), which produces a biocrude oil that can be used as an alternative fuel after a catalytic upgrading [3-7]. The aim of this project is the optimization of HTL of lignocellulosic biomass, specifically pine, eucalyptus and coffee grounds, for bio-oil production in a batch reactor.

Experimental

Batch reactions were carried out in a stainless-steel reactor from Autoclave Engineers. In all reactions, a 12% (w/w) mixture of biomass and water was used. Table 1 shows the reaction conditions studied in this work.

Tab 1. Reaction conditions of batch experiments

	Reaction time	Temperature	pH
Step 1	Evaluate 4 contitions (0-60 minutes)	Fixed (250ºC)	Fixed (natural)
Step 2	Fixed (60 min)	Evaluate 4 contitions (150-350ºC)	Fixed (natural)
Step 3	Fixed (optimized)	Fixed (optimized)	Evaluate 2 contions (acid-basic)

The reaction product was filtered to separate the liquid (hereafter referred to as aqueous phase) from the solid fraction. Bio-oil (or oil phase) was extracted from the solid fraction using acetone, which was later evaporated and recovered using a rotavapor. Gas generated during reaction was also recovered. The following analyses were performed for each phase:

a) Aqueous phase

HPLC analysis was carried out to determine aqueous phase composition, both qualitative and quantitatively, by comparing samples chromatograms with chromatograms of standards for typical bio-oil compounds. Carbon content was determined through Total Organic Carbon (TOC) analysis.

b) Oil phase

Elemental analysis of bio-oil determined its carbon percentage. Besides, a gas-chromatography analysis, with a mass spectrometry detector (GC-MS) was carried out to identify some of the compounds present in the samples.

c) Solid phase

Elemental analysis was also performed to the solid phase to find out carbon content. FTIR (Fourier Transform Infrared) analysis allowed a qualitative identification of molecule bonds.

d) Gas phase

Gas chromatography was performed for both qualitative and quantitative analysis. The analysis with thermal conductivity detector (GC-TCD) identified and quantified main compounds in the sample (CO, CO_2, O_2, N_2, among others), and gas-chromatography with a mass spectrometry (GC-MS) identified other minority compounds of interest.

To evaluate the results, severity factor (t_s) was calculated for each experiment using equation (1). This parameter combines the effect of time and temperature, including heating, isothermal and cooling processing, and provides a useful tool to compare results for hydrothermal processing carried out at different temperatures and times [6, 7].

$$t_s = \sum_{i=1}^{n} t_i \: x \: e^{\left(\frac{T_i - T_b}{\omega}\right)}$$

Eq. 1. Severity Factor equation

Where n is the number of measurements, t_i the reaction time (minutes), T_i the reaction temperature (ºC), T_b the reference temperature (250ºC), and ω a parameter calculated with the activation energy of the reactions in place, which in most studies is based on the activation energy of hemicellulose hydrolysis (111 kJ/mol).

As shown in Figure 1, carbon content (%C) in the aqueous phase was hardly affected by reaction conditions, and only the harshest conditions made it decreased significantly. However, carbon yield in oil and solid phase was affected by reaction conditions, revealing opposite tendencies: at low severity factor, carbon percentage in oil phase was the lowest, increasing gradually when severity factor also increased, showing a maximum at severity factor around 40 - 100 minutes, and then decreasing at higher severities. For the solid phase, this behaviour was reversed, and the lowest carbon content was found at mild severities, around 40-100 minutes, whereas the lowest and highest severities showed the maximum carbon yield.
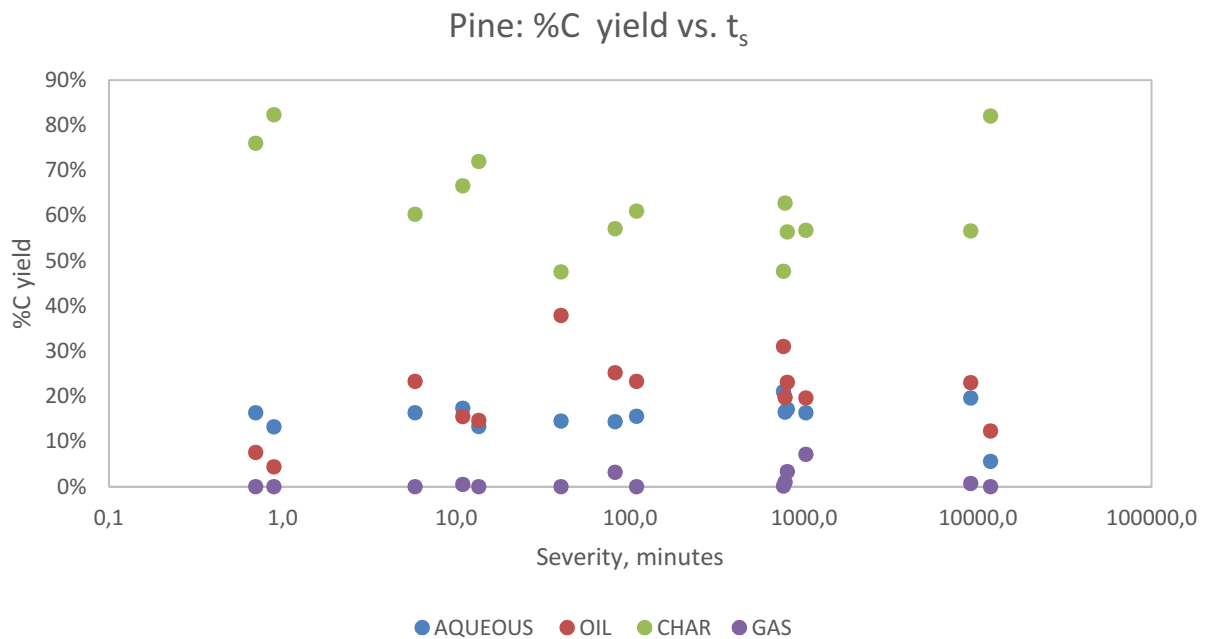

Fig. 1. Carbon yield (%) vs. severity factor for batch experiments with pine

Summary

Hydrothermal liquefaction of lignocellulosic biomass in a batch reactor for bio-oil as a sustainable aviation fuel precursor production has been optimised. Best results, in terms of amount of bio-oil and carbon percentage were obtained at mild reaction conditions.

Acknowledgment

References

|1] Ritchie H., Rosado P. & Roser M. (2020) - "Emissions by sector: where do greenhouse gases come from?" Published online at OurWorldInData.org. Retrieved from: https://ourworldindata.org/emissions-by-sector Accesed 08 March 2024

[2] ATAG. Facts and figures. Available at: https://atag.org/facts-figures/ Accesed 08 March 2024

[3] Martinez-Valencia, L., Garcia-Perez, M., & Wolcott, M. P. (2021). Supply chain configuration of sustainable aviation fuel: Review, challenges, and pathways for including environmental and social benefits. In Renewable and Sustainable Energy Reviews (Vol. 152).

[4] Gundupalli, M. P., Gundupalli, S. P. & Somavarapu Thomas, (2022). Hydrothermal liquefaction of lignocellulosic biomass for production of biooil and by-products: Current state of the art and challenges. Biofuels and Bioenergy: Opportunities and Challenges (pp. 61–84).

[5] Stone, M. L., Webber, M. S. & Mounfield, W. P., (2022). Continuous hydrodeoxygenation of lignin to jet-range aromatic hydrocarbons. Joule, 6(10), 2324–2337.

[6] Cantero-Tubilla, B., Cantero, D. A., Martinez, C. M., Tester, J. W., Walker, L. P., & Posmanik, R. (2018). Characterization of the solid products from hydrothermal liquefaction of waste feedstocks from food and agricultural industries. Journal of Supercritical Fluids, 133, 665–673.

[7] Posmanik, R., Cantero, D. A., Malkani, A., Sills, D. L., & Tester, J. W. (2017). Biomass conversion to bio-oil using sub-critical water: Study of model compounds for food processing waste. Journal of Supercritical Fluids, 119, 26–35.

Extraction of Oil from Waste Tomato Seeds and Waxes from Waste Tomato Peel Using Supercritical Carbon Dioxide

Bojana Mihajlović

Faculty of Technology and Metallurgy, University of Belgrade;

Bioeconomy Research Institute, PressTech Group, Department of Chemical Engineering and Environmental Technology, University of Valladolid;

20233018@estudent.tmf.bg.ac.rs

Introduction

While searching for replacements for fossil fuel-based energy sources with renewable ones, the focus in the research area expanded to further investigate the usage of different waste materials, aiming to avoid their disposal by analyzing the potential recovery of useful compounds. Sustainable decisions and ecological practices are promoted within the industries by finding alternative applications of the products made from waste materials.

Especially interesting are the natural waste materials such as different plant residues. One of the examples is the tomato pomace which is a by-product of the ketchup and tomato juice industry, with the data showing that dried pomace consists of 44% seeds and 56% pulp and skins [1]. These residues come from both preparation and production processes in the tomato industry. To separate the peel and seeds, the pomace has to be first soaked in water in which the peels stay at the surface of the mixture, while the seeds fall at the bottom of it. One of the biggest constituents of the tomato peel is cutin, a biopolyester with a complex 3D network, which makes up between 40% and 85% of the tomato's cuticle [2]. The other important constituents are fatty acids, polysaccharides, polypeptides, phenolic compounds, and several carotenoids. Tomato seeds are also rich in antioxidant, tocopherol, and carotenoid compounds, as well as fatty acids, which are placed in the tomato seed oil that makes up between 19.5% and 25.7% of the tomato seeds [3]. The content of peel and seeds is further analyzed in other research that has shown that the percentages of carbon, hydrogen, oxygen, and nitrogen in tomato peels are 56.8%, 8.1%, 28.8%, and 2.4%, respectively. The same data for the seeds shows that the percentages of these elements in the same order are 57.3%, 8.5%, 25.0%, and 4.9% [3]. Other elements such as chrome, copper, and nickel have a similar amount present in both seeds and peel, while sodium and potassium analyses show that these elements are more

present in peels than seeds [3]. The total amount of carotenoids found in tomato peels is 793.2 µg g^{-1}, out of which 734.0 µg g^{-1} represents lycopene, and the rest represents *α*-carotene, *β*-carotene and *cis-β*-Carotene. The total amount of carotenoids found in tomato seeds is 157.9 µg g^{-1}, out of which lycopene represents 130 µg g^{-1} and the rest represents carotenes [4]. The amount of lycopene in the tomato seed oil, depending on the solvent used, is between 17 µg g^{-1} and 26 µg g^{-1}, while the *β*-carotene found in it is ca. 4 µg g^{-1} regardless of the solvent [5]. Tomato seed oil analyses have shown that the content of the oil is made up of 57% linoleic acid, 21% oleic acid and 14% palmitic acid [3]. Because of the potential use of tomato seed oil as a vegetable oil, as well as the possibility to remove the cuticular waxes from tomato peel as a form of a pretreatment, the idea of this investigation is to extract these compounds and find the optimal conditions of temperature and solvent flow rate in which the maximum yield is achieved.

The standard solvents used for the extraction are organic solvents such as ethanol and hexane. But with the development of the high-pressure fluid technology, it is found that carbon-dioxide in the supercritical state (further used scCO$_2$) could be used as a replacement for organic solvents for extracting polar compounds as its dissolution power increases when compressed above the critical point [6]. The scCO$_2$ is available at a relatively low cost and high purity, and it is a non-toxic, non-inflammable, and non-explosive compound that doesn't require high operating temperatures as its critical point is at 31.1°C and 73.76 bar [6]. One research compares the extracted tomato seed oil yields in the case of three different solvents: hot ethanol, hot hexane and scCO$_2$. Even though the highest yield was achieved with ethanol (23.1%), then hexane (20.0%) and then scCO$_2$ (17.3%), the yield achieved with scCO$_2$ is still high enough to be significant and scCO$_2$ considered as a solvent for this extraction process [5].

Experimental

Two types of experiments were conducted in the extraction pilot plant using scCO$_2$ – extraction of oils placed in the tomato seeds and of waxes placed in the tomato peel. The extraction from tomato seeds was done in four different sets of conditions, while the extraction from tomato peels was done in two different sets, that in both cases varied in the values of scCO$_2$ flow rate and temperature set in the extractor. Reaction curves of the extraction and yields will be shown in the presentation, as well as the interpretation of the results of further analyses of the product, and the feed material before and after the process.

Summary

Waste tomato peels and seeds, which are by-products in the food industry, have not yet found widespread application, although they have significant potential as a source of natural oils and waxes. The development of high-pressure fluid technology enables the use of $scCO_2$ as an efficient and environmentally friendly extraction solvent compared to the standard extraction methods that use organic solvents. In order to promote sustainable development and resource optimization, this study will investigate the possibilities of applying $scCO_2$ for the extraction of waxes and oils from tomato waste under various conditions, and further analyze the obtained products which will provide insight into the efficiency of the method.

Acknowledgment

References

1. Sogi, D. S., & Bawa, A. S. (1998). Studies on dehydration of tomato processing waste. Indian Food Packer, 52(2), 26–29.

2. Cifarelli, A., Cigognini, I. M., Bolzoni, L., & Montanari, A. (2019). Physical-Chemical Characteristics of Cutin Separated from Tomato Waste for the Preparation of Bio-lacquers, Advances in Science and Engineering, 11(1), 33-45.

3. Rossini, G., Toscano, G., Duca, D., Corinaldesi, F., Pedretti, E. F., & Riva, G. (2013). Analysis of the characteristics of the tomato manufacturing residues finalized to the energy recovery, Biomass and Bioenergy, 51, 177-182.

4. Knoblich, M., Anderson, B., & Latshaw, D. (2005). Analyses of tomato peel and seed byproducts and their use as a source of carotenoids, Journal of the Science of Food and Agriculture, 85(7), 1166-1170.

5. Eller, F.J., Moser, J.K., Kenar, J.A., & Taylor, S. L. (2010). Extraction and Analysis of Tomato Seed Oil, Journal of the American Oil Chemists' Society, 87, 755-762.

6. Machado, B. A. S., Pereira, C. G., Nunes, S. B., Padilha, F. F., & Umsza-Guez, M. A. (2013). Supercritical Fluid Extraction Using CO_2: Main Applications and Future Perspectives, Separation Science and Technology, 48(18), 2741–2760.

Valorisation of Beef Bones to Value-Added Natural Products by Using Green Solvents - Process Optimization

Nikol Krusberská[1,2], Ivana Troppová[1], Lenka Matějová[1]

[1]Institute of Environmental Technology, CEET, VŠB – Technical University of Ostrava, 17. listopadu 15/2172, 708 00 Ostrava, Czech Republic

[2]Faculty of Materials Science and Technology, VŠB – Technical University of Ostrava, 17. listopadu 15/2172, 708 00 Ostrava, Czech Republic

Introduction

Biogenic waste (namely secondary animal products - bones, cartilage, skins, plumage, talons etc.) and mixed animal biomass waste e.g. from supermarkets represent a group of large-volume biomass waste which is commonly sell to rendering plants to be treated in spite of the fact that it may be further yielded to value-added natural products such as collagen, aminoacids, cholesterol, fatty acids and hydroxyapatite by using modern green technologies. Supercritical CO_2 extraction (without or with pressurized hot fluids as a co-solvent) or subcritical water extraction belong among these technologies [1, 2]. The yielded natural substances can be used for animal nutrition in agriculture sector or production of animal food and cosmetics. Moreover, developed green technologies may offer the alternative way how to treat/sterilize and dilapidate the bonegrafts e.g. before being implanted in orthopaedic surgery practice [3].

Experimental and aim of the work

The aim of this work is to study the effect of process conditions of supercritical CO_2 extraction and subcritical water extraction on the quality and quantity of yielded natural substances. The effect of pressure, temperature, the addition of co-solvent (water) to $scCO_2$ and extraction by pressurized hot ethanol was investigated on aminoacids yields distribution and the quality of solid bone residue (bonegrafts) by using high-pressure liquid chromathography with mass-spectroscopic detection (HPLC-TQ), thermogravimetric analysis (TGA), organic elementary analysis (OEA) and nitrogen physisorption at 77K. Fresh beef bones (ribs) were taken from Tešínské jatky, s.r.o. (Slezské uzeniny, Česká Republika). They were cryogenically cut to smaller pieces ~5mm. After that 30 g of bone substrate was extracted using 1.) subtrical water at 50-225°C and 10-30 MPa, 2.) supercritical CO_2 at 60°C at 10-70 MPa and 3.) supercritical CO_2 with added 30 and

60 wt.% of H_2O as a co-solvent at 60°C or 150°C at 10 MPa. The set-up used for extraction are shown in Figure 1.

TGA analysis of extracted bones performed on thermogravimetric analyser TGA 701 (LECO, USA) according to the ASTM D7582 standard was done for proximate analysis including determination of moisture, volatile matter, fixed carbon and ash in wt.%. OEA of extracted bonegrafts was realized using CHNS 628 (LECO, USA) according to standard ASTM D3172-13 and D5373-16 in order to do ultimate analysis including determination of elementary C, H, N in wt.%. Nitrogen physisorption at 77 K on extracted bones was measured to characterize textural properties of residual bones such as the specific surface area and pore-size distribution. HPLC-TQ was measured on Shimadzu (Nexera X2) to determine extracted aminoacids.
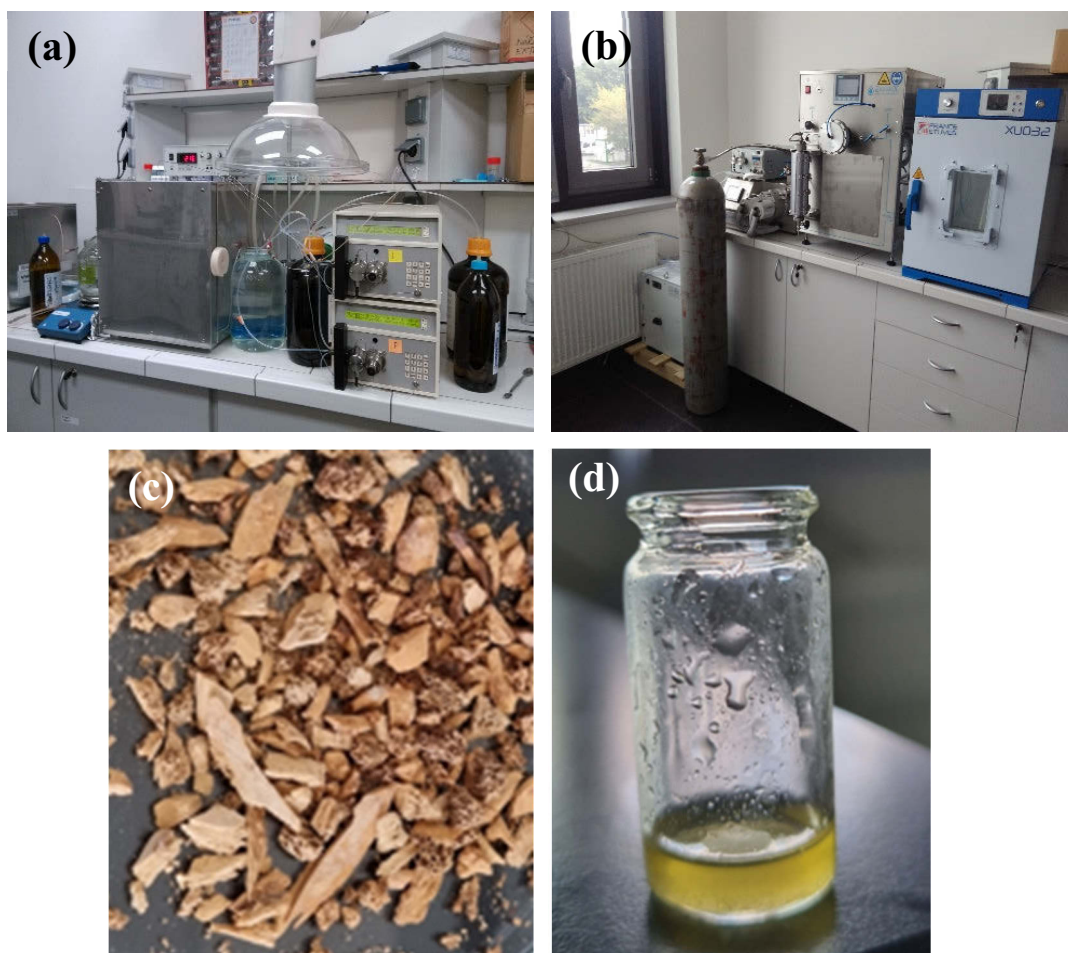

Fig. 1.: Set-up for (a) subcritical water extraction, (b) supercritical CO_2 extraction (without or with a co-solvent), (c) bonegrafts after extraction and (d) fatty acids-based product from extraction.

Since temperature and pressure affect significantly the dielectric constant of solvent characterizing its polarity/nonpolarity and dissolving power, thus, affect the solubility of

valuable natural substances in H_2O, CO_2 and CO_2 enriched with another solvents (H_2O, ethanol etc.), their effects were investigated in yielding of aminoacids and the quality of residual bonegrafts. While using subcritical water extraction the highest yields of alanine, isoleucine and gylcine were achieved, using supercritical CO_2 extraction tyrosin, threonine and phenylalanine were the most frequent yielded aminoacids. Increased temperature of subcritical water extraction (50-225°C at 10 MPa) increased yields of aminoacids and this corresponded to the decreased volatiles amount and increased ash amount in residual bonegrafts. Addition of H_2O as a co-solvent to supercritical CO_2 increased the yields of all aminoacids (in µg/g) by one order, in general. The effect of extraction temperature (60°C vs. 150°C at 10 MPa) on aminoacids yields and quality of bonegrafts was proved.

Summary

Subcritical water extraction and supercritical CO_2 extraction (without and with co-solvent) with CO_2 recycling represent the environmentally-friendly and sustainable ways how to yield valuable natural products from animal waste biomass and treat the bonegrafts.

Acknowledgement

References

[1] Baiano, A. Molecules 2014, 19, 14821-14842.

[2] Silva, J.C., Barros, A.A., Aroso, I.M., Fassini, D., Silva, T.H., Reis, R.L., Duarte, A.R.C. Ind. Eng. Chem. Res. 2016, 55, 6922−6930.

[3] Fages, J., Jean, E., Frayssinet, P., Mathon, D., Poirier, B., Autefage, A., Larzul, D. J. Supercrit. Fluids, 1998, 13, 351–356.

Numerical Modelling of Thermoplastic Foaming by Supercritical CO_2 Assisted Extrusion: Exploring the Process-Microstructure Relationship

M. Altinisik [a, 1], **M. Sauceau** [b, 2], **R. D'Elia** [a, 3], **R. Sescousse** [b, 4],
F. Baillon[b,5] **G. Michon**[a, 6]

[a]*Institut Clément Ader (ICA), UMR-CNRS 5312,"INSA, UPS, Mines Albi, ISAE" 31077, Toulouse, France*

[b] *Centre RAPSODEE IMT Mines Albi, CNRS, Université de Toulouse, 81013, Albi, France*

[1]mustafa.altinisik@isae-supaero.fr; [2]martial.sauceau@mines-albi.fr;
[3]raffaele.delia@mines-albi.fr; [4]romain.sescousse@mines-albi.fr;
[5]fabien.Baillon@mines-albi.fr [6]guilhem.michon@isae-supaero.fr

Introduction

Sandwich structures are largely used in lightweight applications thanks to their enhanced strength-to weigh-ratio. Nomex® and aluminium honeycombs are widely used as core materials due to their mechanical properties, ease of processing along with fire, smoke and toxicity compliancy with standard transportation regulations. However, their lack in sound insulation, damping capabilities and recyclability for Nomex® honeycombs, represent a major concern. A promising and emerging solution consists in the use of multifunctional thermoplastic foams developed by supercritical CO_2 assisted extrusion foaming technology. This green, non-inflammable solvent/solute can be used as physical blowing agent during an extrusion process, allowing a fine control of foaming process and thus of the final foam microstructure. Several functional properties can be associated to the material: enhanced sounds insulation can be obtained for fine open cells, while closed fine cells provide an enhanced thermal insulation capability [1], the nature of the functionality of the foam clearly residing in the structures of the porosity. Starting from this assumption, it is important to establish a clear processing-microstructure relation, in order to tune the foam for a desired functional property. To follow this, we have decided to develop a numerical model of the CO_2-assisted extrusion foaming process. Experimental analyses are associated with numerical modelling as shown in Figure 1. The experimental approach, based on Chauvet and Dimos previous works [2,3], consists in three different phases, spanning from the foam manufacturing by CO_2-assisted extrusion foaming, foam

assembly and final vibro-acoustic characterization using a Kundt tube. These experimental phases will then be simulated using existing literature models. A first step, describing bubble nucleation, growth and coalescence will be implemented in Matlab® using a microscopic approach based on Shafi and Taki models [4,5]. A macroscopic approach will then be implemented in a finite element software, in order to simulate foam assembly and vibro-acoustic response. The objective of this work, in partnership between Institute Clément Ader (ICA) and RAPSODEE laboratories, is therefore to understand and predict by different digital tools the microstructure of a thermoplastic polymer foam extruded and assisted by supercritical CO_2 and establish the link between the foaming/assembly process and vibro-acoustic properties
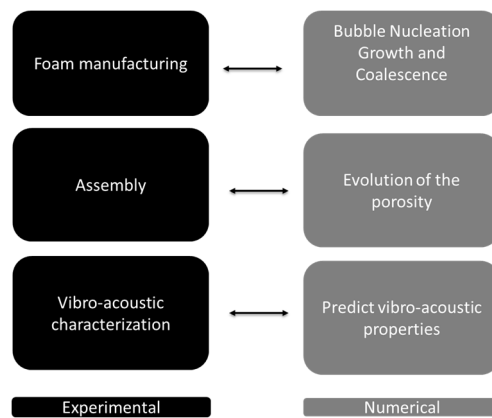
Figure 1: Representation of the main step of the current work

Experimental

Polylactic acid (PLA) foams studied in this work have been fabricated by supercritical CO_2 assisted extrusion process. which offers a route to control porosity parameters such as pore morphology and density. This process consists of 4 majors steps: polymer melting, injection of supercritical CO_2, mixing to have one phase system and finally foaming by pressure drop. As shown in Figure 2, the extrusion process is a continuous process in contrast with batch processes.
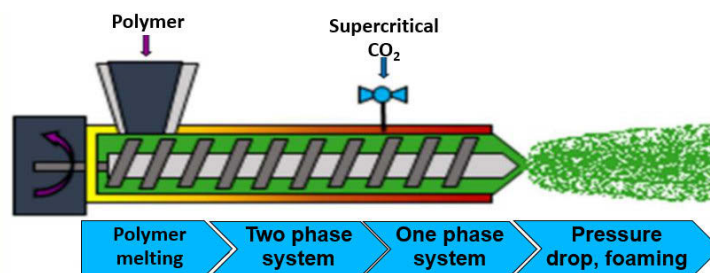
Figure 2: Schema of extrusion process [6]

First experimental results have shown, in Table 1, that processing temperature and CO_2 mass fraction strongly influence density, inner cell's structure and material crystallinity. By dropping the extrusion temperature (90°C), a crystalline foam (crystallinity rate Xc = 24 %) with reduced cells size and diameter is obtained, while at higher extrusion temperature (110°C), as shown in Figure 3, results indicate a more expanded and amorphous foam (Xc = 7 %) with higher cell diameter.

Table 1: Foam characteristics according to extrusion temperature

Die Temperature (°C)	Density (kg/m^3)	Pore diameter (µm)	Cristallinity (%)
110	37	500	7
100	29	290	12
90	23	140	24
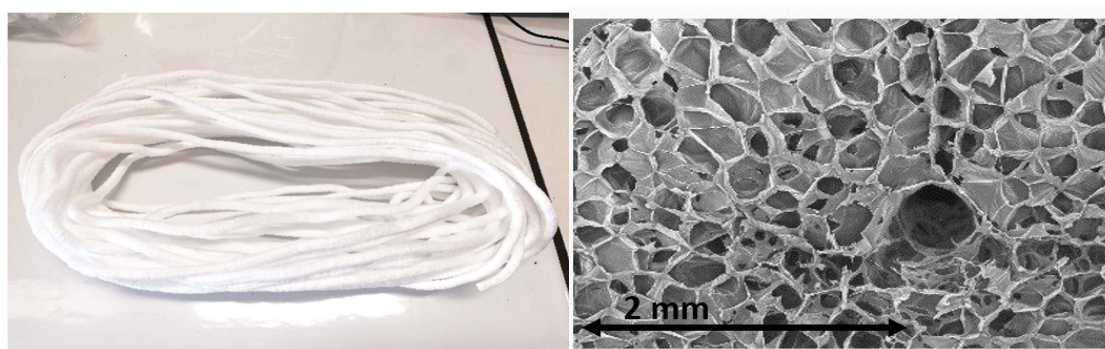
Figure 3 : Foam structure after extrusion process

Modelling Approach

First simulations based on the Shafi and Taki [4,5] models are currently under development and will be used to correlate the processing-microstructure relationship during the continuous extrusion process. The modelling approach employed in this work is based on the influence volume approach (Figure 4), developed by Shafi and coworkers mainly for batch foaming approaches [4]. Bubbles are modelled as non-overlapping cells, with a volume saturated in gas and which cannot be affected to more than a single bubble. This model is described by Equations 1, 2 and 3, while nucleation rate equation is

derivated by Gibbs, Blander and Katz works (Equation 4). Coupling these equations, it is possible to describe the nucleation and growth during the foaming process.
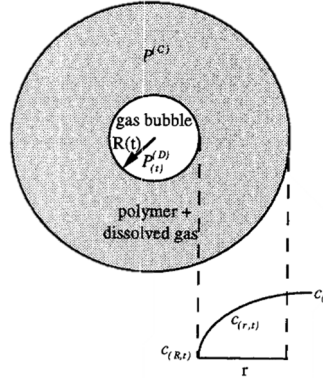
Figure 4: Influence of volume approach

$$\frac{dR}{dt} = \frac{(P_{cell} - P_{polymer})R}{4\eta} - \frac{\gamma}{2\eta}$$

Equation 1: Force balance around the bubble

$$\frac{\partial c}{\partial t} + \frac{\dot{R}R^2}{r^2}\frac{\partial c}{\partial r} = \frac{D}{r^2}\frac{\partial}{\partial r}\left(r^2\frac{\partial c}{\partial r}\right)$$

Equation 2: Gas diffusion in polymer

$$\frac{d}{dt}\left(\frac{4\pi}{3}\frac{P_{cell}R^3}{\Re T}\right) = 4\pi R^2 D \left.\frac{\partial c}{\partial r}\right|_{r=R}$$

Equation 3: Flux of gas into a bubble

$$J_{homogeneous} = N\sqrt{\frac{2\gamma}{\pi m}}\exp(-\frac{16\pi\gamma^3}{3k_bT(P_{bubble}-P_{polymer})^2})$$

Equation 4: Equation needed for nucleation rate

As explained above, depending on the porosity microstructure, foam functional properties can be tuned: in the case of sound insulation, open porosities are required, in order to dissipate the acoustic energy in the intricated open microstructure of the foam, by viscous and thermal dissipative effects. Starting from this assumption, the goal of this work is to extend this approach, successfully implemented by Chauvet [ref] in the case of continuous extrusion processes, in order to integrate bubbles coalescence, thus evaluating the appearance of open porosities during the process. The coalescence and visualisation models employed are derivated from Taki's work [5], where coalescence is regulated by biaxial elongation at bubbles interfaces. The limiting factor to this phenomenon is the polymer viscosity, as shown in Figure 5 and Equation 5.

$$\tau = \frac{6\eta\alpha}{|P_{D1} - P_{D2}|}$$

Equation 5: Convenient time scale of coalescence
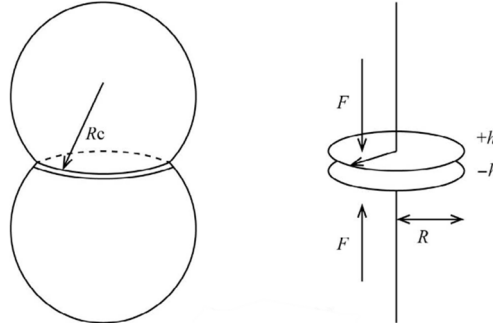
Figure 5: Biaxial elongation model

The last step of this approach is the visualization of the final microstructure in order to compare its distribution with experimental results using tools such as optical microscopy, scan electron microscopy (SEM) and micro-tomography. The numerical results export and analysis, such as bubbles position, radius and coalescence will be performed using Paraview® software. An example of the preliminary results is shown in Figure 6.
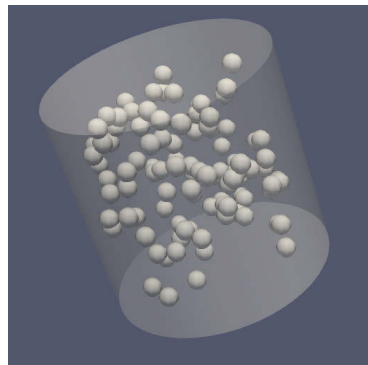
Figure 6: Porosity visualization (without coalescense)

References

[1]G.WU, P.XIE, H.YANG, K.DANG, *J. Mat Sci*. Vol. 56 **2021** 1-26, DOI: 10.1007/s10853-021-06034-6

[2]M.CHAUVET, PhD, IMT Mines Albi, **2017**

[3]E.DIMOS, R. D'ELIA, M.SAUCEAU, R.SESCOUSSE, L.CORTES, L.SANCHES, G.MICHON, *ECCM20* **2022**, 1472-1479, DOI: 10.5075/epfl-298799_978-2-9701614-0-0

[4]M.A. SHAFI, J.G.LEE, R.W.FLUMERFELT, *J. Polym. Eng. Sci.,* 36.**1996**, *1950-1959*, DOI: https://doi.org/10.1002/pen.10591

[5]K.TAKI,H.HAYASHIZAKI,K.FUKADA,*J. ISIJ Int.,* 54 **2014**, 2493–2502, DOI : https://doi.org/10.2355/isijinternational.54.2493

[6] VILLAMIL, J.A.; LE MOIGNE, N.; BÉNÉZET, J.-C.; SAUCEAU, M.; SESCOUSSE, R.; FAGES, *J. Mol* **2020**, *25*, 3408. DOI: https://doi.org/10.3390/molecules25153408

Characterization of Mass Transport of Pure Gases and Mixtures in Bio-Based Polymeric Membranes for Carbon Capture Applications

Zahra Maghazeh

Department of Civil, Chemical, Environmental and Materials Engineering,

Alma Mater Studiorum - University of Bologna, Via Terracini, 28, Bologna, Italy

zahra.maghazeh2@unibo.it

Introduction

Among different carbon capture technologies, membrane separation has gained a lot of attention due to lower energy consumption with respect to solvent-based methods. Despite the high potential of polymeric membranes and their versatile characteristics, they are subjected to permeability/selectivity trade-off which limits their performance.

The trade-off is depicted by an empirical correlation known as Robeson upper bound which allows comparing the performance of polymeric membranes based on this shortcoming [1]. To surpass the mentioned bound, different agents can be explored to maintain a facilitated transport through the membrane which result in an enhanced selectivity of CO_2 rather than transport via solution diffusion mechanism. These agents, which have high affinity for CO_2, act as carriers and speed up its transfer by binding with CO_2 reversibly and forming a complex while other gases (such as N_2) diffuse through the membrane which is a much slower process.

In general, the preferred membrane should have high thermo-mechanical properties, stability, durability along with high separation performance for an efficient performance [2]. Beside the choice of material, operating conditions such as feed pressure and temperature can have a significant impact on the potential of the developed membrane for separation [3].

Also, humidity can affect the microstructure of the membrane depending on its chemical structure of the polymeric material and it is possible to exploit humidity as a privilege for transport of CO_2 [4]. Therefore, it is required to explore this effect along with variations of operating conditions for a thorough characterization of a polymeric membrane during separations.

Another important consideration is the membrane's robustness and stability for a long-term, effective performance. Several phenomena such as plasticization, degradation and carrier saturation (in case of facilitated transport membranes) can reduce the efficiency of the membrane by reducing its permeability and selectivity. These phenomena can be

induced by exposure to CO_2, moderately high pressure, temperature and humidity. The stability and durability of the membrane depends on the resilience that each material show with respect to these parameters which can be challenging to sustain [5].

Lowering the thickness of the membrane can be an important factor in increasing its energy efficiency. However, fabrication of a defect-free thin film membrane which can maintain the same separation performance is difficult and challenging. Both fabrication method and processibility of the polymer play an important role in development of a thin-film membrane. Besides, using a suitable support layer with a good compatibility with the polymer is an important parameter to consider for a successful result. For reducing the thickness of the selective layer, choosing a suitable fabrication method and addition of CO_2-philic agents are necessary to improve the processibility of the membrane.

With proper knowledge about polymeric material, it is possible to exploit the unique properties of each material. Optimizing the separation performance can be achieved through adjusting different parameters such as addition of a compatible carrier, functionalization, crosslinking and even adjusting humidity after a comprehensive study and experimentation on the effect of each parameter on the separation.

In this case, the project will be mainly focused on selection and characterization of bio-based polymers for development of a "green" membrane for CO_2 separation. The focus on natural-based biopolymers is due to their biodegradability which fulfils global sustainability and goals of circular economy [6].

As an example, natural biopolymers like nanocellulose and chitosan are abundant, renewable, nontoxic and biodegradable. Although they have gas barrier properties in dry state, several studies have explored their gas permeability properties upon exposure to humidity which makes their microstructure moisture sensitive [7], [8]. Natural biopolymers with different functional groups have a great potential for different chemical modifications which makes them flexible to suite specific applications [6]. However, these materials must exhibit high durability and resistance to withstand a wide range of operating conditions and exposure to degrading agents. This requirement poses one of the primary challenges in developing polymeric membranes from green sources.

Experimental

Each membrane is thoroughly assessed in terms of its chemical structure, separation performance, and surface morphology to achieve comprehensive characterization. Additionally, different fabrication methods—including solvent-casting, layer-by-layer

technique, knife casting, and spin coating—will be evaluated and compared to develop defect-free membranes with varying thicknesses.

FTIR analysis can be used to determine the chemical structure both before and after gas permeation test to determine any possible modifications on the structure during the separation process. Also, the evaluation of surface morphology by AFM technique is another aspect which will be studied for characterization of the developed membranes.

Due to high importance moisture and its effects on biopolymers, it is crucial to study the effect of water on the membrane including its swelling and water sorption. This effect can be studied by various methods such as pressure decay apparatus and automated spring balance as well as a simple method like immersion in water and mass measurement.

The separation performance of the membranes can be evaluated through a single-gas or mixed-gas permeation test under certain operating conditions. The permeability is measured in a thermostatic manometric system which operates based on constant volume/variable pressure according to the following scheme. The magnetic stirrer on the upstream side of the cell helps with preventing concentration polarization by ensuring a homogeneous mixture during the test. The upstream and downstream pressures are monitored by manometers and recorded through LabView software during the test. Presence of two different manometers on the downstream side of the cell makes it possible to conduct the test both in low pressure (via PT02) or high pressures up to 500 psia (via PT03).
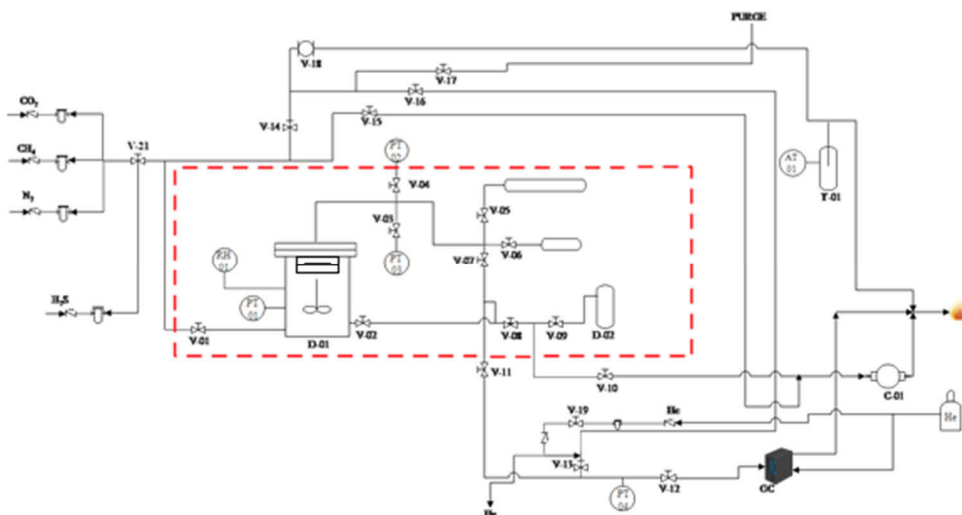
Figure 1-Scheme of Gas Permeation System

This apparatus allows measurements in both dry and humid conditions to evaluate the effect of water sorption and swelling on separation efficiency of the membrane which is of

high importance for bio-based polymers. The humid permeation tests are done in static mode by equilibrating the membrane with desired relative humidity for an adequate amount of time. This process in controlled via monitoring the pressure by downstream manometer. A scheme of a mixed and pure gas permeation system can be observed in Figure 1.

The results of the permeation tests are used to calculate the inherent property of each material for permeation of each gas. Selectivity of each material for CO_2 with respect to different gases can also be evaluated based on permeability of each gas for selected material.

Apart from single-gas permeation, this apparatus makes it possible to use a gas chromatography technique for conducting a mixed-gas permeation test and evaluate the efficiency of separation when the membrane is exposed to different gases at the same time.

Summary

Despite various studies on polymeric materials, the development of a green membrane based on biopolymers has yet to be fully optimized and requires more detailed investigation. Characteristics such as low environmental impact, biodegradability, abundance, non-toxicity, low cost, and versatile inherent functionalization make biopolymers a promising option for exploration. However, to address their limitations, it is essential to explore different techniques such as chemical modification, functionalization, and the implementation of compatible carriers to achieve durable, long-lasting, and efficient operation. Characterization of membranes will be conducted under various conditions to evaluate the effects of temperature, pressure, humidity, and modifications on this group of biopolymers, with a focus on providing a green solution for CO_2 capture applications.

Acknowledgment

adopted by the Italian Ministry of University and Research, CUP F53C22000560006, ECCSELLENT — Development of ECCSEL-R.I. Italian facilities: user access, services and long-term sustainability.

References

[1]   L. M. Robeson, "The upper bound revisited," *J Memb Sci*, vol. 320, no. 1–2, pp. 390–400, Jul. 2008, doi: 10.1016/J.MEMSCI.2008.04.030.

[2]   S. Nithin Mithra and S. S. Ahankari, "Nanocellulose-based membranes for CO2 separation from biogas through the facilitated transport mechanism: a review," *Materials Today Sustainability*, vol. 19, p. 100191, Nov. 2022, doi: 10.1016/J.MTSUST.2022.100191.

[3]   S. Li, Z. Wang, X. Yu, J. Wang, and S. Wang, "High-Performance Membranes with Multi-permselectivity for CO2 Separation," *Advanced Materials*, vol. 24, no. 24, pp. 3196–3200, Jun. 2012, doi: 10.1002/ADMA.201200638.

[4]   L. Ansaloni, J. Salas-Gay, S. Ligi, and M. G. Baschetti, "Nanocellulose-based membranes for CO2 capture," *J Memb Sci*, vol. 522, pp. 216–225, Jan. 2017, doi: 10.1016/J.MEMSCI.2016.09.024.

[5]   Z. Dai, L. Ansaloni, and L. Deng, "Recent advances in multi-layer composite polymeric membranes for CO2 separation: A review," *Green Energy & Environment*, vol. 1, no. 2, pp. 102–128, Jul. 2016, doi: 10.1016/J.GEE.2016.08.001.

[6]   F. Seidi *et al.*, "Biopolymer-based membranes from polysaccharides for CO2 separation: a review," *Environmental Chemistry Letters 2021 20:2*, vol. 20, no. 2, pp. 1083–1128, Jan. 2022, doi: 10.1007/S10311-021-01349-X.

[7]   M. Minelli *et al.*, "Investigation of mass transport properties of microfibrillated cellulose (MFC) films," *J Memb Sci*, vol. 358, no. 1–2, pp. 67–75, Aug. 2010, doi: 10.1016/J.MEMSCI.2010.04.030.

[8]   L. A. El-Azzami and E. A. Grulke, "Carbon dioxide separation from hydrogen and nitrogen by fixed facilitated transport in swollen chitosan membranes," *J Memb Sci*, vol. 323, no. 2, pp. 225–234, Oct. 2008, doi: 10.1016/J.MEMSCI.2008.05.019.

Influence of Hop (*Humulus lupulus*) and its Components (α-Acids and β- Acids) on Micellization

Tjaša Skarlovnik [a], Urban Bren [a, b, c], Gregor Hostnik [a]

[a] Faculty of Chemistry and Chemical Engineering, University of Maribor,

[b] Faculty of Mathematics, Natural Sciences and Information Technologies, University of Primorska,

[c] Institute for Environmental Protection and Sensors, Maribor, Slovenia

tjasa.skarlovnik@um.si

Introduction

Excessive use of antibiotics causes the bacteria in the microbe to become increasingly resistant, making such treatment less effective. This problem can be reduced by limiting the use of antibiotics in animals and humans and discovering new compounds that have antibacterial properties [1] . One of promising candidates are the components of hops (α- and β-acids), which also have antioxidant, anticancer, antiviral, antifungal and anti-inflammatory properties due to their composition [2-5]. Hops have been used in the past to treat diseases and symptoms [3, 6, 7]. However, the utilisation of its antibacterial properties is limited by poor bioavailability and therefore low biological efficacy [6, 8-10]. Bioavailability can be improved by micellization [8, 9, 11]. This is achieved by adding surface-active substances that form a micelle at a certain concentration, the so-called critical micelle concentration. The value of the critical micelle concentration varies from the type of surfactant, the temperature, the solvent, the addition of salt and other dissolved substances, the pH value and the ionic strength [12]. Therefore, research into the influence of Hop and its constituents on the micellization of surface-active substances is of crucial importance for developing or discovering new compounds that would be suitable for treating diseases.

Experimental

The value of the critical micelle concentration was determined using fluorescence. The measurements were carried out with a Jasco FP-8550 spectrofluorometer (Jasco, Japan) at a temperature of 25 °C and between wavelengths of 350 to 650 nm. The excitation wavelength of fluorescein was 491 nm and the initial concentration in the cuvette was

$2,5 \cdot 10^{-6}$ M. We selected the three most frequently analysed surfactants (dodecytrimethylammonium bromide - DTAB, tetradecytrimethylammonium bromide - TTAB and hexadecyltrimethylammonium bromide - HTAB) so that the measured values could be compared with literature values. The initial concentration of cohumulone (CH) in the cuvette was 1 mM. In Figure 1 structures of cohumulone (left) and surfactants (right), (n values are 10, 12, and 14 for DTAB, TTAB, and HTAB, respectively) are depicted.
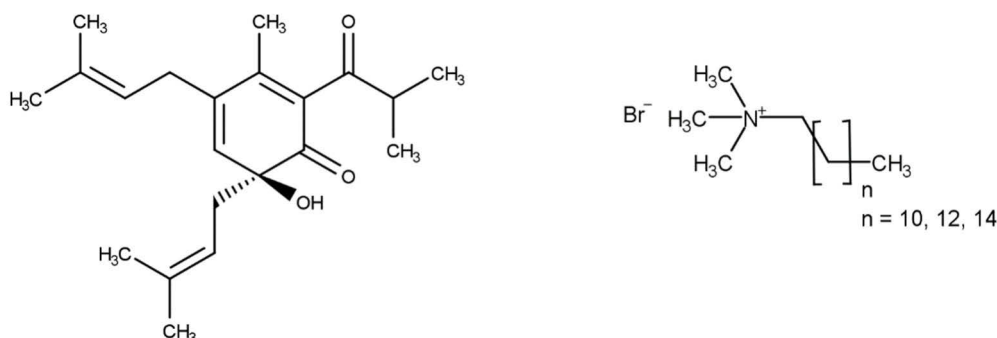
Fig. 1.: Structure of cohumulone (left) and surfactants (right).

Figure 2 shows the experimental measurements for DTAB, TTAB and HTAB, and the fitting curve. If we compare plots a and d, b and e and c and f, we can see that the shape of the sigmoid curve changes and its inflection point, which represents the value of the critical micelle concentration, also shifts, when cohumulone is added to surfactants.
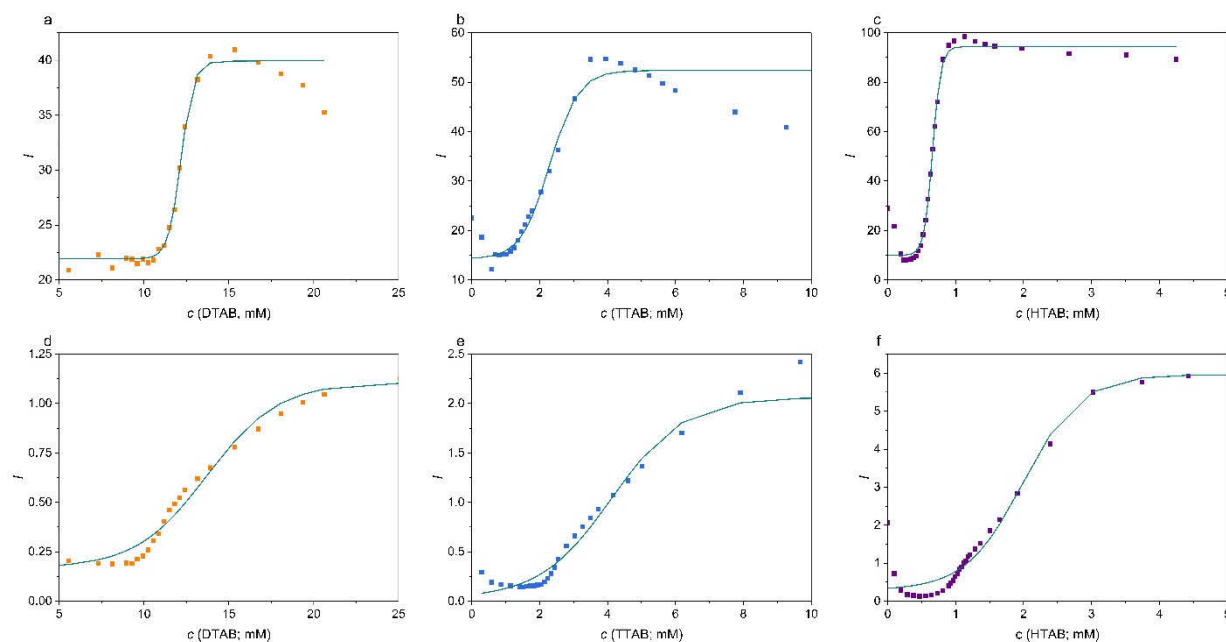
Fig. 2.: Plots of fluorescein in a DTAB, b TTAB and c HTAB solution and with added cohumulone in d DTAB, e TTAB and f HTAB and the fitted curves.

When cohumulone is added to the surfactant, 2 inflection points can be observed on the curve, one in the premicellar region and the other in the micellar region, where the critical micellar concentration is determined. In Table 1 we can see that the value of the critical micelle concentration increases slightly after the addition of cohumulone. The addition of cohumulone also increases the value of Δx, which represents the width of the inflection point (transition) of the curve.

Tab. 1.: Values of critical micelle concentration and Δx without and with cohumulone.

	DTAB		TTAB		HTAB	
	without CH	with CH	without CH	with CH	without CH	with CH
CMC (mM)	12,2	13,7	2,3	4,1	0,7	2,0
Δx	$3,74 \cdot 10^{-4}$	$2,10 \cdot 10^{-3}$	$4,39 \cdot 10^{-4}$	$1,06 \cdot 10^{-3}$	$6,24 \cdot 10^{-5}$	$4,21 \cdot 10^{-4}$

Summary

We investigated the influence of cohumulone on the micellization of the three most commonly used surfactants. We found that cohumulone changes the value of the critical micelle concentration (the peak of the sigmoid curve) and also changes the shape of the curve itself.

Acknowledgment

References

(1) Kolenc, Z.; Langerholc, T.; Hostnik, G.; Ocvirk, M.; Štumpf, S.; Pintarič, M.; Košir, I. J.; Čerenak, A.; Garmut, A.; Bren, U. Antimicrobial Properties of Different Hop (Humulus lupulus) Genotypes. *Plants* **2023**, *12* (1), 120.

(2) Chen, L.; Zhao, Q.; Jin, H.; Zhang, X.; Xu, Y.; Yu, A.; Zhang, H.; Ding, L. Determination of xanthohumol in beer based on cloud point extraction coupled with high performance liquid chromatography. *Talanta* **2010**, *81* (1-2), 692-697. DOI: 10.1016/j.talanta.2010.01.004 From NLM Medline.

(3) Sun, S.; Wang, X.; Yuan, A.; Liu, J.; Li, Z.; Xie, D.; Zhang, H.; Luo, W.; Xu, H.; Liu, J.; et al. Chemical constituents and bioactivities of hops (Humulus lupulus L.) and their effects on beer-related microorganisms. *Food and Energy Security* **2022**, *11* (2). DOI: 10.1002/fes3.367.

(4) Knez Hrnčič, M.; Španinger, E.; Košir, I. J.; Knez, Ž.; Bren, U. Hop Compounds: Extraction Techniques, Chemical Analyses, Antioxidative, Antimicrobial, and Anticarcinogenic Effects. *Nutrients* **2019**, *11* (2). DOI: 10.3390/nu11020257 From NLM.

(5) Bocquet, L.; Sahpaz, S.; Bonneau, N.; Beaufay, C.; Mahieux, S.; Samaillie, J.; Roumy, V.; Jacquin, J.; Bordage, S.; Hennebelle, T.; et al. Phenolic Compounds from Humulus lupulus as Natural Antimicrobial Products: New Weapons in the Fight against Methicillin Resistant Staphylococcus aureus, Leishmania mexicana and Trypanosoma brucei Strains. *Molecules* **2019**, *24* (6). DOI: 10.3390/molecules24061024 From NLM Medline.

(6) Karabin, M.; Hudcova, T.; Jelinek, L.; Dostalek, P. Biologically Active Compounds from Hops and Prospects for Their Use. *Compr Rev Food Sci Food Saf* **2016**, *15* (3), 542-567. DOI: 10.1111/1541-4337.12201 From NLM PubMed-not-MEDLINE.

(7) Zanoli, P.; Zavatti, M. Pharmacognostic and pharmacological profile of Humulus lupulus L. *J Ethnopharmacol* **2008**, *116* (3), 383-396. DOI: 10.1016/j.jep.2008.01.011 From NLM Medline.

(8) Mahli, A.; Seitz, T.; Freese, K.; Frank, J.; Weiskirchen, R.; Abdel-Tawab, M.; Behnam, D.; Hellerbrand, C. Therapeutic Application of Micellar Solubilized Xanthohumol in a Western-Type Diet-Induced Mouse Model of Obesity, Diabetes and Non-Alcoholic Fatty Liver Disease. *Cells* **2019**, *8* (4). DOI: 10.3390/cells8040359 From NLM Medline.

(9) Khayyal, M. T.; El-Hazek, R. M.; El-Sabbagh, W. A.; Frank, J.; Behnam, D.; Abdel-Tawab, M. Micellar solubilization enhances the anti-inflammatory effect of xanthohumol.

Phytomedicine **2020**, *71*, 153233. DOI: 10.1016/j.phymed.2020.153233 From NLM Medline.

(10) Harish, V.; Haque, E.; Śmiech, M.; Taniguchi, H.; Jamieson, S.; Tewari, D.; Bishayee, A. Xanthohumol for Human Malignancies: Chemistry, Pharmacokinetics and Molecular Targets. *International Journal of Molecular Sciences* **2021**, *22* (9), 4478.

(11) Savjani, K. T.; Gajjar, A. K.; Savjani, J. K. Drug solubility: importance and enhancement techniques. *ISRN Pharm* **2012**, *2012*, 195727. DOI: 10.5402/2012/195727 From NLM PubMed-not-MEDLINE.

(12) Salanci, E.; Malík, I.; Šandrik, R.; Pecher, D.; Andriamainty, F. Determination of the critical micelle concentration and thermodynamic parameters of phenylcarbamic acid derivatives using a fluorescence method. *Chemical Papers* **2021**, *75* (7), 3081-3090. DOI: 10.1007/s11696-021-01539-5.

Implementation of a Multi-Zone Autoclave in the High-Pressure Polymerization Process

Christoph Weigel, Markus Busch*

Ernst-Berl-Institute of Technical and Macromolecular Chemistry, Technical University of Darmstadt, 64287 Darmstadt/Germany, *e-mail: markus.busch@pre.tu-darmstadt.de

Introduction

Polyethylene (LDPE) is produced by radical polymerization at temperatures of up to 300 °C and pressures of up to 3000 bar. During the process, long- and short-chain branches are formed which are important for the properties of the material.[1, 2]

Autoclaves and tubular reactors are used for the industrial production of LDPE. The advantage of tubular reactors is their surface-to-volume ratio which allows a conversion of up to 35 %. The LDPE from these reactors is characterized by a comb-like structure due to the few long-chain branches and by a narrow molecular weight distribution. Compared to tubular reactors, industrial autoclave reactors exhibit back-mixing. This produces LDPE products with a broader molecular weight distribution and an increased number of long chain branches, resulting in a tree-like branched structure. The autoclave leads to a lower conversion of 20 % because of the reduced surface-to-volume ratio, which hinders the removal of polymerisation heat. Both structural features are important for extrusion coating applications.[3, 4]

Multi-zone autoclaves are used to combine the unique tree-like branched structure of autoclave-produced LDPE with the higher conversion of tubular reactors. This type of autoclave gives a similar conversion to tubular reactors due to multiple fresh ethylene feeds and a moderate temperature increase along the autoclave. The tree-like branched structure is obtained by back-mixing.[3, 4]

Experimental

All multi-zone autoclave experiments are carried out in a continuous high-pressure polymerization plant, which is located in a reinforced concrete room. The flow sheet of this plant is shown in Figure 1.
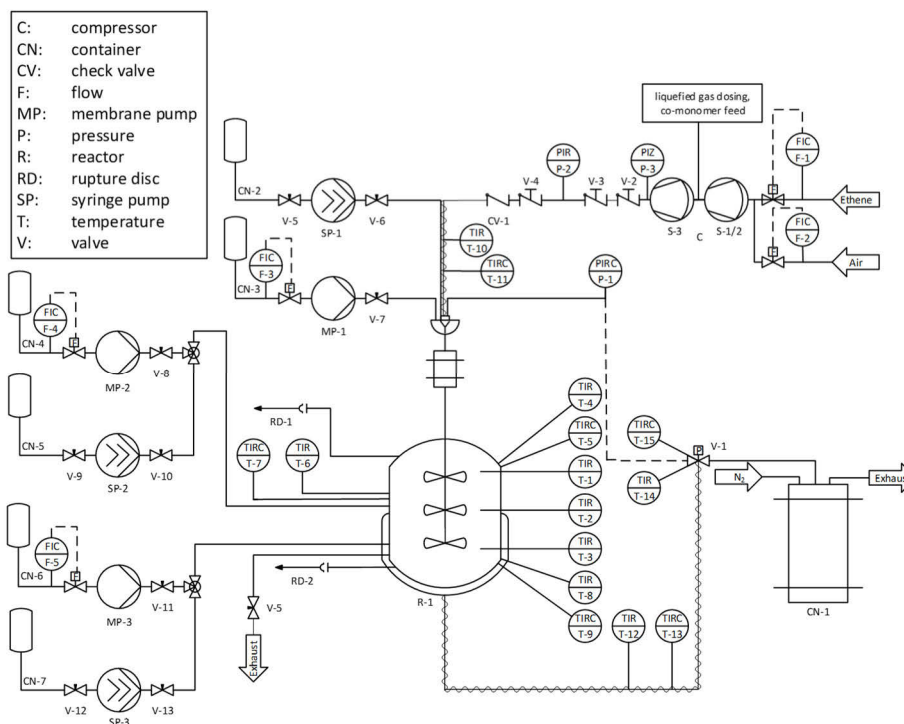
Fig. 1.: Schematic flow sheet of the continuous high-pressure multi-zone autoclave.

Ethene is compressed by a *Hofer* three stage membrane compressor and enters the multi-zone autoclave from the top. Between the second and the third stage, chain transfer agents (CTAs) can be supplied by a *Lewa* membrane pump. Other chemicals can be added between the same stages by a *Fink Chem+Tech* high-pressure dosing pump. In the reinforced concrete room initiators can be supplied by syringe pumps. Chemicals that need to be pumped at higher flow rates are added to the multi-zone autoclave by using an *Orlita* membrane pump. To add initiator from the side of the autoclave, a side feed is required. This feed requires one syringe pump for the initiator and one membrane pump for the carrier feed. The carrier feed is necessary to flush the initiator into the multi-zone autoclave due to the low flow rate. The polymer produced is transferred in a collecting vessel via a heated outlet line. The autoclave is heated by ceramic heating jackets. The pressure is controlled by a pneumatic outlet valve. This leads to periodic fluctuations in the temperature and the pressure throughout the experiment. Outside the reinforced concrete room, the process parameters are measured, recorded and controlled by a *Beckhoff* Automation unit using *LabVIEW*.

The multi-zone autoclave can be operated at a maximum pressure of 2500 bar and a maximum temperature of 300 °C. The volume of the autoclave is 300 mL and it is made of 1.7707 steel. The Computer Aided Design (CAD) of the multi-zone autoclave is shown in Figure 2.
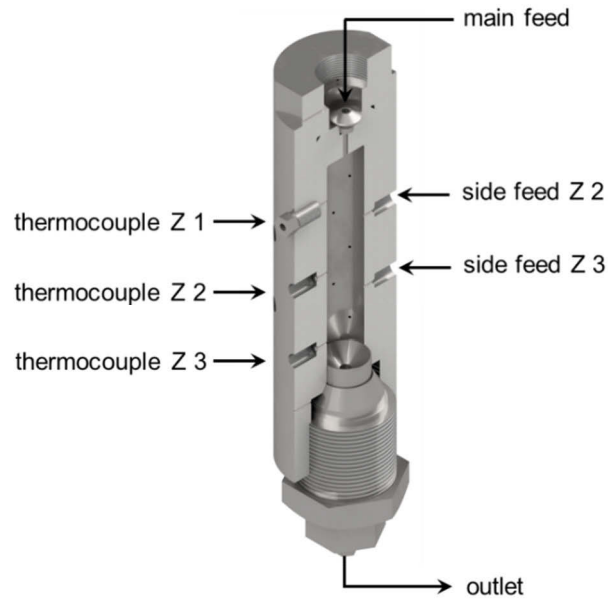
Fig. 2.: Cross section of the high-pressure multi-zone autoclave.

The multi-zone autoclave is divided into three reaction zones by the design of the agitator. The temperature of each zone can be measured by a thermocouple. For adding substances into the second and the third zone a side feed is required.

Figure 3 shows a typical temperature profile of an LDPE-experiment in the multi-zone autoclave.[5]
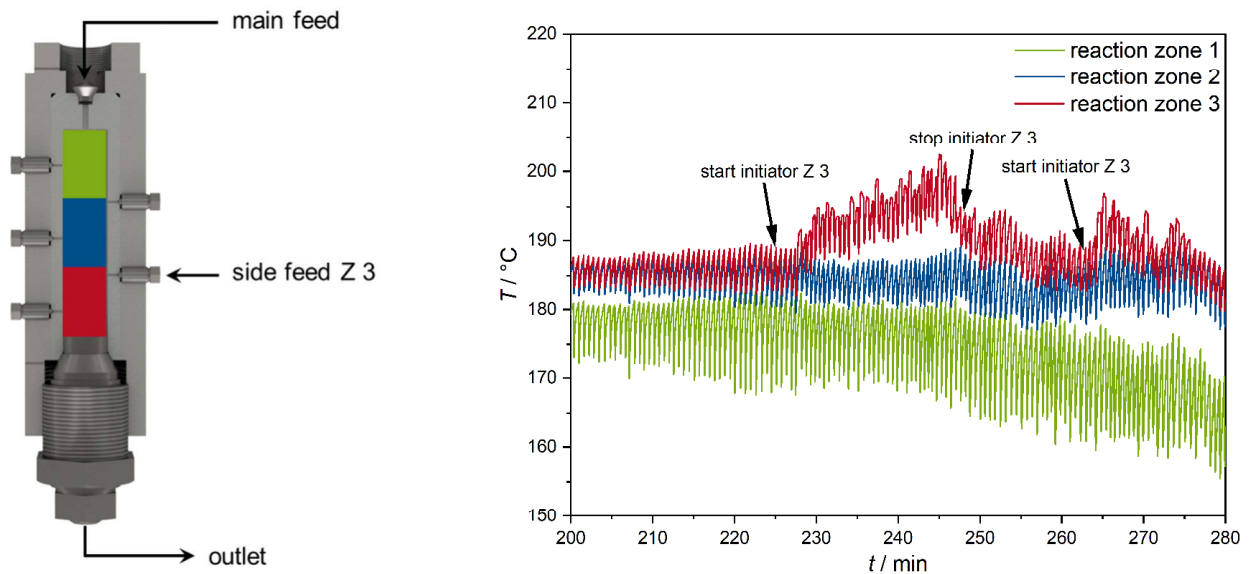
Fig. 3.: Temperature profile of an LDPE-experiment after the start of the initiator feed into the third zone of the multi-zone autoclave.

The multi-zone autoclave shown on the left is color coded to illustrate the zones. The first zone (green) is the coldest because there the cold ethylene feed enters the autoclave. In the diagram on the right the switch-on and switch-off behavior is illustrated. After initiator has been added to the third zone (red) the temperature of this zone increases. This can be explained by the fact that the initiator starts new exothermic reactions in the radical process. After the initiator supply was stopped, the temperature dropped. After 263 minutes, the initiator was added again and the temperature rose again. The advantage of this is that the temperature can be increased in a controlled manner, which means that the final product properties can be influenced.

Figure 4 also shows a temperature profile of an LDPE-experiment.
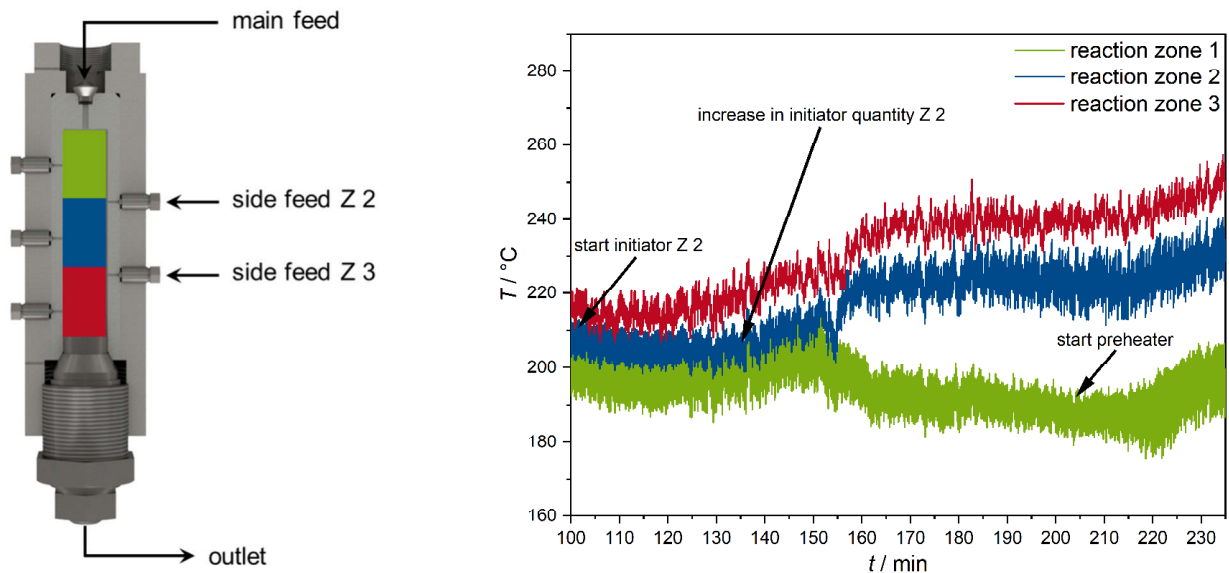
Fig. 4.: Temperature profile of an LDPE-experiment after the start of the initiator feed into the second zone of the multi-zone autoclave.

Until the 100th minute, initiator was only added to the third zone from the side and from above. Then initiator was also added to the second zone. After 152 minutes the starting behavior of the initiator in the second zone occurs. This can be seen by the slight drop in temperature. After the drop, the temperature of the second and the third zone increases. As a result, a temperature gradient of 52 °C is achieved in the multi-zone autoclave. This means that the second zone of the autoclave can also be addressed. It is also recognizable that the temperature difference between the first and second zone is bigger than the temperature difference between the second and third zone. The preheater can

be used to heat the main feed that enters the first zone of the multi-zone autoclave. This is also shown in the diagram in Figure 4.

Summary

The majority of mini-plants for high-pressure polymerization around the world focus on CSTRs, while industrial autoclaves are used as multi-zone autoclaves. To move closer to industrial scale, a 300 mL multi-zone autoclave was designed to operate at 2500 bar and 300 °C. Further scale-up strategies are investigated to obtain representative samples on a small low-cost scale. In this work, the targeted addressing of the individual zones of the multi-zone autoclave was shown. A switch-on and switch-off behavior of the autoclave was demonstrated by adding initiator to the third zone. Furthermore, a temperature gradient of 52 °C along the autoclave was achieved by adding initiator to the second zone. Here, the temperature difference between the first and second zone was the biggest. The main feed could also be heated by a preheater, which made the first zone warmer.

References

[1] M. D. Lechner, K. Gehrke, E. H. Nordmeier, Makromolekulare Chemie, 2014.

[2] N. Maraschin, Encyclopedia of Polymer Science and Technology: Ethylene Polymers, 2002.

[3] C. Kiparissides, J. F. MacGregor, G. Verros, J. Macromol. Sci. Rev. Macromol. Chem. Phys. 1993, 33, 437.

[4] K. S. Whiteley, in Ullmann's Encyclopedia of Industrial Chemistry: Polyethylene, 2000.

[5] N. Schreiner, C. Weigel, J. Kirsch, L Gockel, M. Busch, Commissioning and Scalability of a High-Pressure Multi-Zone Autoclave for Polymer Synthesis, unpublished proceedings of the ASME 2024.

Formulation of Rutin to Improve its Bioavailability

Sara Pahino Villardón

Chemical Engineering and Environmental Technology, University of Valladolid,

sara.pahino@uva.es

Introduction

Polyphenols are natural compounds found in plants, which is why they are present in many plant-based foods and beverages. They are known for their antioxidant, antimicrobial and anti-inflammatory properties, as well as their ability to reduce the risk of metabolic disorders, cardiovascular disease, type 2 diabetes and some types of cancer. Their antioxidant power makes them excellent candidates for protecting and preventing the body from oxidative stress. For this reason, and because of the direct relation between diet, good health and disease prevention, the presence of quality foods rich in polyphenols in the diet has generated a great deal of consumer interest (Nazzaro et al., 2022).

However, it has been established that, although polyphenolic compounds are present in many diets, the health benefits depend not only on the nature and quantity of the polyphenols ingested, but also on their bioavailability and bioaccessibility, which in the case of flavonoids is poor (Bié et al., 2023)

Bioavailability is defined as the fraction of a nutrient ingested from food that remains available for absorption in the intestine and metabolic processing and storage (Jackson, 1997, Cited in Hedrén et al., 2002). Structural differences between the various compounds affect their bioavailability (Bié et al., 2023)

The positive influence of polyphenols on wellbeing and health and the versatility of the properties represents a great opportunity for industries. In particular, the pharmaceutical and food industries, allowing them to formulate new technological processes or new functional products that can improve the properties of polyphenols such as their water solubility and thus their bioavailability. (Nazzaro et al., 2022)

In order to improve their solubility, different techniques have been developed such as micronisation and particle encapsulation (Wang et al., 2023). The formulation of natural substances with a biocompatible or biodegradable carrier material to form composites or encapsulates is of great importance in various industries. Various supercritical fluid precipitation methods can be successfully implemented to produce these materials, most notably the SAS process (Cocero et al., 2009).

The objective is therefore to develop a formulation of rutin by studying its precipitation and encapsulation in Eudragit® using the SAS technique, in order to enhance its dissolution rate and improve its bioavailability.

Rutin is a polyphenol that belongs to the flavonoid group and is found in the flavonols, being the glycosylated form of quercetin. Its molecular formula is $C_{27}H_{30}O_{16}$. As its nomenclature indicates, it is a rutinoside formed by quercetin (aglycone) to which a rutinose disaccharide (glucose and rhamnose) is attached at position 3 of the C ring (as a substituent to the C3 hydroxy group) (Moravkar et al., 2023; Remanan & Zhu, 2023 , Figure 1).

Rutin consists of the basic phenolic part attached to the sugar molecule (Patel & Patel, 2019). It usually appears together with quercetin as a consequence of rutin hydrolysis, which occurs due to the action of glucosidase, giving rise to quercetin with rutinose (Frutos et al., 2019).
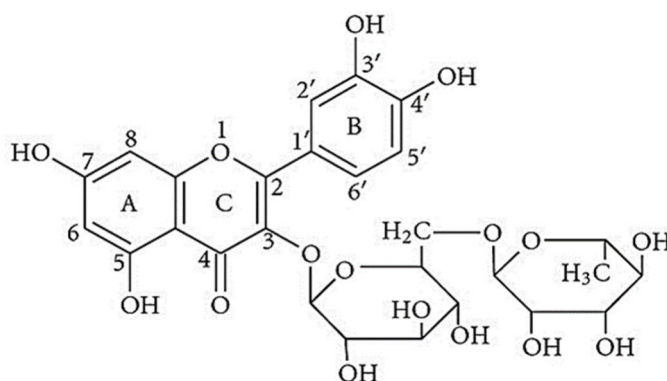
Figure 1: Chemical structure of rutin (Remanan & Zhu, 2023)

The main characteristic of rutin, and of most flavonoids, is its antioxidant activity, as it acts by scavenging free radicals. Its antioxidant power is associated with the hydroxyl groups present in its aromatic rings (Frutos et al., 2019)

Rutin can be found in various plants, especially in fruits and vegetables. Its main sources among these are grapes and buckwheat (Frutos et al., 2019; Remanan & Zhu, 2023)

Rutin has a low water solubility of 0.125 g/L (Frutos et al., 2019), which limits its incorporation in foods and food supplements. In addition, its stability under processing conditions and possible interactions with other components must be taken into account. Therefore, the application of rutin to the development of functional foods, which affects its bioavailability and absorption, is a problem (Frutos et al., 2019)

Regarding the general uses of rutin, its main applications are in the pharmaceutical industry, medicine, animal feed, cosmetics and the chemical industry (Patel & Patel, 2019). Rutin exhibits different pharmacological activities: cardiovascular activity,

anticancer activity, anti-inflammatory activity, antidiabetic activity or antioxidant activity (Semwal et al., 2021).

Therefore, rutin has excellent therapeutic potency, but despite these benefits, it has limitations such as poor water solubility, low bioavailability and poor absorption. Due to these drawbacks of rutin, different techniques such as encapsulation are investigated as a strategy that can overcome these limitations (Frutos et al., 2019; Remanan & Zhu, 2023)

To improve the bioavailability of these molecules, in addition to facilitating product dosage and reducing their storage volume requirements, the aim is to create particles of specific size and morphology. Apart from size reduction, amorphous compounds are more soluble than crystalline ones (Rodríguez-Rojo et al., 2022)

The SAS technique can be used for the preparation and formation of pharmaceutical granules, generating ultrafine particles and microcapsules (Wang et al., 2023)

Supercritical carbon dioxide (SC-CO$_2$) is commonly used as an antisolvent in SAS, as it has a relatively low critical point (31.26°C and 73.8 bar), is inexpensive and non-toxic (Wang et al., 2023)

The SAS technique takes advantage of the low solubility of solid organic molecules and bioactive compounds in supercritical carbon dioxide and the high or complete miscibility of most solvents in SC-CO$_2$. To obtain a good final product, the organic solvent must be completely miscible with CO$_2$ under the operating conditions. Typical pressure and temperature conditions are in the range of 80-150 bar and 35-50°C respectively (Fraile et al., 2014; Rodríguez-Rojo et al., 2022).

During the process, the solute is dissolved in an organic solvent to form a solution that is pressurised and mixed with CO$_2$. The anti-solvent fluid (SC-CO$_2$) supersaturates this solution, expanding it and inducing precipitation or co-precipitation/encapsulation of the solute in the form of dry micro- or nanoparticles (Machado et al., 2022; Rodríguez-Rojo et al., 2022)

The SAS process can also be used for co-precipitation or co-precipitation of an active compound with a support material (Fraile et al., 2014). When the precipitation process occurs with a single solute, micro- and nanoparticles with a large specific surface area are formed, thus increasing their bioavailability (Machado et al., 2022).

The precipitation of composite systems (or co-precipitation) gives rise to microcapsules that have the capacity to be used in the controlled delivery of bioactives (Machado et al., 2022)

Experimental

In the first part of this work, the precipitation of rutin and its encapsulation in Eudragit® was studied using the SAS (supercritical antisolvent) technique with supercritical CO2, to develop a formulation that improves the bioavailability of rutin and its solubility in solvents and polar substances such as water. A schematic of the SAS process is shown below:
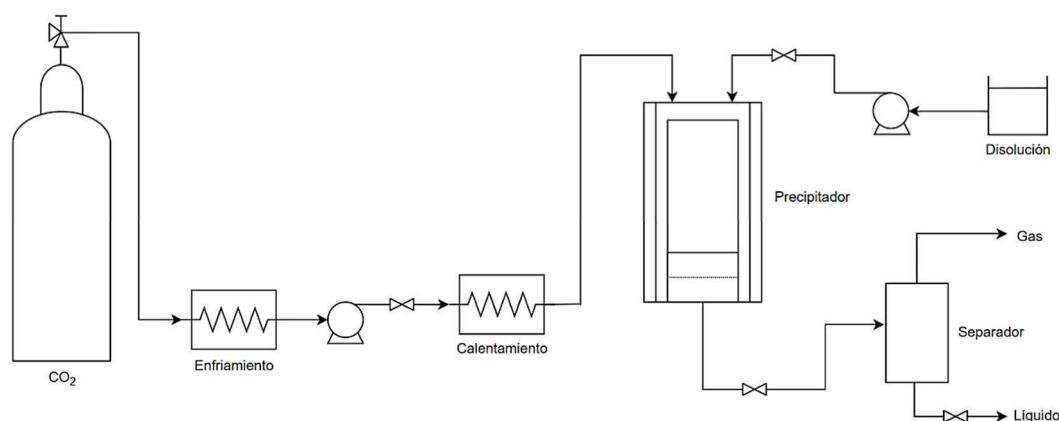
Figure 2: Scheme of the SAS process

First, supercritical CO_2 was introduced into the precipitator (flowrate 2kg/h) until the desired pressure and temperature conditions were reached (in this case 100 bar and 40 ºC, respectively). These conditions were kept constant throughout the experiment. The solution was then injected at a rate of 5 ml/min. Finally, once all the solution had been introduced into the vessel, the flow of supercritical CO_2 was kept constant for a further 30 minutes in order to eliminate the remaining organic solvent from the precipitate so that it would be completely dry.

Once these three steps were completed, the precipitator was decompressed with the help of the back pressure valve and the particles were collected from the filter and the vessel walls for further analysis. These samples were examined by scanning electron microscopy (SEM) and X-ray diffraction.

In this second part, in vitro release assays were performed simulating intestinal fluids and using the rutin products obtained in the precipitation and encapsulation with SAS previously performed. To begin with, the solution that simulates intestinal fluid must be prepared. To do this, 6.8 g of potassium phosphate is weighed and dissolved in 1 L of ultrapure distilled water (miliQ). The pH is then adjusted to the desired value, in this case 6.8, by adding NaOH from a previously prepared solution.

The rutin product is placed in a basket which is immersed in the intestinal fluid solution and kept at constant temperature and agitation. The experiments were performed with a gut fluid volume of 475 mL, at a temperature of 37°C and a speed of 100 rpm.

During the experiment, 3 mL samples are withdrawn at various time points and an equivalent volume of fresh intestinal fluid is added. The defined periods of sample extraction are 2, 5, 10, 20, 20, 30, 30, 40, 40, 50, 60, 60, 70, 80, 90, 100, 110 and 120 min.

To remove undissolved particles from the samples, they are filtered using cellulose acetate syringe filters with a pore size of 0.22 µm. They are thus prepared for further analysis in the spectrophotometer.
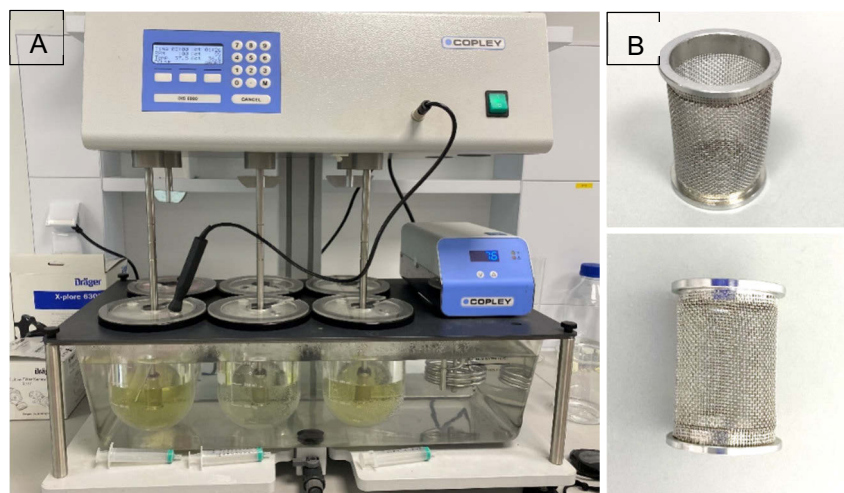
Figure 3: (A) Equipment used for in vitro release testing (B) Detail of the basket containing the rutin sample during testing

In vitro dissolution experiments were carried out with:

- Pure rutin samples
- Physical mixtures of pure rutin with Eudragit® L-100 (1:1 ratio)
- Physical mixtures of pure rutin with Eudragit® E-100 (1:1 ratio)
- Rutin samples processed with SAS
- Rutin samples coprecipitated with Eudragit® L-100
- Rutin samples co-precipitated with Eudragit® E-100
-

Results

The product obtained from the SAS experiments was studied in order to characterise its morphology and crystalline structure. Figure 4 shows that the pure rutin has irregular particle aggregates. The processed rutin shows very porous particles and a reduced size distribution. It is shown that the characteristics of the processed rutin particles are favoured by the SAS process.
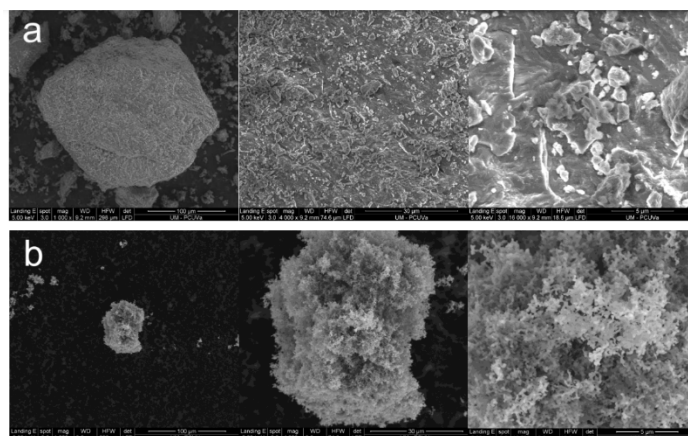
Figure 4: SEM images of: (a) pure unprocessed rutin and (b) SAS-processed rutin. The magnification ratio of the images from left to right is 1000x, 4000x, 16000x and their scale is 100 μm, 30 μm and 5 μm, respectively (Giraldes Fernández, 2022).

For coprecipitation of rutin and Eudragit®, it can be seen how the particle growth has been restricted by the polymer coating the rutin core. The polymer surrounds the particle and enters the particle interstices to achieve complete encapsulation.
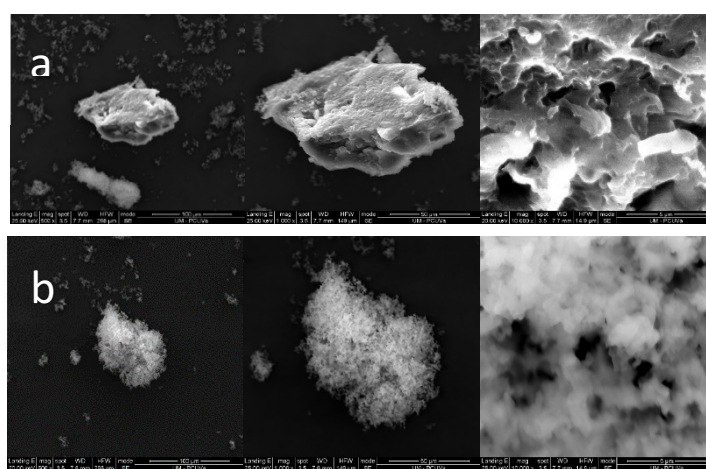
Figure 5: SEM images of: (a) rutin and Eudragit® E-100 co-precipitated with SAS and (b) rutin and Eudragit® L-100 co-precipitated with SAS. The magnification ratio of the images from left to right is 1000x, 4000x, 16000x and their scale of 100 μm, 30 μm and 5 μm.

For in vitro release tests, looking at Figure 6, the most significant result can be seen with the SAS-processed rutin, which shows a much faster dissolution than the other samples, as well as a higher final solubility. This behaviour can be attributed to the particle size reduction achieved by SAS micronisation, which increases their available surface area.

On the other hand, samples obtained from a physical homogenisation of rutin with Eudragit® at a 1:1 ratio revealed a higher solubility and faster dissolution compared to pure rutin samples. This increase in solubility is possibly due to the modification of the solution properties with the addition of Eudragit® polymers, which may improve the dissolution of the active compound.

Finally, samples coprecipitated with Eudragit® show a much more controlled release than those corresponding to the physical mixtures. When processing these samples with SAS, the rutin is coated with the polymer, which can lead to a much slower release and dissolution. This behaviour could also be favourable for the application of the formulation, as the controlled release could improve the stability of rutin in the gastrointestinal tract.
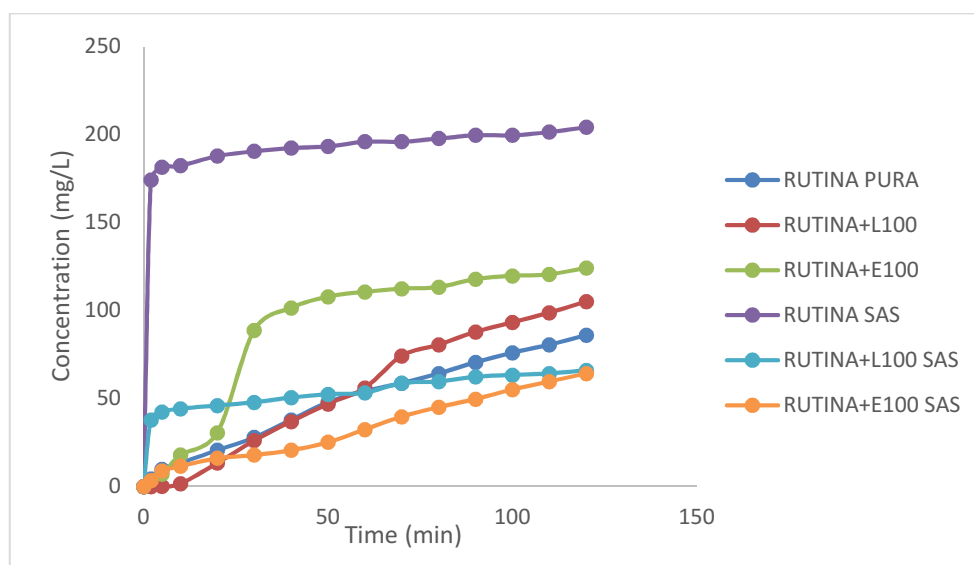
Figure 6: Results of drug release tests in simulated intestinal fluid

Summary

The main objective of this work is to develop a formulation able to potentially improve the water solubility and bioavailability of rutin in order to apply its potential benefits in industry and human health.

To achieve this objective, first, rutin was precipitated with the SAS (Supercritical Antisolvent) technique, and then rutin was co-precipitated with different polymers of Eudragit® as support material by encapsulation with the same technique.

Subsequently, the morphology and structure of the particles were characterised by scanning electron microscopy (SEM) and X-ray diffraction. The results indicated a significant reduction in particle size and crystallinity.

Finally, dissolution tests were carried out in simulated intestinal fluid and the results showed an improvement in the dissolution behaviour of the rutin with respect to the untreated compound.

References

Bié, J., Sepodes, B., Fernandes, P. C. B., & Ribeiro, M. H. L. (2023). Polyphenols in Health and Disease: Gut Microbiota, Bioaccessibility, and Bioavailability. *Compounds 2023, Vol. 3, Pages 40-72*, *3*(1), 40–72. https://doi.org/10.3390/COMPOUNDS3010005

Cocero, M. J., Martín, Á., Mattea, F., & Varona, S. (2009). Encapsulation and co-precipitation processes with supercritical fluids: Fundamentals and applications. *The Journal of Supercritical Fluids*, *47*(3), 546–555. https://doi.org/10.1016/J.SUPFLU.2008.08.015

Fraile, M., Buratto, R., Gómezgómez, B., Ngel Martín, A.´, & Josécocero, M. J. (2014). *Enhanced Delivery of Quercetin by Encapsulation in Poloxamers by Supercritical Antisolvent Process*. https://doi.org/10.1021/ie5001136

Frutos, M. J., Rincón-Frutos, L., & Valero-Cases, E. (2019). Rutin. *Nonvitamin and Nonmineral Nutritional Supplements*, 111–117. https://doi.org/10.1016/B978-0-12-812491-8.00015-1

Giraldes Fernández, I. N. (2022). *Encapsulación de antioxidantes naturales mediante proceso Supercritical Anti Solvent (SAS)*.

Hedrén, E., Diaz, V., & Svanberg, U. (2002). Estimation of carotenoid accessibility from carrots determined by an in vitro digestion method. *European Journal of Clinical Nutrition 2002 56:5*, *56*(5), 425–430. https://doi.org/10.1038/sj.ejcn.1601329

Machado, A. P. da F., Nascimento, R. de P. do, Moya, A. M. T. M., Baptista, R. de C., & Marostica Junior, M. R. (2022). Development of natural bioactive delivery systems through pressurized fluids-modern techniques. *Herbal Bioactive-Based Drug Delivery Systems: Challenges and Opportunities*, 331–369. https://doi.org/10.1016/B978-0-12-824385-5.00010-8

Moravkar, K. K., Laddha, U. D., Patil, M. D., Kale, S. S., Girase, N., Bhairav, B. A., Bhaumik, J., & Chalikwar, S. S. (2023). Extraction of rutin from tagetes erecta (Marigold) and preparation of peroral nano-suspension for effective antitussive/expectorant therapy. *Carbohydrate Polymer Technologies and Applications*, *5*, 100320. https://doi.org/10.1016/J.CARPTA.2023.100320

Nazzaro, F., Fratianni, F., De Feo, V., Pimentel, T. C., Coppola, R., & Cruz, A. G. (2022). Polyphenols applications in food industry sector. *Technologies to Recover*

Polyphenols from AgroFood By-Products and Wastes, 301–336. https://doi.org/10.1016/B978-0-323-85273-9.00002-8

Patel, K., & Patel, D. K. (2019). The Beneficial Role of Rutin, A Naturally Occurring Flavonoid in Health Promotion and Disease Prevention: A Systematic Review and Update. *Bioactive Food as Dietary Interventions for Arthritis and Related Inflammatory Diseases*, 457–479. https://doi.org/10.1016/B978-0-12-813820-5.00026-X

Remanan, M. K., & Zhu, F. (2023). Encapsulation of rutin in Pickering emulsions stabilized using octenyl succinic anhydride (OSA) modified quinoa, maize, and potato starch nanoparticles. *Food Chemistry*, *405*, 134790. https://doi.org/10.1016/J.FOODCHEM.2022.134790

Rodríguez-Rojo, S., Moreno, T., Gonçalves, V. S. S., Martín, Á., Navarrete, A., & Cocero, M. J. (2022). *Chapter 13. Post-extraction Processes: Improvement of Functional Characteristics of Extracts*. 591–626. https://doi.org/10.1039/9781839165894-00591

Semwal, R., Joshi, S. K., Semwal, R. B., & Semwal, D. K. (2021). Health benefits and limitations of rutin - A natural flavonoid with high nutraceutical value. *Phytochemistry Letters*, *46*, 119–128. https://doi.org/10.1016/J.PHYTOL.2021.10.006

Wang, C., Yan, T., Yan, T., & Wang, Z. (2023). Fabrication of hesperetin/hydroxypropyl-β-cyclodextrin complex nanoparticles for enhancement of bioactivity using supercritical antisolvent technology. *Journal of Molecular Structure*, *1279*, 134947. https://doi.org/10.1016/J.MOLSTRUC.2023.134947

Development of a Supercritical CO₂ Assisted Process Combining Simultaneous Extraction and Encapsulation of a Bioactive Component Derived from Agricultural Waste: Enhancing Stability and Bioavailability

Adeline Leluc, Suênia De Paiva Lacerda, Jean-Jacques Letourneau, Fabienne Espitalier

Centre RAPSODEE (UMR CNRS 5302) IMT Mines Albi,

adeline.leluc@mines-albi.fr

Introduction

Poor management of agricultural waste leads to environmental pollution due to by-products from intensive agricultural production as well as those from the processing of raw agricultural materials into finished products. However, some bioactive components derived from fruit, plants and vegetable waste are considered interesting from a health perspective. Indeed, they can play an essential role as anticancer, antiviral, antioxidant, anti-inflammatory, antimutagenic agents, etc. For example, essential oils, carotenoids, phenolic acids, polyphenol and vitamins can be mentioned.

Nowadays, tea is the second most consumed beverage in the world after water, with 18 to 20 billion cups of tea consumed every day (Debnath *et al.*, 2021). The increase in tea production involves significant agricultural waste (leaves, buds, stems) or infusion residues. Furthermore, tea is well known for its health benefits. Indeed, tea is rich in polyphenols, and the main composition of tea waste is presented in Tab. 1. It contains 25 to 30% polyphenols (dry mass). Polyphenols are a family of molecules that can be divided into two main groups: flavonoids (flavones, flavonols, anthocyanidins, isoflavones, flavanones, catechins) and non-flavonoids (resveratrol, phenolic acids, lignans).
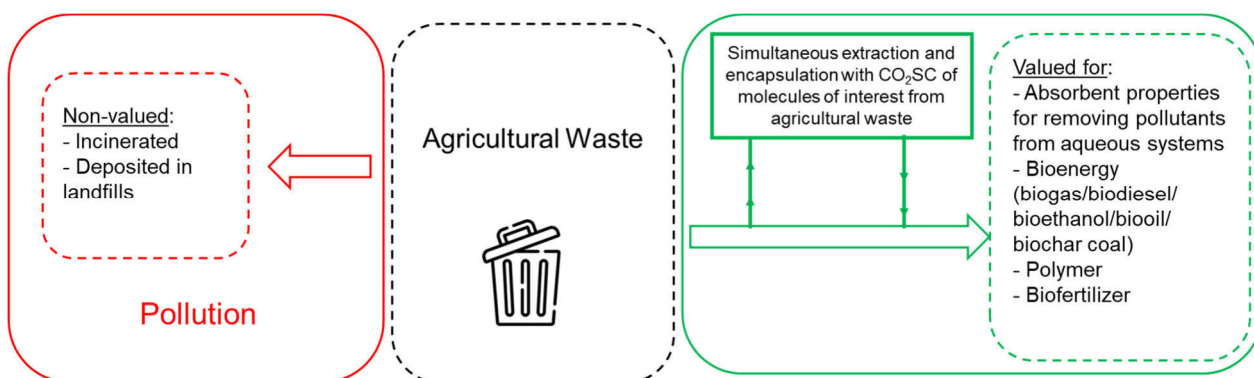
Fig. 1.: The positioning of our approach in the valorisation of agricultural waste

In tea, the most abundant flavonoids are catechins, which offer numerous benefits (cardioprotective, neuroprotective, hepatoprotective, etc.) (Bedrood *et al.*, 2018; Rodrigues *et al.*, 2013). In green tea waste, catechins include epigallocatechin gallate (48 to 55% of total flavonoids), epicatechin gallate, epigallocatechin, and epicatechin (respectively 9 to 12%, 9 to 12%, and 5 to 7% of total flavonoids) (Debnath *et al.*, 2021). Based on catechins physico-chemical properties, it is necessary to control temperature, pH, oxygen concentration, ions, and exposure to light to prevent epimerization, hydrolysis, and oxidation of catechins during the process *(Ananingsih et al., 2013; Mehmood et al., 2022; Rodrigues et al., 2013).* Encapsulation using a polymer thus protects catechins from external factors that could degrade them and increases the stability of the molecules over time. The second advantage of encapsulation is to improve the bioavailability of the active molecules during administration by enabling targeted and controlled release.

Classical molecule extraction methods use large amounts of organic solvents (Soxhlet, maceration, distillation) and require a significant amount of energy (heating, drying, etc.). Moreover, these methods still rely on organic solvents such as chloroform, acetone, acetonitrile, methanol, which contributes strongly to the waste stream, higher toxicity and consequently are not suitable in the agri-food and pharmaceutical fields (Agrawal *et al.*, 2020; Serdar *et al.*, 2017; Vuong *et al.*, 2010). For these reasons, it is needed to establish a green extraction method for tea catechins without the use of organic solvents. Unlike the classical method, supercritical CO_2 extraction does not require high-temperature heating, avoids the use of harmful solvents, consumes less energy, and it is suitable for sensitive molecules to heat and organic solvents.

The main objective of this project is to develop a process for the simultaneous extraction and encapsulation of molecules of interest extracted from agricultural waste, as well as to develop a pharmaceutical formulation for the oral administration of catechins in order to improve their stability and bioavailability.

Tab. 1.: Main components of a tea leaf as a percentage of dry mass

Compounds	%	Compounds	%	Compounds	%
Polyphenols	25 to 30	Lignin	6,5	Organic acids	1,5
Fibre	26	Minerals	5	chlorophylls	0,5
Proteins	15 to 20	Lipids	2	Carotenoids	0,5
Carbohydrate	5 to 7	Amino acids	1 à 4	Vitamins	

Experimental

The extraction and encapsulation of catechins are carried out using the supercritical CO_2, shown in Fig. 2, adapted from that of T. Massias PHD thesis (Massias, 2020). In the first autoclave (Fig. 2. A), CO_2 is cooled to the liquid state and pressurized beyond its critical pressure with a pump (Fig. 2. P), then heated beyond its critical temperature (Fig. 2. HE) to obtain supercritical CO_2. The supercritical CO_2 then reaches another autoclave (Fig. 2. B) containing the tea waste, where it dissolves the molecules of interest (catechins), which are then sent to the atomization nozzle (Fig. 2. N). Simultaneously, a polymer in solution (Fig. 2. D) is pumped to the nozzle using an HPLC pump. Thus, in the recovery autoclave (Fig. 2. C), tea extracts rich in catechins will be obtained.

Once the process is optimized, this study can potentially be extended to other agricultural wastes. A biopolymer will be used for encapsulation (like chitosan), helping to prevent degradation of the molecules of interest and to improve its bioaccessibility and/or bioavailability. An HPLC analytical method has been developed to quantify catechins in tea waste. This method allows bioactive compounds assay (*i.e.* catechin, epicatechin, epigallocatechin, epicatechin gallate, epigallocatechin gallate). Dissolution tests simulating gastrointestinal environment will be also conducted to assess the release of catechins over time.
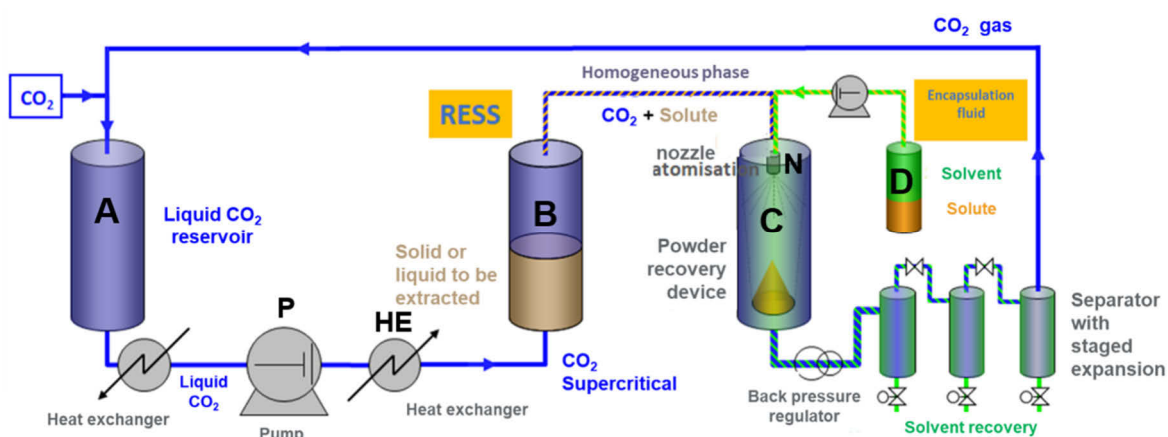
Fig. 2.: Supercritical CO_2 extraction and encapsulation process

Summary

In summary, this study aims to develop a one-step method for extracting and encapsulating bioactive molecules from tea agricultural waste, simultaneously.

A preliminary bibliographic study was conducted to select a model waste, namely tea, and

an analytical method using HPLC was implemented to quantify the extracted catechins. In parallel with the supercritical CO_2 extraction, a physico-chemical and biopharmaceutical characterization of extracts obtained will be performed in order to evaluate the process and encapsulation impact on bioactive compound stability and behaviour in a simulated gastrointestinal environment.

Acknowledgment

References

Agrawal, M., Dubey, S.K., Khan, J., Siddique, S., Ajazuddin, Saraf, S., Saraf, S., et al. (2020), "Chapter 3 - Extraction of catechins from green tea using supercritical carbon dioxide", in Inamuddin, Asiri, A.M. and Isloor, A.M. (Eds.), Green Sustainable Process for Chemical and Environmental Engineering and Science, Elsevier, pp. 41–66, doi: 10.1016/B978-0-12-817388-6.00003-9.

Ananingsih, V.K., Sharma, A. and Zhou, W. (2013), "Green tea catechins during food processing and storage: A review on stability and detection", Food Research International, Vol. 50 No. 2, pp. 469–479, doi: 10.1016/j.foodres.2011.03.004.

Bedrood, Z., Rameshrad, M. and Hosseinzadeh, H. (2018), "Toxicological effects of Camellia sinensis (green tea): A review", Phytotherapy Research: PTR, Vol. 32 No. 7, pp. 1163–1180, doi: 10.1002/ptr.6063.

Debnath, B., Haldar, D. and Purkait, M.K. (2021), "Potential and sustainable utilization of tea waste: A review on present status and future trends", Journal of Environmental Chemical Engineering, Vol. 9 No. 5, p. 106179, doi: 10.1016/j.jece.2021.106179.

Massias, T. (2020), Développement et Caractérisation d'une Forme Pharmaceutique Pour Application Cutanée à Partir de Solides Sursaturés, These en préparation, Lyon 1.

Mehmood, S., Maqsood, M., Mahtab, N., Khan, M.I., Sahar, A., Zaib, S. and Gul, S. (2022), "Epigallocatechin gallate: Phytochemistry, bioavailability, utilization challenges, and strategies", Journal of Food Biochemistry, Vol. 46 No. 8, p. e14189, doi: 10.1111/jfbc.14189.

Rodrigues, C.F., Ascenção, K., Silva, F. a. M., Sarmento, B., Oliveira, M.B.P.P. and Andrade, J.C. (2013), "Drug-delivery systems of green tea catechins for improved stability and bioavailability", Current Medicinal Chemistry, Vol. 20 No. 37, pp. 4744–4757, doi: 10.2174/09298673113209990158.

Serdar, G., Demir, E. and Sökmen, M. (2017), "Recycling of Tea Waste: Simple and Effective Separation of Caffeine and Catechins by Microwave Assisted Extraction (MAE)", International Journal of Secondary Metabolite, İzzet KARA, Vol. 4 No. 2, pp. 78–89, doi: 10.21448/ijsm.288226.

Vuong, Q.V., Golding, J.B., Nguyen, M. and Roach, P.D. (2010), "Extraction and isolation of catechins from tea", Journal of Separation Science, Vol. 33 No. 21, pp. 3415–3428, doi: 10.1002/jssc.201000438.

HS3, An Innovative Solvent for CO_2 Capture

Matteo Gilardi and Filippo Bisotti

SINTEF Industry, Process Technology, Chemical and Environmental Process
Engineering, Sem Sælands vei 2A, 7034, Trondheim, Norway

Introduction

Carbon Capture and Storage (CCS) is a promising technology to reduce Greenhouse Gas emissions from the industrial sector [1]. Based on promising outcomes from two distinct pilot plant test campaigns, the novel solvent HS3, namely a blend of a primary (3-amino-1-propanol, AP) and tertiary (2-hydroxy-ethyl-pyrrolidine, PRLD) amine, is proposed as an alternative blend to benchmark monoethanolamine (MEA) 30 wt% to reduce the energy requirements of the CO_2 capture process and increase its economic and environmental sustainability [2]. The work mainly includes the development of a model of the new amine blend in a process simulator, its validation, and its testing for CO_2 capture from a real refinery.

Model development and validation

Model implementation

The HS3 model has been implemented in Aspen Plus® V11.0 according to the ELECNRTL framework, dealing with vapor-liquid equilibrium first and then adding kinetics and mass transfer. The reaction scheme has been defined following previous modelling works on similar blends, and equilibrium constants have been retrieved from the literature. In-house data have been exploited to regress the thermodynamic models for the vapor pressure, Henry constant and physical properties such as density, viscosity, heat capacity and heat of vaporization. Lab-scale VLE data have been used to tune interaction coefficients between molecules and ions. The proposed model accounts for only 24 temperature-independent and 10 temperature-dependent coefficients to avoid overfitting. The model stability is confirmed by a correlation matrix among the regressed parameters and the smoothness and accuracy of the VLE model have been checked (Fig. *1*a) and compared against the available experimental data at different temperatures using a statistical test. As a matter of fact, the developed Aspen Plus® model can provide reasonable speciation in the liquid phase and can estimate the absorption reaction heat with an AARD lower than 8% in a temperature range between 40°C and 100°C (Fig. *1*b).

This outcome is extremely relevant since an accurate estimate of the reaction heat is essential to demonstrate the correctness of energy balances and to achieve a consistent calculation of the process energy requirements. Further details on the experimental data, physical properties definition, and the ELECNTRL model are available in Gilardi et al. (2023) [3].
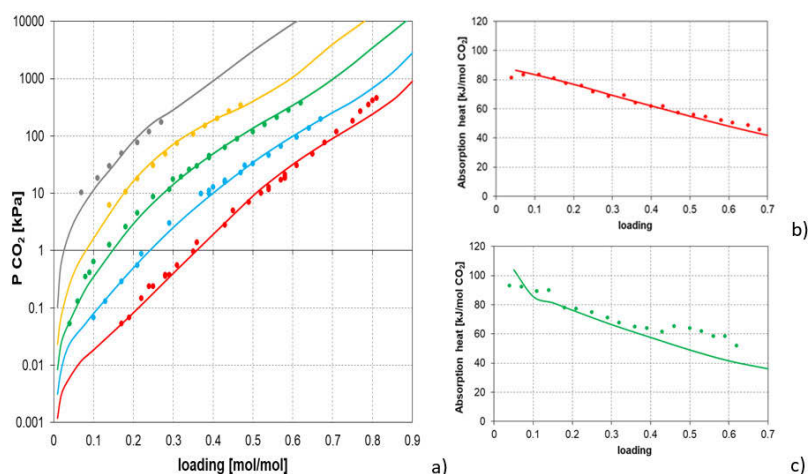
Fig. 1.: Comparison between the Aspen model (solid lines) and the experimental data (dots) for (A) CO_2 partial pressure and (B, C) heat of absorption (estimated through enthalpy balance by simulating a reactive flash) at different temperatures: 40°C (red), 60°C (light blue), 80°C (green), 100°C (yellow), and 120°C (grey).

Kinetic constants for the global reactions between amines, water and CO_2 have been retrieved from the literature, and a liquid mixture (AP-water and PRLD-water) viscosity model has been tuned to published experimental data for an accurate implementation of the Wilke-Chang method to account for diffusion of CO_2 in the bulk liquid. The Nernst-Hartley and the Chapman-Enskog-Wilke-Lee methods have been adopted to characterize the ions' diffusivity and the molecular diffusivity in the gas phase, respectively. Additional pieces of information can be retrieved from Gilardi et al. (2024) [4].

Model validation

The final comprehensive model (VLE with kinetics and mass transfer) has been validated over pilot scale data collected at the Tiller plant (SINTEF CO_2Lab, Trondheim, Norway). To this aim, the absorber and stripper have been simulated providing input conditions compliant with the experimental conditions, while the CO_2 captured flow, the released flow from the stripper, the temperature profiles in both columns and the loadings were the compared outputs. The proposed model can predict all the KPIs of the CO_2 capture process with an AARD (average absolute relative deviations) lower than 5% and an ARD (average relative deviation) close to zero (Fig. 2), which indicates that the proposed model

neither under- nor overestimates. Also in temperature profiles, the maximum observed discrepancy did not overcome 5°C in all the tested runs. These results demonstrate the reliability of the developed Aspen model to model and optimize the design of carbon capture plants. The validated model has been further validated on a close loop simulation of the Tiller plant, which further confirmed the quality of model prediction in terms of predictivity of amine lean and rich loadings. Indeed, the AARD on cycling capacity remains always below 10%. The details of the statistical analysis are provided in Gilardi et al. (2024) [4].
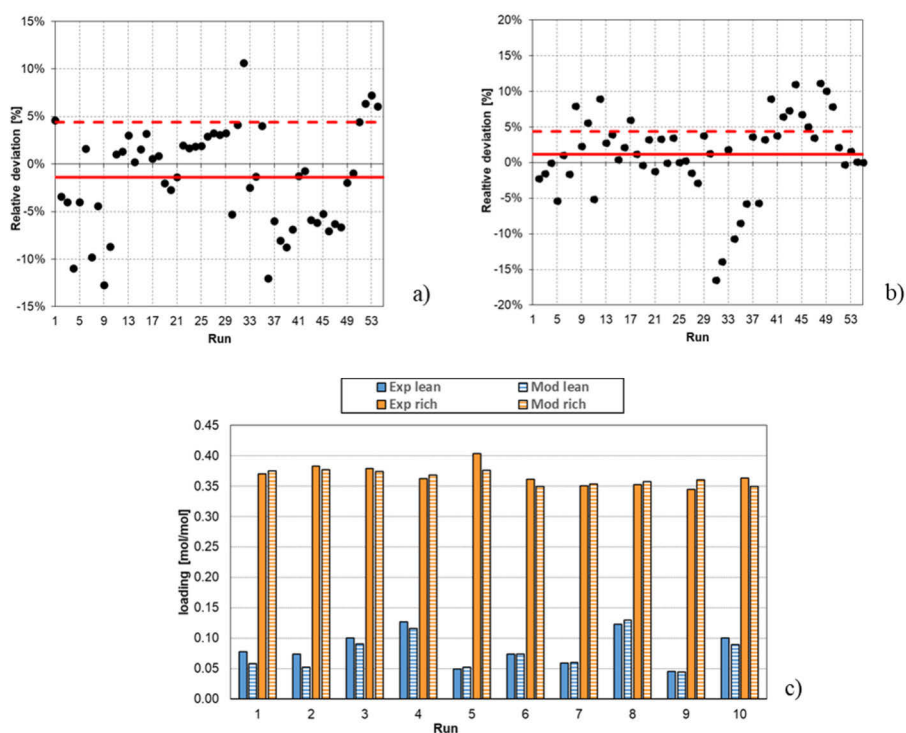
Fig. 2.: Aspen model validation over the Tiller pilot plant data: residuals (•), ARD% (—) and AARD% (- - -) for (a) CO_2 captured flow (open-loop) and (b) CO_2 desorbed flow (open-loop); (c) experimental and predicted lean and rich loadings (close-loop).

Design and simulation for a carbon capture plant in an oil refinery

The validated model has been exploited to design and optimize a CO_2 capture plant for treating flue gas streams from an oil refinery with CO_2 content higher than 2 vol%. For the sake of comparison, the same simulations have been set up also for the benchmark MEA solvent using a consistent methodology. For MEA modelling, the default template proposed by AspenTech has been used. The CO_2 capture plant has been designed according to the layout drawn in Fig. *3*. This is a conventional carbon capture facility with a Direct Contact Cooler (DCC), an absorber with a water wash section on top, and stripper with reboiler for the solvent regeneration. The simulations included a heat exchanger

network (HR-1 to HR-10) to recover the heat for producing part of the steam for solvent regeneration. The uncovered demand for steam is compensated by a steam boiler whose flue gas is conveyed to the absorber with the stacks from the refinery. The capture ratio is assumed of 90%.
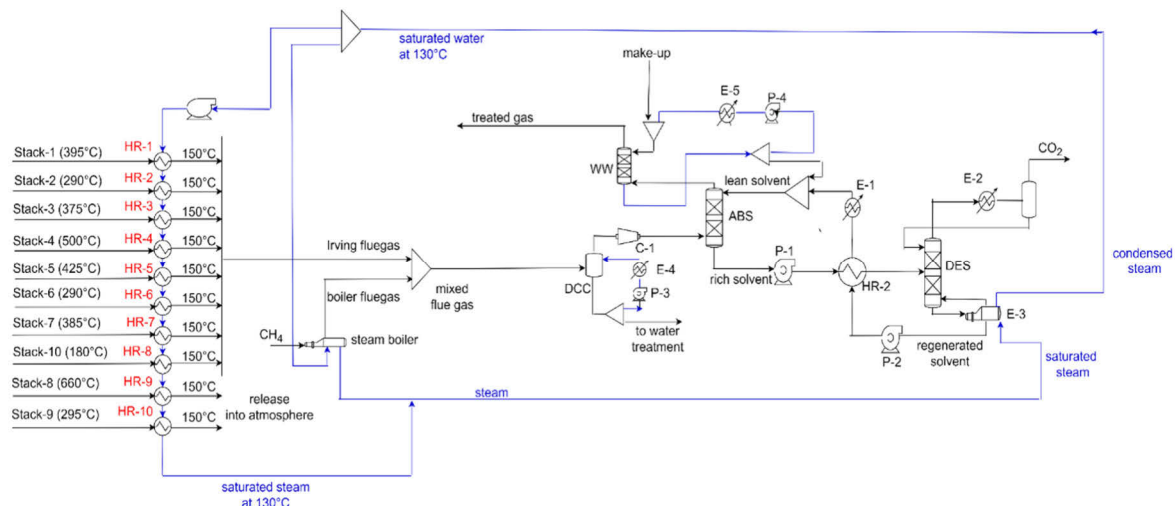
Fig. 3.: Flowsheet of the plant designed for CO_2 capture from the oil refinery with preliminary heat recovery section.

Tab. 1.: Results from the Aspen simulation for the capture plant for the refinery case study.

Parameter	HS3	MEA	Variation
Flue gas from steam boiler [t/h]	11.63	27.72	-58.0%
Flue gas from stacks [t/h]	280.3	280.3	
Cycling capacity [mol_{CO2}/mol_{amine}]	0.287	0.266	+7.90%
Liquid/Gas ratio [kg/kg]	1.65	2.00	-18.8%
Absorber Diameter (D) [m] / Height (H) [m]	5.60 / 18.0	5.86 / 10	
Water wash H [m]	4.90	2.10	+133%
Stripper D [m] and H [m]	2.69 / 12.0	3.12 / 8.0	
Reboiler duty [MWth]	24.45	33.05	-26.0%
Specific reboiler duty (SRD) [$MJ_{th}/kg_{CO2\ capt}$]	2.98	3.78	-21.2%
Specific steam requirement [$MJ_{th}/kg_{CO2\ capt}$]	0.77	1.70	-54.7%
Energy recovered from flue gas [%]	74.3	55.0	+35.1%
Cooling water in DCC [t/h]	935.0	991.0	-5.70%
Cooling water in water wash [t/h]	446.0	644.0	-30.8%

Assumptions for the flowsheet development and justification of the adopted simplification are reported in Gilardi et al. (2024) [4]. Tab. *1* summarizes and compares the performance of the same capture facility when HS3 and MEA solvents are adopted. The most relevant and commonly used key performance indicators (KPIs) are reported.

Summary

HS3 blend allows for having smaller and more compact columns while reducing the total energy demand and water consumption to run the cooling system. Despite these relevant features, the cost of the solvent may represent a hurdle to its deployment as well as the need to enlarge the water wash section to abate the amine emission to the environment. Tab. *2* tries to summarise the main understanding of the HS3 blend (compared to MEA).

Tab. 2.: Comparison between HS3 and MEA solvents (for the refinery case study)

HS3 advantages	HS3 disadvantages	Equal performance to MEA
- 24% solvent flow - 19% L/G ratio	Slower kinetics (higher packing)	Purity of delivered CO_2 stream (>97%)
- 26% reboiler duty	Higher column packing heights	Easy retrofitting (same plant layout)
-21% specific reboiler duty (SRD)	Higher volatility (larger water wash section)	Similar pressure drop in columns (similar energy demand for the blower)
-45% specific steam requirement (SSR)	Higher initial solvent cost (due to higher production of cyclic amine)	
Smaller absorber and stripper diameters (due to lower L/G ratio)		
More compact ancillary devices due to less flue gas and solvent circulating		

Acknowledgement

References

[1] M. Bui, C.S. Adjiman, A. Bardow, E.J. Anthony, A. Boston, S. Brown, P.S. Fennell, S. Fuss, A. Galindo, L.A. Hackett, J.P. Hallett, H.J. Herzog, G. Jackson, J. Kemper, S. Krevor, G.C. Maitland, M. Matuszewski, I.S. Metcalfe, C. Petit, G. Puxty, J. Reimer, D.M. Reiner, E.S. Rubin, S.A. Scott, N. Shah, B. Smit, J.P.M. Trusler, P. Webley, J. Wilcox, N. Mac Dowell, Carbon capture and storage (CCS): the way forward, Energy Environ. Sci. 11 (2018) 1062–1176. https://doi.org/10.1039/C7EE02342A.

[2] Demonstrating a Refinery-Adapted Cluster-Integrated Strategy to Enable Full-Chain CCUS Implementation | REALISE Project | Fact Sheet | H2020, CORDIS | European Commission (2020). https://cordis.europa.eu/project/id/884266 (accessed January 16, 2024).

[3] M. Gilardi, F. Bisotti, A. Tobiesen, H.K. Knuutila, D. Bonalumi, An approach for VLE model development, validation, and implementation in Aspen Plus for amine blends in CO2 capture: the HS3 solvent case study, International Journal of Greenhouse Gas Control 126 (2023) 103911. https://doi.org/10.1016/j.ijggc.2023.103911.

[4] M. Gilardi, F. Bisotti, H.K. Knuutila, D. Bonalumi, HS3 as a novel solvent for carbon capture: Model validation and an industrial case study with comparison against 30 wt% MEA, Journal of Cleaner Production 447 (2024) 141394. https://doi.org/10.1016/j.jclepro.2024.141394.

Extraction of Phenolic Compounds from Spruce Bark by Supercritical CO₂ Extraction with Ethanol and Ethyl Acetate Co-Solvents

Martin Štosel, Richard Nadányi, Aleš Ház

Institute of Natural and Synthetic Polymers/Department of Wood, Pulp and Paper,

Slovak University of Technology,

martin.stosel@stuba.sk

Introduction

Forests cover approximately 3,870 million hectares of our planet, of which more than a quarter belong to Europe, approximately 1,040 million hectares [1]. The European Union and its member states account for 5% of the world's forest area, which is approximately 158 million hectares, covering 37.7% of the EU's territory. Between 1990 and 2010, the forested area in the EU expanded by 11 million hectares [2]. A similar trend can be observed in the territory of the Slovak Republic, where since 1990, the forest area has increased by 1%, and currently, forests represent 41.3% of Slovakia's territory [3]. The largest share of EU forests is coniferous forests, 42%, followed by broadleaf forests at 40%, and mixed forests at 18% [4]. In contrast, broadleaf forests predominate in Slovakia, representing 64.25% of the total forest area in the country [3]. Despite the dominance of broadleaf forests in our region, the processing of coniferous wood is significantly widespread in our territory, whether for the paper industry or the construction industry, where coniferous wood serves as a construction material. Conifers also have a significant advantage in growth rate and wood mass increase compared to the slow-growing hardwood of broadleaf trees. Due to their relatively rapid growth and widespread presence across almost all of Europe, coniferous forests represent a suitable renewable source of raw materials.

European forests are a significant source of renewable biomass. Approximately half of the renewable resources for energy production come from wood. Harvested wood is largely used in the energy sector, up to 42%, with 24% of the harvested wood used in sawmills, 17% in the paper industry, and 12% of the total harvested wood used to produce wooden boards [2]. The industrial processing of wood generates a substantial number of by-products, such as bark, leaves, needles, and fruits/cones, which are primarily used for energy purposes today.

Many studies, however, suggest that these by-products of the forestry, wood, and paper industries contain valuable substances, particularly those with phenolic characteristics. It is generally known that these substances have significant effects, such as antioxidant, antiviral [5], antibacterial, antifungal [6], cardio- and neuroprotective [7], [8], anti-inflammatory [9], [10], and primarily anticancer [10], [11] properties. These properties of phenolic substances, as secondary plant metabolites, make them the subject of interest for many studies.

Thanks to their mentioned effects, these substances have a wide range of uses in the pharmaceutical industry, cosmetics, and the food industry, where they are used to increase food shelf life [12]. There are also efforts to use phenolic substances as additives to polymers, mainly for their antioxidant properties [13]. Additionally, these phytochemical compounds find their application in agriculture for plant protection, primarily against harmful insects [14].

These properties are mainly attributed to their structure, which consists of at least one benzene ring substituted with one or more –OH groups. The hydrogens of the –OH groups readily provide hydrogen in radical reactions, making these substances good radical scavengers [15].

It is known that supercritical CO2 extraction is a safe and environmentally friendly alternative to conventional extraction techniques that use large volumes of organic solvents. Supercritical CO2 extraction is primarily used for the isolation of lipophilic compounds; however, by adding a cosolvent such as ethanol, the polarity value is shifted, thereby broadening the spectrum of extracted substances. Thanks to the use of cosolvents, this technique can also isolate natural phytochemicals such as phenols, which are relatively abundantly present in phytomass [16], [17].

Experimental

Sample Preparation

Spruce (*Picea abies*) bark was manually collected in May 2023. It was then air-dried at laboratory temperature. The dried sample was ground to a fraction of 1 – 1.5 mm. The prepared sample was then stored in the dark and dry conditions until further use.

The moisture content of the spruce bark was determined using the gravimetric method by drying at a temperature of 105°C. This drying continued until a constant weight of the dried

material was achieved. Approximately 1 g of the spruce bark sample was used to determine the moisture content, which was found to be 9.39%.

Supercritical CO_2 Extraction

The extraction of natural substances from spruce bark was carried out using the SFT – 150 SFE SYSTEM laboratory equipment from Supercritical Fluid Technology, Inc. Extractions were performed using pure CO_2 (> 99%, Messer) as the extraction agent. Cosolvents used in the extraction were pure ethanol (> 94%, Centralchem) and pure ethyl acetate (> 99.7%, Centralchem). Both cosolvents were used in a 1:1 ratio in a batch extraction process.

For this work, a designed experiment was conducted with a temperature range of 40 – 140 °C and a pressure range of 80 – 480 bars. Approximately 20 g was weighed and subsequently extracted for each experiment. The flow rate of the extraction agent mixture during the discharge of the extraction space was maintained at 2 ml/min.

The extraction proceeded in static mode for 60 minutes, followed by the collection of the obtained extract in a vial with a septum, which was cooled in an ice bath. The samples of the extracted spruce bark were lyophilized for 24 hours in a Lyovac GT2 (Leybold-Heraeus) lyophilizer. The resulting yield of the extraction was determined as the difference in the weight of the absolutely dry fresh sample compared to the extracted and lyophilized bark.

Summary

The designed experiment was designed to optimize the extraction conditions, specifically temperature and pressure, for the highest possible extraction yield. In this experiment, a total of 13 extractions were performed across a temperature range of 40 – 140°C and a pressure range of 80 – 480 bars. The obtained extracts were collected in cooled vials to prevent the undesirable evaporation of volatile extracted compounds as well as the evaporation of the solvents used (ethanol and ethyl acetate, 1:1 v/v). After completing all experiments, we proceeded to evaluate the optimal extraction conditions. Our mathematical model selected for this work revealed that extraction temperature has a significant impact on yield for supercritical extraction of spruce bark with carbon dioxide. The optimal conditions for the highest extraction yield of spruce bark are temperature 47.7°C and pressure 80 bars, for which extraction will be carried out to confirm the results of the planned experiment. The results of the planned experiment show an inverse relationship between temperature and extraction yield. In the further stages of this work,

we plan to identify the individual extracts using gas chromatography coupled with mass spectrometry. Subsequently, we will conduct an analysis of antioxidant activity using the DPPH (2,2-Diphenyl-1-picrylhydrazyl) method and determine the total phenolic content (TPC) according to the Folin-Ciocalteu method.

Acknowledgment

References

[1]   "Výmera lesov Európy - ForestPortal," Národné lesnícke centrum. Accessed: Apr. 08, 2023. [Online]. Available: https://www.forestportal.sk/odborna-sekcia-i/informacie-o-lesoch/zakladne-informacie-o-lesoch/vymera-lesov-europy/

[2]   F. Nègre, "THE EUROPEAN UNION AND FORESTS," Apr. 2022. Accessed: Apr. 06, 2023. [Online]. Available: https://www.europarl.europa.eu/ ftu/pdf/en/FTU_3.2.11.pdf

[3]   "Správa o lesnom hospodárstve v Slovenskej republike za rok 2021 - Zelená správa," Národné lesnícke centrum. Accessed: Mar. 31, 2023. [Online]. Available: https://web.nlcsk.org/zelena-sprava-2021/

[4]   "Europe's Forests in the Spotlight," in *4th Ministerial Conference on the Protection og Forests in Europe*, 2003, p. 5.

[5]   V. A. Tirado-Kulieva, E. Hernández-Martínez, and T. J. Choque-Rivera, "Phenolic compounds versus SARS-CoV-2: An update on the main findings against COVID-19," *Heliyon*, vol. 8, no. 9, p. e10702, Sep. 2022, doi: 10.1016/J.HELIYON.2022.E10702.

[6]   Z. Burčová *et al.*, "Antibacterial and antifungal activity of phytosterols and methyl dehydroabietate of Norway spruce bark extracts," *J Biotechnol*, vol. 282, pp. 18–24, Sep. 2018, doi: 10.1016/J.JBIOTEC.2018.06.340.

[7]   A. Freyssin, G. Page, B. Fauconneau, and A. Rioux Bilan, "Natural stilbenes effects in animal models of Alzheimer's disease," *Neural Regen Res*, vol. 15, no. 5, p. 843, May 2020, doi: 10.4103/1673-5374.268970.

[8] S. D. Rege, T. Geetha, G. D. Griffin, T. L. Broderick, and J. R. Babu, "Neuroprotective effects of resveratrol in Alzheimer disease pathology," *Front Aging Neurosci*, vol. 6, no. AUG, pp. 1–27, Sep. 2014, doi: 10.3389/FNAGI.2014.00218/BIBTEX.

[9] M. M. Lesjak *et al.*, "Juniperus sibirica Burgsdorf. as a novel source of antioxidant and anti-inflammatory agents," *Food Chem*, vol. 124, no. 3, pp. 850–856, Feb. 2011, doi: 10.1016/J.FOODCHEM.2010.07.006.

[10] A. Ali Redha, "Review on Extraction of Phenolic Compounds from Natural Sources Using Green Deep Eutectic Solvents," *J Agric Food Chem*, vol. 69, no. 3, pp. 878–912, Jan. 2021, doi: 10.1021/ACS.JAFC.0C06641/ASSET/IMAGES/LARGE/JF0C06641_0002.JPEG.

[11] E. Burlacu and C. Tanase, "Anticancer Potential of Natural Bark Products - A Review," *Plants 2021, Vol. 10, Page 1895*, vol. 10, no. 9, p. 1895, Sep. 2021, doi: 10.3390/PLANTS10091895.

[12] N. C. da Silva, T. T. de Barros-Alexandrino, O. B. G. Assis, and M. Martelli-Tosi, "Extraction of phenolic compounds from acerola by-products using chitosan solution, encapsulation and application in extending the shelf-life of guava," *Food Chem*, vol. 354, p. 129553, Aug. 2021, doi: 10.1016/J.FOODCHEM.2021.129553.

[13] M. D. Samper, E. Fages, O. Fenollar, T. Boronat, and R. Balart, "The potential of flavonoids as natural antioxidants and UV light stabilizers for polypropylene," *J Appl Polym Sci*, vol. 129, no. 4, pp. 1707–1716, Aug. 2013, doi: 10.1002/APP.38871.

[14] F. A. Neis, F. De Costa, A. T. De Araújo, J. P. Fett, and A. G. Fett-Neto, "Multiple industrial uses of non-wood pine products," 2019, doi: 10.1016/j.indcrop.2018.12.088.

[15] L. A. de la Rosa, J. O. Moreno-Escamilla, J. Rodrigo-García, and E. Alvarez-Parrilla, "Phenolic Compounds," *Postharvest Physiology and Biochemistry of Fruits and Vegetables*, pp. 253–271, Jan. 2019, doi: 10.1016/B978-0-12-813278-4.00012-9.

[16] N. Bukhanko *et al.*, "Extraction of cones, branches, needles and bark from Norway spruce (Picea abies) by supercritical carbon dioxide and soxhlet extractions techniques," *Ind Crops Prod*, vol. 145, p. 112096, Mar. 2020, doi: 10.1016/J.INDCROP.2020.112096.

[17] S. M. Ghoreishi, A. Hedayati, and S. Mohammadi, "Optimization of periodic static-dynamic supercritical CO2 extraction of taxifolin from pinus nigra bark with ethanol as entrainer," *J Supercrit Fluids*, vol. 113, pp. 53–60, Jul. 2016, doi: 10.1016/J.SUPFLU.2016.03.015

Continuous Hydrothermal Fractionation of Carrot Waste using Subcritical and Supercritical Water, Purification and Application to Produce Bio-Based Films

Andrea Arribas Sanchidrián

Department of Chemical Engineering and Environmental Technology,

University of Valladolid, andrea.arribas.sanchidrian@estudiantes.uva.es

Introduction

In this work the best way to pretreat discarded carrots was studied and a hydrothermal fractionation process was developed using five different subcritical and supercritical water conditions in a continuous system. The aim is to separate the biopolymers present in these carrots and to use the fibre obtained as a reinforcement in bio-based films made with soy protein and glycerol.

Two major current problems are the use of petrochemical plastic packaging (Zhang et al., 2001) and the production of food waste (Rajinipriya et al., 2018): plastic waste has become a huge part of municipal solid waste and about 10% of global greenhouse gas emissions are related to food that is not consumed (United Nations Environment Programme, 2021).

Therefore, it is intended to provide a solution to both problems by using discarded carrots from which valuable components can be extracted such as cellulose and used to create biodegradable packaging materials (Mostafa et al., 2023). The purpose is to achieve an alternative to conventional plastics in order to reduce the use of non-renewable raw materials and thus contribute to a circular economy model (Asgher et al., 2020).

The biorefinery for food waste management has a positive environmental and economic impact due to the reduction of the environmental load produced by its disposal, the reduction of greenhouse gas emissions, the decrease in the consumption of primary raw materials, less dependence on fossil sources and the reduction of water, soil and atmospheric pollution (United Nations Environment Programme, 2021), (Nayak & Bhushan, 2019).

Furthermore, pressurized water extraction processes with subcritical or supercritical water used are one of the most efficient technologies and are aligned with sustainability, as it avoids the use of organic solvents and reduces the reaction time and the water consumption compared to traditional extraction technologies (Baiano, 2014).

One of the advantages of using water as a solvent is that, as it is one of the constituents of biomass, it is not necessary to dry it previously, which means great energy savings (Peterson et al., 2008).

Experimental

In order to achieve the objective of this work, firstly, the most efficient way of pretreatment of the biomass to enable subsequent hydrothermal fractionation was studied. In this pretreatment the discarded carrots were cooked and then a wet milling process was carried out.

This was followed by a suitable carrot fractionation process that extracts the different biopolymers present in the carrots, such as cellulose and hemicelluloses. In this process, five different subcritical and supercritical water conditions were used in a continuous system, which can be consulted in the following table.

Table 1. Operating conditions in the continuous hydrothermal fractionation plant.

Condition	C1	C2	C3	C4	C5
Temperature (^{o}C)	220	280	330	380	440
Pressure (barg)	200	200	200	200	240

Part of the products obtained after hydrothermal fractionation was used for HPLC, FTIR and SEM analysis, among others.

Another part was conditioned by washing and centrifuging cycles in order to remove the free sugars present and obtain a clean fibre, which was used as a reinforcement material in the bio-based films made with glycerol and soy protein as a matrix.

Soy protein isolate is obtained from soybean cake, which is the agricultural waste material from the soybean oil industry. Glycerol was used as a bio-plasticizer.

Different films were made using fibre obtained in each of the treatment conditions mentioned above. Moreover, for some cases, different percentages of fibre loading were added to evaluate the effect on the properties of the films, such as mechanical strength.

The feasibility of making bio-based films from carrot fibre alone, without the addition of soy protein, was also investigated by optimising the processing conditions.

The following table shows the necessary quantities of each component used depending on the desired loading and humidity content of each hydrolysis product.

Table 2. Quantity of compounds used for the production of films.

	Soy film	C1			C2		C3		C4	C5
		C1.1	C1.2	C1.3	C2.1	C2.2	C3.1	C3.2		
Humidity	-	94%	94%	94%	94%	94%	95%	95%	92%	91%
Desired amount of carrot fibre (%)	-	5%	15%	30%	5%	15%	5%	14,6%	5%	5%
Water (mL)	100	95,3	85,6	71,2	95,3	85,9	94,3	22,5	96,6	96,9
Hydrolysis product (g)	-	5,0	15,3	30,6	5,0	15,0	6,0	25	3,8	3,3
Soy protein (g)	6	6	6	6	6	6	6	-	6	6
Glycerol (g)	3	3	3	3	3	3	3	1	3	3

As can be seen, a film was made only with soy protein and glycerol, without carrot fibre, which was useful as a control to compare the properties of the films containing and not containing carrot.

Below is the visual appearance of several of the films made.

Figure 1. Soy film and bio-based films reinforced with 5% fibre obtained under different hydrolysis conditions (C1-C5).
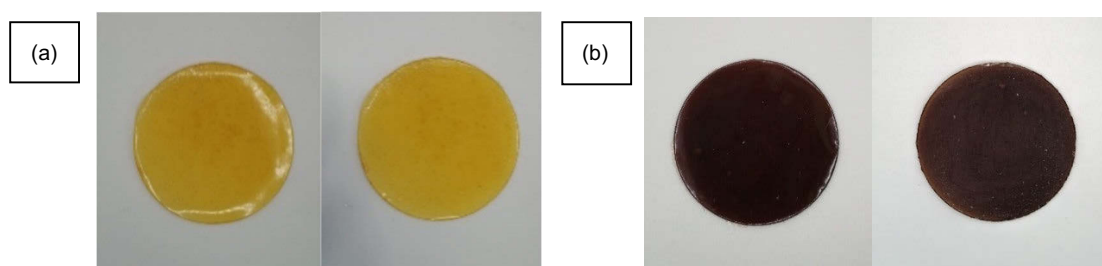
Figure 2. Bottom and top side of bio-based films reinforced with 15% C2 fibre (a) and 5% C4 fibre (b).

Tensile tests were carried out on the films to determine their mechanical properties. The most important properties studied are tensile modulus and tensile strength, which are a measure of the stiffness of the film, as well as strain at tensile strength, which indicates tenacity. Thus, the interest lies in having high stiffness and toughness.

It is worth mentioning that it was not possible to realize the mentioned tests on the film made with 5% of C1 fibre because it was not in a appropriate condition to carry them out. Neither could they be performed on the film made only with carrot fibre because mold appeared on it during the drying process.

The results are in table 3.

Table 3. Tensile properties of bio-based films.

Film	Carrot fiber (%)	Tensile Modulus (MPa)	Tensile strenght (MPa)	Strain at tensile strength (%)
Soja	-	44,56 ± 5,05	3,29 ± 0,54	207,28 ± 26,63
C1	15%	30,86 ± 0,91	2,00 ± 0,31	19,09 ± 7,36
	30%	71,41 ± 20,27	4,51 ± 0,94	26,03 ± 2,24
C2	5%	49,56 ±10,50	2,58 ± 0,53	16,39 ± 4,06
	15%	118,04 ± 20,43	6,55 ± 0,41	26,40 ± 2,79
C3	5%	238,55 ± 22,60	6,79 ± 0,25	9,63 ± 3,60
C4	5%	41,91 ± 8,17	2,51 ± 0,11	73,26 ± 23,87
C5	5%	57,08 ± 8,78	2,89 ± 0,22	13,69 ± 2,36

These three properties were plotted against the temperature applied in the hydrothermal fractionation to obtain each hydrolysis product. Additionally, the percentage of carrot fibre that has been used to reinforce each film is shown.

Figure 3. Plot of Tensile Modulus of films vs. temperature of hydrolysis conditions.

Figure 4. Plot of tensile strength of films vs. temperature of hydrolysis conditions.
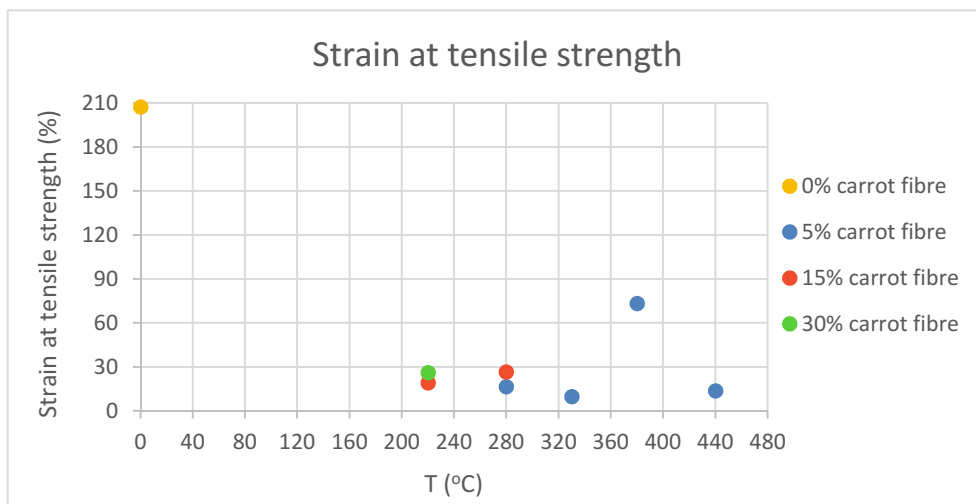
Figure 5. Strain at tensile strength of films vs. temperature of hydrolysis conditions.
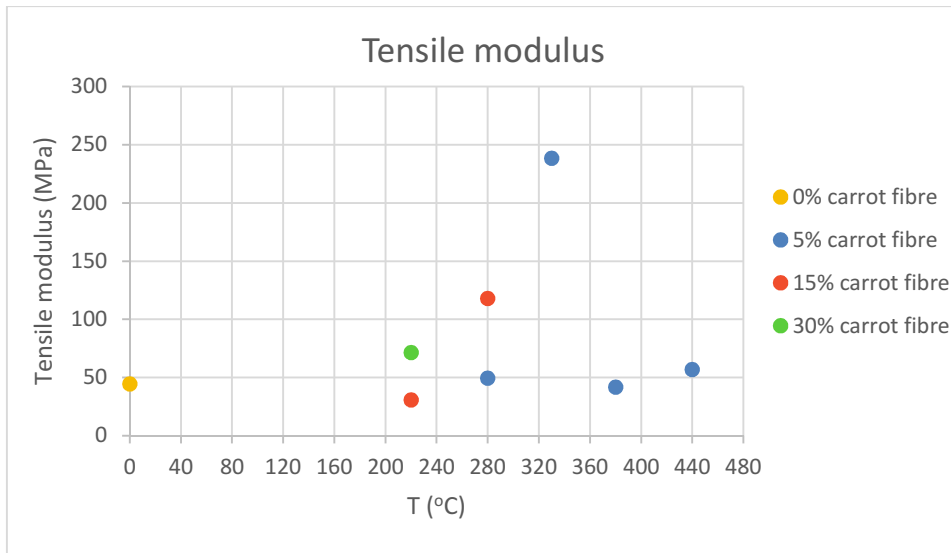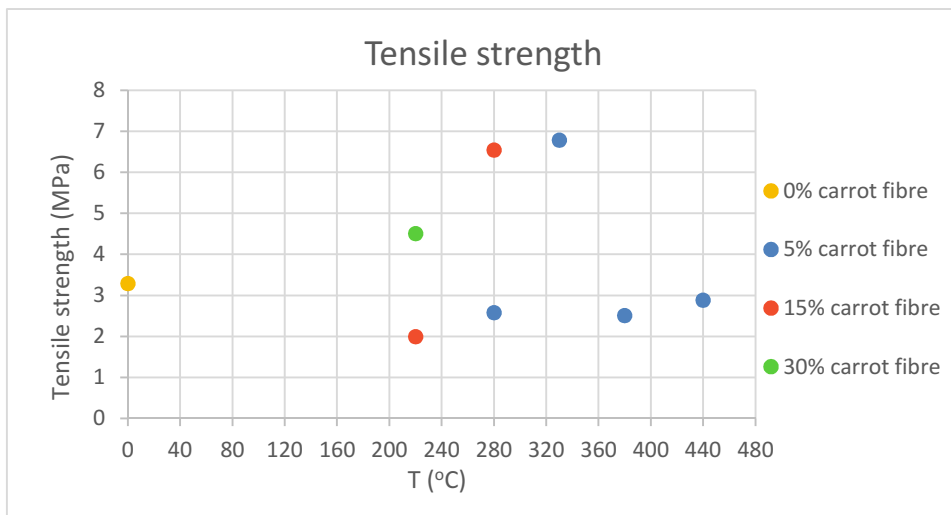
Evaluating the effect of incorporating different percentages of carrot fibre loadings on the properties of the films, it can be concluded that higher percentages of fibre obtained under the same pressure and temperature conditions provide greater rigidity and toughness.

None of the treatments succeeded in increasing the elongation at break with respect to the film made solely from soya. However, it has been possible to obtain films with higher stiffness.

Particularly, with the addition of 30% C1 or 15% C2 fibre, a higher Young's modulus and tensile strength are achieved, making them a good option for increasing stiffness, especially the latter.

There is another film, in which 5% carrot fibre from the C3 treatment was added, which manages to increase the Young's modulus by more than five times compared to the soy film and is much higher than that of the other reinforced films. Despite this great property, it has a lower elongation.

This gives an idea that the C3 treatment may have changed the particle size, dispersion, distribution or compatibility between carrot and soy, as its properties deviate from those of the other films with the same percentage of fibre.

Summary

To sum up, the biorefinery concept was used to reduce food waste carrots and use their components extracted by hydrothermal fractionation to manufacture bio-based films that could become substitutes for conventional plastic packaging.

In order to improve both rigidity and toughness, it would be necessary to optimize the compatibility between carrot and soy with a small particle size of carrot fibre and a high size distribution.

It could be also added an additive to prevent the growth of mold, which should be a natural antifungal that respects the principles of green chemistry so that the film remains a sustainable alternative.

Acknowledgements

References

Asgher, M., Qamar, S. A., Bilal, M., & Iqbal, H. M. N. (2020). Bio-based active food packaging materials: Sustainable alternative to conventional petrochemical-based packaging materials. *Food Research International*, *137*. https://doi.org/10.1016/j.foodres.2020.109625

Baiano, A. (2014). Recovery of biomolecules from food wastes - A review. In *Molecules* (Vol. 19, Issue 9, pp. 14821–14842). MDPI AG. https://doi.org/10.3390/molecules190914821

Mostafa, H., Airouyuwaa, J. O., Hamed, F., Wang, Y., & Maqsood, S. (2023). Structural, mechanical, antioxidant and antibacterial properties of soy protein isolate (SPI)-based edible food packaging films as influenced by nanocellulose (NC) and green extracted phenolic compounds from date palm leaves. *Food Packaging and Shelf Life*, *38*. https://doi.org/10.1016/j.fpsl.2023.101124

Nayak, A., & Bhushan, B. (2019). An overview of the recent trends on the waste valorization techniques for food wastes. In *Journal of Environmental Management* (Vol. 233, pp. 352–370). Academic Press. https://doi.org/10.1016/j.jenvman.2018.12.041

Peterson, A. A., Vogel, F., Lachance, R. P., Fröling, M., Antal, M. J., & Tester, J. W. (2008). Thermochemical biofuel production in hydrothermal media: A review of sub- and supercritical water technologies. *Energy and Environmental Science*, *1*(1), 32–65. https://doi.org/10.1039/b810100k

Rajinipriya, M., Nagalakshmaiah, M., Robert, M., & Elkoun, S. (2018). Homogenous and transparent nanocellulosic films from carrot. *Industrial Crops and Products*, *118*, 53–64. https://doi.org/10.1016/j.indcrop.2018.02.076

United Nations Environment Programme. (2021). *FOOD WASTE INDEX REPORT 2021*.

Zhang, J., Mungara, P., & Jane, J. (2001). Mechanical and thermal properties of extruded soy protein sheets. *Polymer*, *42*(6), 2569–2578. www.elsevier.nl/locate/polymer

Production of Bioaerogels for Biomedical Applications Using Supercritical CO₂

Nika Atelšek Hozjan[a], Gabrijela Horvat[a], Zoran Novak[a]

[a] Faculty of Chemistry and Chemical Engineering, University of Maribor

nika.atelsek@um.si

Introduction

As the world's population ages rapidly, various health conditions are becoming a significant problem. Among them are chronic wounds, traumatic injuries, bone defects caused by burns, diabetes, accidents, and age-related diseases such as osteoporosis. These conditions affect millions of people worldwide and generate high healthcare costs. They also cause pain, reduced mobility, and generally harm patients' quality of life. To overcome these challenges, effective treatments are needed to prevent long-term disability and improve patient well-being. In response, the research community has focused its efforts on regenerative medicine strategies, such as the development of advanced bio-based materials for tissue engineering. This includes the production of bioaerogels, which represent an innovative and promising solution for various biomedical applications [1–3].

Bioaerogels are materials made from naturally occurring polysaccharides and biopolymers. Due to their origin, they are biodegradable, biocompatible, and non-toxic, meaning they are well tolerated by the human body [4]. The porous structure, high specific surface area, good fluid absorption, and ability to encapsulate active ingredients make these materials unique and suitable for various applications such as wound healing, controlled drug delivery, and tissue regeneration. Their mechanical and physical properties can be improved by combining different biopolymers, resulting in materials that can also be used as scaffolds for bone regeneration [2].

Experimental

The key element in producing all types of aerogel structures (including organic, inorganic and hybrid) is forming a three-dimensional network with high porosity and sufficient stability. The traditional method for preparing all types of aerogels is a wet-chemical synthesis technique known as "sol-gel reaction" [1]. This process generally

involves several main steps: the mixing of precursors to form a "sol", gelation to convert the "sol" into a gel, and subsequent ageing and drying of the gels [5].

After gelation, the wet gel contains a three-dimensional network of pores filled with a solvent, which can be water, an organic substance, or a mixture of both. An aerogel is formed by replacing the liquid in the pores with gas without collapsing the structure of the wet gel. This outcome can only be achieved through supercritical drying, where supercritical fluids (SFs) are used as the working medium. SFs have a density like liquids and a viscosity like gases, allowing them to act as solvents and enable better mass transfer. Supercritical CO_2 (SC CO_2) is the most common choice for aerogel synthesis, as it transitions to a supercritical phase at temperatures and pressures exceeding its critical values: 31 °C and 73.8 bar, respectively. With its low viscosity and surface tension, SC CO_2 easily penetrates the gel pores, mixes with the solvent, and enables its removal [5].

Since water solubility in SC CO_2 is limited, it cannot be extracted effectively and is replaced by a solvent with better solubility in SC CO_2, such as ethanol, which converts the initial hydrogels into alcogels. The alcogels are then placed in a high-pressure container with an excess of solvent to prevent evaporation of the pore liquid and maintain the gel structure. Once the working conditions (temperature and pressure) are established, a constant stream of SC CO_2 is introduced into the high-pressure vessel, which infiltrates the pores of the material. SC CO_2 reaches the surface of the gel by convection and diffuses from there into the central pores of the gel. At the same time, the alcohol diffuses from the inner pores to the surface pores. This simultaneous transfer takes place as SC CO_2 combines with the alcohol in the pores, increasing the total volume of the liquid and allowing excess liquid to enter the external SC CO_2 stream. Initially, the mass flow of the liquid from the pores into the external SC CO_2 stream is accelerated due to the high concentration gradient. During the drying process, the concentration gradient decreases, resulting in reduced convective liquid transfer from the gel surface and less efficient solvent extraction from the pores. As drying progresses, the concentration of liquid in the pores gradually decreases, while the concentration of CO_2 in the pores increases. The supercritical drying process continues until all the solvent in the pores is replaced by SC CO_2.

The final step in the drying process is reducing the pressure in the high-pressure vessel. During this step, the pores of the gel are filled with SC CO_2, which gradually escapes from the pores as the pressure decreases. When the pressure drops below the critical value (73.8 bar), SC CO_2 turns into gaseous CO_2 and fills the aerogel pores. The

pressure must be reduced at an appropriate rate. If the rate is too high, the pressure outside the gel will drop faster than inside, leading to changes in pore size and porosity, causing the structure of the finished material to collapse. As the pressure decreases, the mixture of dissolved CO_2 and alcohol expands and forms two phases: a CO_2-rich gas phase and a liquid phase, which is essentially the solvent. The solvent-rich phase is collected and disposed of, while the CO_2 stream is returned to the system via a pump or compressor for reuse.

The result of supercritical drying is an aerogel with the same structure as the alcogel but with gaseous CO_2 in its pores instead of alcohol. The use of SC CO_2 in the synthesis of aerogels preserves their porosity, and high specific surface area and improves mechanical strength. It is also an environmentally friendly alternative, as SC CO_2 can be recycled and reused in the aerogel synthesis process.

In this work, we produced various aerogels from polysaccharides and biopolymers. We selected xanthan gum (XA), agar-agar (A), and polylactic acid (PLA) as starting materials. The gels were prepared using the "sol-gel synthesis" method (Fig. 1). First, we mixed the polysaccharides in water and the biopolymer in ethyl lactate. After gelation, and before supercritical drying, the solvents in the gels were replaced with absolute ethanol, turning them into alcogels. The alcogels were then stored in ethanol for 24 hours before being converted to aerogels using supercritical CO_2 technology. The final materials were characterized using advanced analytical methods to study their porosity, specific surface areas and morphology. The Brunauer-Emmett-Teller (BET) method was used to determine the surface area (m^2/g) and Barrett-Joyner-Halenda (BJH) method to determine the pore size and pore volume of the samples during nitrogen (N_2) adsorption-desorption analysis. Their morphology was analysed by scanning electron microscopy (SEM).

The results of the N_2 adsorption measurements are presented in Tab. *1*. The values in the table indicate that all the aerogels produced have a mesoporous structure, as the size of the pores is in the range of 2 to 50 nm. Additionally, the specific surface areas are high, reaching up to 396 m^2/g. These results confirm that supercritical drying preserves the porosity of the original gels without causing the inner structure to collapse.
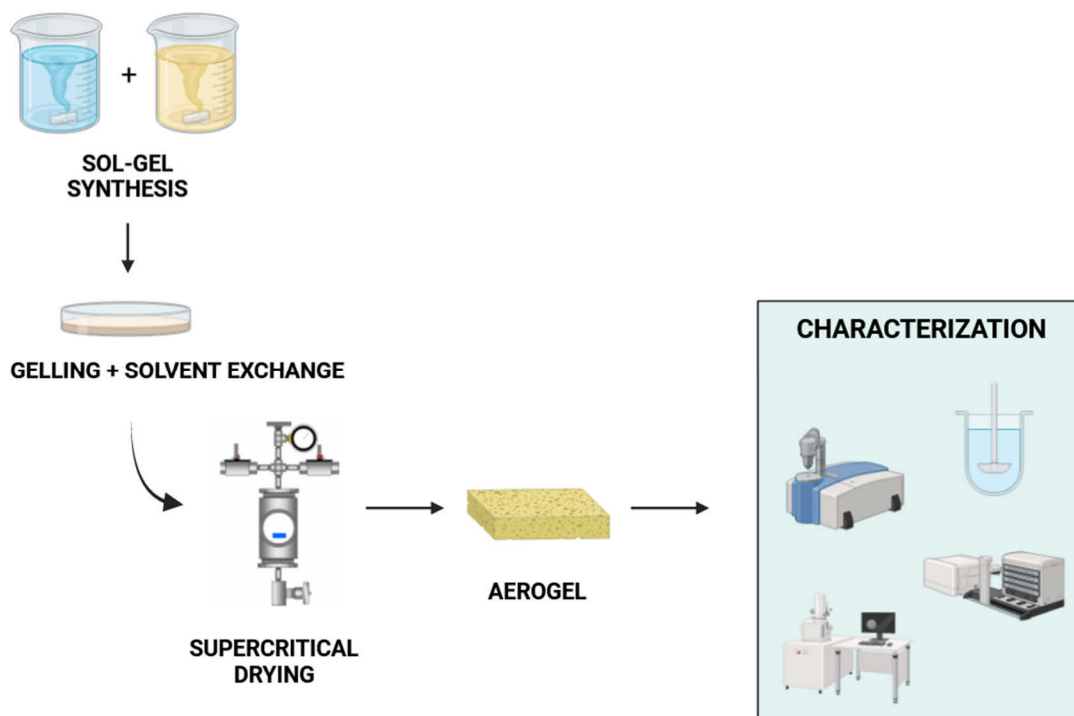
Fig. 1: Process scheme of bioaerogel production and characterization.

Tab. 1: Pore size, pore volume and specific surface areas (BET) of prepared aerogels.

Sample	Pore volume [cm³/g]	Pore size [nm]	BET [m²/g]
1XA4:2PLA4	1.92	18.10	342.26
1XA4:1PLA2	1.74	16.45	396.15
2A	0.63	9.14	272.30
6A	0.93	10.14	375.14
10A	0.87	10.23	314.17

XA - xanthan gum; PLA – polylactic acid; A – agar-agar

The results of the SEM analysis are shown in Fig. 2. These images confirm that all aerogels have a three-dimensional structure. Additionally, high porosity is observed, corresponding with the N_2 adsorption measurements. These findings validate the effectiveness of the supercritical drying method in preserving the inner structure of the starting gels, which is crucial for successful aerogel production.
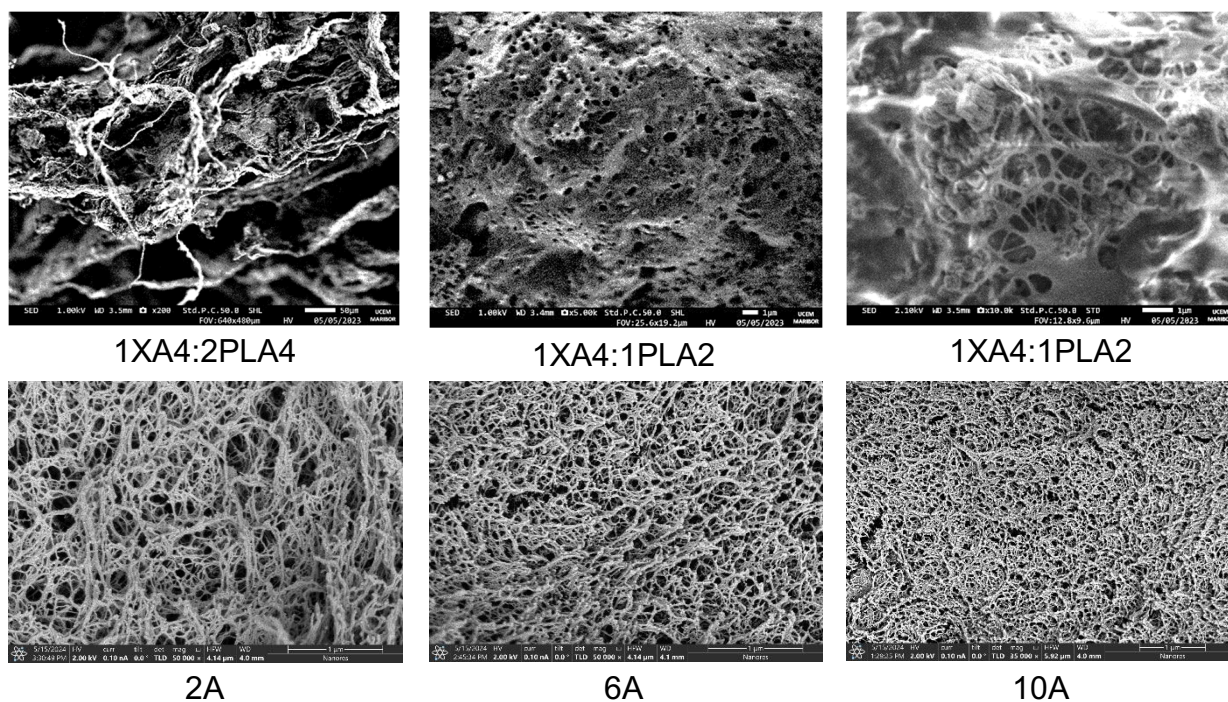
Fig. 2: SEM images of aerogels.

Summary

Various aerogels were prepared from the polysaccharide agar-agar and a combination of the polysaccharide xanthan gum and the biopolymer polylactic acid, resulting in a hybrid aerogel material. All aerogels were synthesised using the "sol-gel method" and supercritical drying with CO_2 to preserve the internal structure of the gels. The final materials were characterised by N_2 adsorption measurements and SEM analyses to determine their porosity and morphology. The results show that all aerogels produced have a 3D network with high porosity and a high specific surface area of up to 396 m^2/g. Additionally, all materials have pore sizes ranging from 2 to 50 nm, indicating a mesoporous structure. The SEM analysis results are consistent with the N_2 adsorption analysis, revealing a highly porous morphology. Our findings confirm that the supercritical drying method effectively preserves the internal structure of the initial gel and produces materials with high porosity and specific surface area - properties that are crucial for use in biomedical applications.

Acknowledgment

References

[1]   Soorbaghi FP, Isanejad M, Salatin S, et al. Bioaerogels: Synthesis approaches, cellular uptake, and the biomedical applications. Biomedicine & Pharmacotherapy. 2019;111:964–975.

[2]   Karamikamkar S, Yalcintas EP, Haghniaz R, et al. Aerogel-Based Biomaterials for Biomedical Applications: From Fabrication Methods to Disease-Targeting Applications. Advanced Science. 2023;10:2204681.

[3]   Bernardes BG, Del Gaudio P, Alves P, et al. Bioaerogels: Promising Nanostructured Materials in Fluid Management, Healing and Regeneration of Wounds. Molecules. 2021;26:3834.

[4]   Stergar J, Maver U. Review of aerogel-based materials in biomedical applications. J Sol-Gel Sci Technol. 2016;77:738–752.

[5]   Dervin S, Pillai S. An Introduction to Sol-Gel Processing for Aerogels. 2017. p. 1–22.

Mini-Plant Scaled Semi-Batch Experiments for Kinetic Investigations of Metallocene Catalyzed Solution Polymerizations

Phillip Weigmann, Markus Busch*

Ernst-Berl-Institute of Technical and Macromolecular Chemistry, Technical University of Darmstadt, 64287 Darmstadt/Germany, *e-mail: markus.busch@pre.tu-darmstadt.de

Introduction

The ever-increasing demand for versatile light-weight materials means that polyolefins such as polyethylene will continue to play a key role in world economics. Catalysis enabled the production of linear homo- and co-polymers of ethene, high-density (HDPE) and linear-low-density polyethylene (LLDPE). Additionally, catalysts allow industry to use low-pressure slurry and solution processes. Nowadays, alongside heterogeneous the ZIEGLER-NATTA- or PHILLIPS-type catalysts, molecular metal-organic compounds such as metallocenes are deployed under homogeneous conditions in solution polymerizations. Their uniform active sites enable a variety of reactions, including cross-couplings, metathesis as well as olefin polymerizations.[1] For olefin polymerizations, metallocene catalysts are of special interest due to their high catalytic activity.[2] Molecular weights and co-monomer incorporation are a result of the reaction kinetics which depend on the reaction conditions and catalyst used. Full understanding of a catalytic system for reaction engineering therefore requires knowledge of the influence of reaction conditions on kinetics. These necessary investigations can be carried out with semi-batch experiments in solution polymerization mini-plants.

Experimental

Known methodologies for kinetic investigations of metallocene catalysts use experimental semi-batch approaches at low pressures for fast and easy access to relevant kinetic parameters while allowing for variable process conditions.[2,3] Here, a mini-plant with a 260 mL autoclave by *Büchi* allows for experiments at up to 200 bar and 300 °C. A simplified flowsheet is shown in figure 1. The set-up includes multiple *Fink Chem+Tech* high-pressure dosing pumps for liquid components as well as two *IDEX* sample loops for precise injection of the catalyst and activator solutions. The gas fed into the reactor at any time is recorded by an individual *miniCORI flow* mass flow meter by *Bronkhorst*.
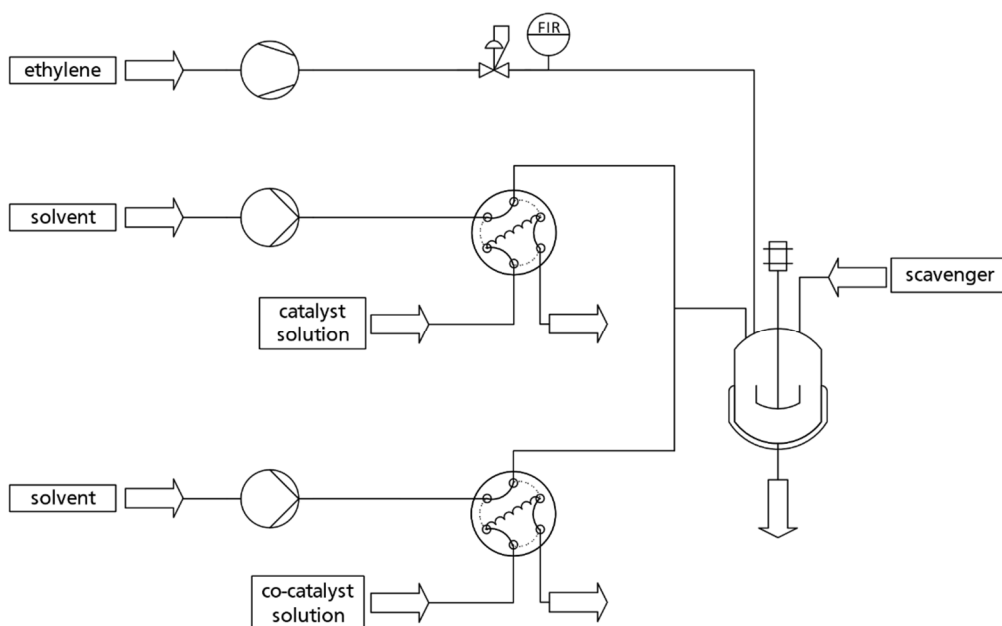
Fig. 1.: Simplified flowsheet of the mini-plant used to investigate the reaction kinetics of metallocene catalysts with semi-batch experiments.

The low-pressure semi-batch approach is carried out at a pressure of 14 bar which results in a heterogeneous phase equilibrium made from the solvent *n*-hexane and the monomer ethene. Those semi-batch experiments consist of three main procedural stages from which different information can be taken. First, the reactor is filled with solvent and heated to the desired temperature. In the second stage, the gaseous component ethene is fed to saturate the system with a pressure of 14 bar. The total amount of ethene flown into the reactor are recorded by the flow meter. A simulation-assisted evaluation methodology was set up and used to depict the state the phase equilibrium.[2,3] The PC-SAFT equation of state is implemented in *KBC Multiflash* which gives the amounts of each compound in each phase. It uses the ethene uptake form this stage as input parameters. Figure 2 shows the amount of ethene dissolved in the liquid phase at 14 bar and different reaction temperatures as calculated by the PC-SAFT model. It can be seen that the ethene concentration in the liquid phase increases significantly when lowering the temperature from 170 °C to 130 °C. This pure thermodynamic influence is an important factor considering the following polymerization only takes place in the liquid phase.
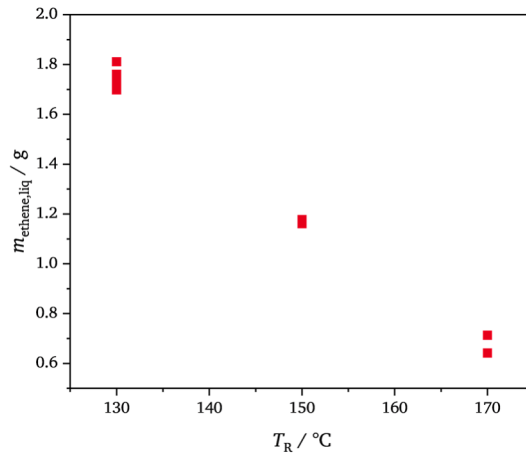
Fig. 2.: Ethene amount dissolved in the liquid phase for homo-polymerizations of ethene at different temperatures and 14 bar calculated with the PC-SAFT model.

To start the polymerization, a defined amount of the catalytic system is injected into the reactor through the sample loops. The pressure in the reactor is held constant so that consumed ethene is equaled out at an instant. Kinetic analysis is carried out by adapting a literature known linear regression concept by SOARES and MEHDIABADI [5,6] based on the gas flown into the reactor recorded by the flow meter. It accesses the rates of propagation and rate of deactivation. Figure 3 a) shows the estimated kinetic parameters for the homo-polymerization of ethene at different reaction temperatures.
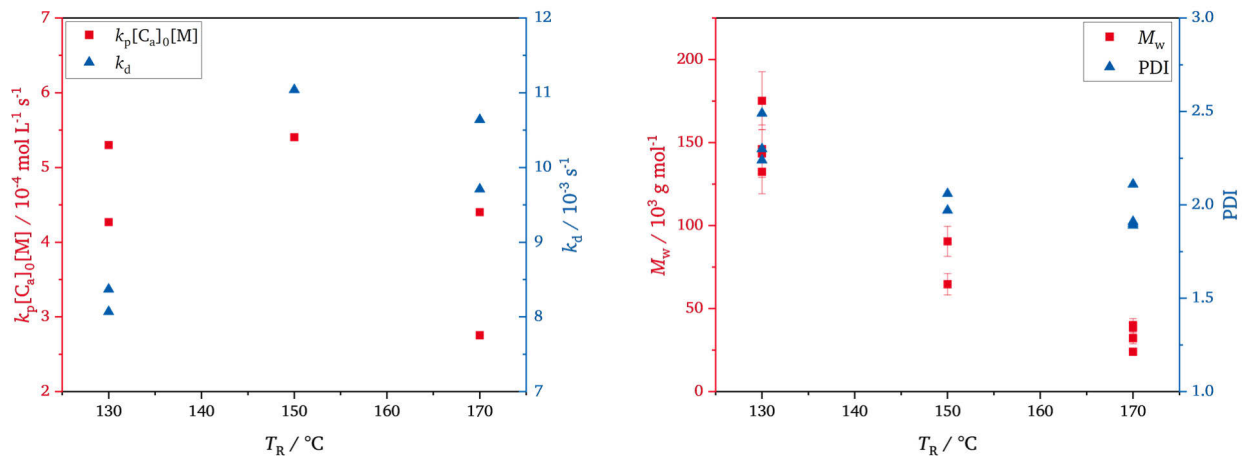
Fig. 3.: Kinetic evaluation and polymer properties of metallocene catalyzed ethene polymerizations at 14 bar with different reaction temperatures. a) Estimated rates of propagation (red) and deactivation (blue) for the homo-polymerization of ethene. b) Weight average molecular weight (red) and polydispersity (blue) of ethene homo-polymers produced at 14 bar with different reaction temperatures.

The estimated rates of propagation increase with lower reaction temperatures. Polymerizations are exothermic reactions and therefore favor lower temperatures. The

determined rate of deactivation allows for estimation of the lifespan of a catalyst molecule. Increasing values for deactivation indicate a shorter lifespan due to the decay of the molecular structure at higher temperatures. Figure 3 b) displays molecular weights of polymers produced analyzed with high-temperature size-exclusion chromatography. It was observed that the weight-average molecular weight increases when decreasing the reaction temperature. Those observations agree with the former thermodynamic and kinetic findings of figure 2 and 3 a). The combined effect of higher monomer concentration and the longer lifespan of the catalyst at lower temperatures yield longer polymer chains with very narrow molecular weight distributions. The slight increase in polydispersity at 130 °C is a result of temperature variation caused by the emitted reaction heat which is more pronounced at lower temperatures.

Summary

The mini-plant scaled semi-batch experiments allow with the modelling assisted evaluation of the phase equilibrium and the reaction kinetics lead to a better understanding of metallocene catalyzed polyethylene synthesis. The reaction temperature effects the state of the phase equilibrium. Lower temperatures increased the ethene amount dissolved in the liquid phase. In addition, kinetic analysis showed that at those lower reaction temperatures, the rate of propagation as well as the lifespan of the catalyst increases. Molecular weights were shown to decrease at higher temperatures which is caused by the combined effects of thermodynamic phase behavior and reaction kinetics.

References

[1]   A. Behr, P. Neubert, *Applied homogeneous catalysis*, 1. ed., Wiley-VCH-Verl.,Weinheim, **2012**.

[2]   W. Kaminsky, A. Laban, *Appl. Catal., A*, **2001**, *222*, 47–61.

[3]   I. Kronshorst, *PhD Thesis*, unpublished work.

[4]   L. Ständecke, *PhD Thesis*, unpublished work.

[5]   S. Mehdiabadi, J. Soares, D. Bilbao, J. Brinen, *Macromol. React. Eng.*, **2011**, *5*, 418–430.

[6]   S. Mehdiabadi, J. Soares, J. Brinen, *Macromol. React. Eng.*, **2017**, *11*, 1600044.

Catalytic Carbon Dioxide Reduction

Fernando Caballero Rojo

Departament of Chemical Engineering and Environmental Technology,

University of Valladolid, fernando.caballero@uva.es

Introduction

In recent years, climate change is one of the main topics of concern around the world. The high concentrations of greenhouse gases, among which carbon dioxide stands out. Within this framework, all institutions are working to reduce CO2 emissions, and thereby reduce the temperature of the planet. The Paris Agreement aims to limit global warming to less than 2 C above the temperature in pre-industrial times (del Río et al., 2021).

In this framework, institutional recommendations promote the use of renewable energies, but the need to continue using fossil fuels makes the use of carbon dioxide capture and storage technologies of vital importance for the future. This is where the importance of this project arises, in which we will work with a technology based on amines to achieve the capture and storage of CO2, and to study the reduction of emissions(Andérez-Fernández et al., 2018).

In this way, we will work with a hydrothermal conversion process of carbon dioxide through capture with amines. It is a known and studied process, which provides great advantages to the conversion of CO2. The objective of the project is to create a kinetic model of the catalytic reaction through which the conversion of CO2 occurs.

Experimental

Materials

The products used in the process are:

- Palladium in carbon as a catalyst, from the Aldrich brand,
- 3-amino-1-propanol amine, 99% pure, also from the Aldrich brand.

Regarding the team:

- Non-stirred reactor, Parr, Model 4791, volume 25 mL, T316 stainless steel.
- Aggregated Parr reactor, with a volume of 50 mL

Amine charge

For the preparation, an aqueous solution of this amine is made and CO_2 is loaded into it. Once the solution has been made in the fume hood, it is transferred to a bottle with a stopper containing holes. The carbon dioxide is pumped through one of the holes. The CO_2 bottles are also in a separate booth, and once opened, the tube is introduced into the solution, so that the carbon dioxide begins to load into the solution. This process is carried out with low pressures in the CO_2 line, controlling the pressure at all times so that the pipes do not freeze, and ensuring that no problems occur in them. The CO_2 loading process is maintained for half an hour. Once the amine has been loaded, it is subjected to a total organic carbon analysis in a TOC device to determine the amount of carbon in the amine.

Reactions

For the experiments, it is shown with a batch reaction system, in which the reagents and catalyst are loaded, and once connected to the piping system, can be introduced into the gas. In the laboratory of the University of Valladolid, we work with a two-reactor system, which follows the diagram shown in Figure 1. This system allows us to work both with a single reactor and with the two batch reactors at the same time. The reactors are reactors prepared to work under high pressure conditions and also withstand high temperatures, to which they are subjected when heated.

Fig. 1.: Process flow diagram

As can be seen in the diagram, there are two lines for the gas feed to the reactors, one for the nitrogen feed and one for the hydrogen feed. In the case of our laboratory, the hydrogen is contained in a bottle in a small hut outside the laboratory for safety reasons. Each time the hydrogen is to be filled, the bottle and several intermediate valves along the entire line have to be opened. As soon as all the venting has been done and the reactor has been loaded with hydrogen, all the lines containing nitrogen are vented again and the cylinder is closed to ensure safety.

The nitrogen bottle is located in the same room as the reactors and, like the hydrogen bottle, has a valve to control the pressure. In both reactors, there is a nitrogen valve on the inlet line and another one on the outlet line, the first one for feeding the reactors, and the second one so that, when venting the hydrogen from the reactor, it is diluted in nitrogen and does not release hydrogen only through the vent. In addition, there is a vent valve on the outlet of each of the reactors, to vent the reactor, and another on the inlet line, which serves to vent this line.

Fig. 2.: Image of the 25 mL reactor

Palladium in carbon is being used as a catalyst. As it is a batch process, the reactor must be loaded first with the amine and the catalyst. In one of the reactors, we work with a volume of amine of 20 mL, in which, in the case of palladium in carbon, 0.1 grams of catalyst must be added. With the rest of the catalysts, the amount that needs to be added depends on the catalyst. In the other reactor, whose volume is half, 10 mL of amine must be added, and the amount of catalyst is also half.

The larger volume reactor has a mechanical stirring system using a stirrer located on the reactor lid, which is subsequently connected to a mechanical motor that rotates it. In the case of the smaller volume reactor, the stirring is magnetic, so when loading the reagents, a stirring magnet must be added, which will then rotate thanks to this magnetic stirring.

Once the reactors have been filled, they are closed with the lid by placing a clamp system that is tightened with screws, which guarantees the correct closure of the reactor and that there are no leaks. With this, the reactor pipes are joined with those of the plant, incorporating the reactor into the system. The first step prior to the reaction is venting with nitrogen, to eliminate any air that may remain. This venting is carried out four times, passing nitrogen through the reactor, at a pressure similar to that at which the hydrogen will be introduced. After this, the reactor is vented with hydrogen, passing it three times, to eliminate any nitrogen that may remain present. Whenever hydrogen is vented, the nitrogen valve on the outlet line must remain open, as undiluted hydrogen cannot be vented for safety reasons.

Fig. 2.: Image of the 50 mL reactor

Once all the venting has been carried out, the reactor is filled with hydrogen to operating pressure. The heating of the reactor is carried out by means of a heating jacket, which covers the entire reactor, and which electrically heats the reactor to the indicated temperature. Before starting the reaction, a jacket of insulating material is placed to cover

both the heating system and the reactor, and the upper part is also covered with insulating material to guarantee correct cooling. In the case of the reactor where the agitation is given by a motor, there is a water cooling system in the part where the agitation is, to avoid overheating in that area. As already said, the hydrogen detector is passed at all times during the reaction, and if a leak is detected, the reaction is stopped.

Experiments are being carried out at three different temperatures, three different pressures and three different catalyst concentrations. Once the reaction has concluded, the heating system is removed and the reactor is placed in a bath of cold water with ice, to accelerate cooling. When the temperature has decreased, the hydrogen is emptied from the reactor, and it is vented up to three times with nitrogen to eliminate all the hydrogen. When everything is depressurized, the reactor is removed from the system and the reactor is opened.

Samples analysis

The contents of the reactor are filtered by vacuum filtration, so that the liquid sample is prepared for analysis, and the solid catalyst is taken to the corresponding drying system for subsequent recovery. Liquid sample analysis is performed on a liquid chromatography column. The HPLC equipment (Waters, Alliance separation module e2695) has an IR detector (Waters, model 2414) and an Aminex HPX-87H column to analyse the samples. The mobile phase used is a solution of sulfuric acid that circulates with a flow of 0.6 mL/min, for half an hour for each sample. The column temperature is 60ºC and the detector temperature is 30ºC.

Safety system

In addition, high safety measures are in place at all times when hydrogen is used. In the room where the reactors are located, there is a detector that detects hydrogen from 4000 parts per million, 10% of the explosive limit. As soon as it detects this, the system automatically closes the hydrogen line. In addition, there is a manual hydrogen detector that detects hydrogen from 40 ppm. This detector is being passed around the reactor while it is being loaded with hydrogen, and during the reaction it is passed every few seconds to ensure that there are no leaks. If it detects any hydrogen in the environment, the reaction is stopped and the reactor and the line are vented.

Summary

In summary, various catalysts are being tested in CO_2 reduction processes in reactions with amines, previously loaded with carbon dioxide, for the determination of the kinetic model of the reaction. These reactions are carried out in batch reactors, pressurized with hydrogen, at a certain temperature and with stirring. With the results obtained from all the reactions, the reaction model will be determined methodically, which is the objective of the project.

Acknowledgements

References

Andérez-Fernández, M., Pérez, E., Martín, A., & Bermejo, M. D. (2018). Hydrothermal CO2 reduction using biomass derivatives as reductants. *The Journal of Supercritical Fluids*, *133*, 658–664. https://doi.org/10.1016/J.SUPFLU.2017.10.010

del Río, J. I., Pérez, E., León, D., Martín, Á., & Bermejo, M. D. (2021). Catalytic hydrothermal conversion of CO2 captured by ammonia into formate using aluminum-sourced hydrogen at mild reaction conditions. *Journal of Industrial and Engineering Chemistry*, *97*, 539–548. https://doi.org/10.1016/j.jiec.2021.03.015

Investigation of the Pressure and Power Characteristics of Planetary Roller Extruders

Daniel Terhorst

Mechanical Engineering/Particle Technology

Ruhr-Universität Bochum

Daniel.Terhorst@ruhr-uni-bochum.de

Introduction

The planetary roller extruder was invented by Ludwig Wittrock in 1953 and was initially only used in the PVC calendaring industry. Since the mid-1980s, its potential for new fields of application was discovered. Today, for example, it is used in powder coatings and the production of wood-polymer compounds. [1,2]

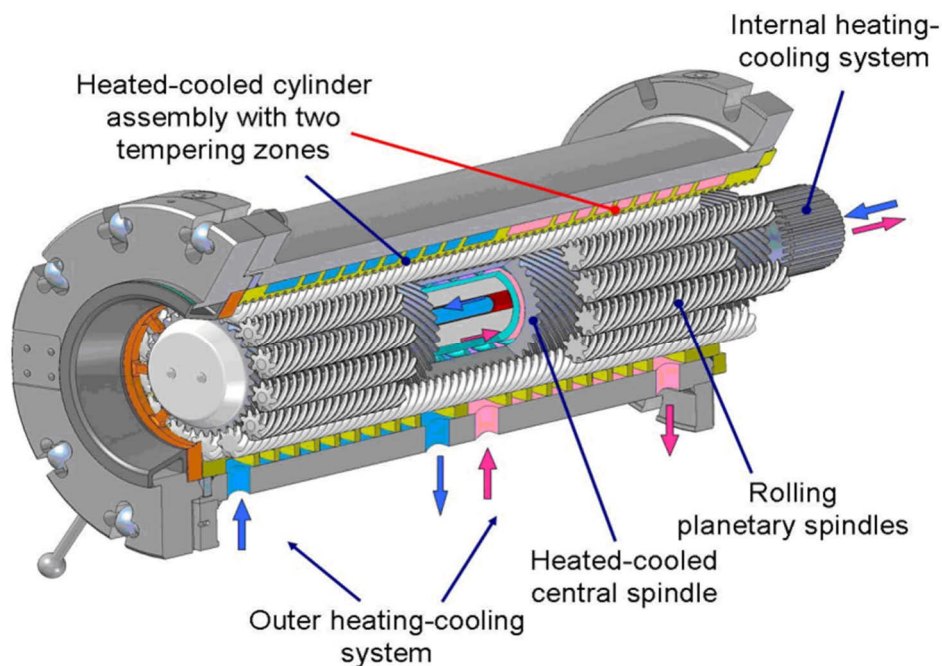Figure 1 planetary roller extruder [3]

Despite the long history of development and the advantages of the planetary roller extruder, there is a lack of knowledge about the transportation behavior of the planetary roller extruder [4]. For other extruders, like the single-screw and twin-screw extruders, there is an extensive knowledge of the power/throughput and pressure/throughput characteristics.

In the progress of my work, a methodology for analysing these characteristics will be developed for the planetary roller extruder. The challenge here is that the planetary roller extruder differs from the single-screw and twin-screw extruders in terms of its geometry and transportation mechanisms.

This methodology is to be applied to existing test data from tests with two materials on the PWE30 and PWE70 from the ENTEX Rust & Mitschke GmbH. The characteristics are to be derived and their main influencing variables from rotation speed, temperature, mass flow, extruder configuration, extruder size and material identified. In addition, an outlook on the prediction of the characteristics of operating parameters that have not yet been investigated is also a goal of my work.

Experimental

There are two planetary roller extruders used in the experiment, which have a diameter of 35.4 and 70.7 mm and consist of two roller cylinders, separated by a dispersing ring. The second roller cylinder has a nozzle at the end which can be closed.

The materials investigated are the two structurally viscous polymers HD-PE 53090 and LD-PE MP 20.

In the first rolling cylinder there are five nab spindles for picking up and melting the material in each test, while between three to six standard or nab spindles are installed in the second rolling cylinder. The different spindles can be seen in Figure 2.
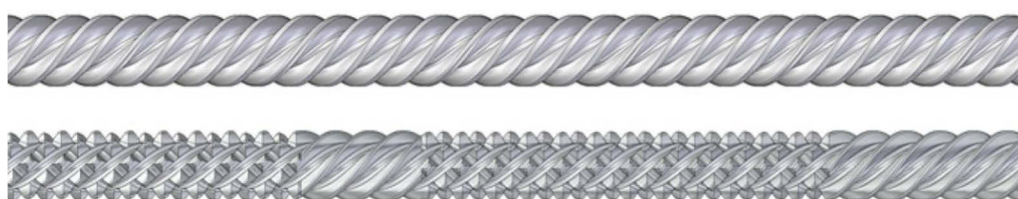
Figure 2 different spindles, standard spindle at the top and nab spindles at the bottom [1]

The two series of tests carried out are a residence time test with an open nozzle and a pressure build-up test with a closed nozzle. In the pressure build-up test, experiments are carried out with different filling levels, while the flow rate is varied in the residence time test.

In addition, different temperatures and rotation speeds of the central spindle are considered in the experiments.

For the characteristics, the dimensionless quantities from Pawlowski [5] were used, which can be used to describe the transportation behavior of single-screw extruders. In these quantities, the pressure difference and the drive power are set as a dependency of the screw speed and the volume throughput.

Throughput number: $$Q = \frac{\dot{V}}{N \cdot D^3} \qquad \text{eq. 1}$$

Pressure number: $$K = \frac{\Delta p \cdot D}{\eta \cdot N \cdot L} \qquad \text{eq. 2}$$

Power number: $$\Pi = \frac{P}{\eta \cdot N^2 \cdot L \cdot D^2} \qquad \text{eq. 3}$$

Summary

The dimensionless quantities enable a pressure-throughput characteristic for HD-PE 53090 that is similar to the known characteristic curves of other extruders. The pressure number decreases when the throughput number increases. This also occurs with LD-PE MP 20 in the PWE70. In the Experiments at the PWE30, a different characteristic is formed, the pressure number initially falls and then rises again as the throughput number increases.

The main factor influencing the pressure number is the throughput number. The number of spindles and the spindle configuration also have a major influence on the pressure number. A high number of spindles results in lower pressure numbers and ensures that the pressure number decreases more slowly as the throughput number increases. Nab spindles also ensure a lower gradient of the pressure-flow characteristic than standard spindles. It is not possible to determine whether the material or the size of the extruder had a greater influence on the tests. HD-PE 53090 and a larger size of extruder ensure a lower gradient of the characteristic. The rotation speed has a smaller influence. A higher rotation speed results in a lower pressure coefficient. A clear influence of the temperature could not be determined.

In the partially filled range, the power/throughput characteristic behaves analogously to the known characteristic curves from the literature. The power number increases as the throughput number increases. However, the power/throughput characteristics in the fully filled range in the planetary roller extruder differs from other extruders. While the power number in the fully filled range decreases with increasing the throughput number in the

single-screw and twin-screw extruders, it continues to increase in the planetary roller extruder.

The main factor influencing the power number is the throughput number. The material also has a major influence. LD-PE MP 20 has a higher power number than HD-PE 53090. A reduction in the number of spindles also results in higher power numbers. The influence of the size of the extruder is different for both materials. For LD-PE MP 20, the power numbers are higher in PWE70 than in PWE30, while this does not influence HD-PE 53090. The spindle type has a fewer influence, while the power number is lower for nab spindles than for standard spindles. Rotation speed and temperature have the fewest influence. A higher temperature and a lower rotation speed result in an increased power number. In addition, a higher rotation speed causes the power/throughput characteristic to increase more quickly.

References

[1] Klemens Kohlgrüber, Michael Bierdel und Harald Rust, Polymer-Aufbereitung und Kunststoff-Compoundierung: Grundlagen, Apparate, Maschinen, Anwendungstechnik. München: Hanser, 2019.

[2] T. Birr, "Verarbeitung von langglasfaserverstärten Thermoplasten für Spritzgussanwendungen auf dem Planetwalzenextruder," Dissertation, Technische Universität Berlin, Berlin, 2016

[3] Michael W. Batton, Harald Rust, " Adhesive Processing using a Planetary Extruder", ENTEX Rust & Mitschke GmbH, Bochum, Germany, 2021

[4] J. Rudloff, "Modellbildung und Vorabschätzung für das Betriebsverhalten eines Planetwalzenextruders," Dissertation, Technische Universität Ilmenau, Ilmenau, 2021.

[5] J. Pawlowski, Transportvorgänge in Einwellen-Schnecken: Förder-, Homogenisier- und Wärmeaustausch-Verhalten, 1. Aufl. (Grundlagen der chemischen Technik). Frankfurt am Main, Aaarau, Frankfurt am Main, Salzburg: Salle; Sauerländer, 1990

Investigating CO_2 Transport Properties in High-Pressure Conditions for Applications in the CCUS Supply Chain Through Experimental and Modelling Methods

Roberta Di Carlo

Department of Civil, Chemical, Environmental and Materials Engineering,

Alma Mater Studiorum - University of Bologna, via Terracini 28, Bologna, Italy

roberta.dicarlo5@unibo.it

Introduction

Carbon capture utilization and storage (CCUS) is a process aimed at separating carbon dioxide from mixed gaseous streams and transporting for use or storage. It is a powerful short-term solution to significantly reduce greenhouse gas emissions and mitigate global warming effects. Since carbon dioxide represents 75% of these emissions, to lower its emission in the atmosphere is a critical and challenging concern [1]. The IPCC (Intergovernmental Panel on Climate Change) has set a 40% reduction of global CO_2 emissions as a target by 2030 and the net zero achievement by 2050 to meet the goals of the Paris Agreement. CCUS is composed of 4 different stages:

1. Carbon capture involves the separation of CO_2 from mixed gas streams generated by industrial processes.
2. Carbon transport deals with the transportation of CO_2 to designed sites.
3. Carbon utilization refers to the use of CO_2 in various industrial processes and applications.
4. Carbon storage involves storing the captured carbon dioxide in geological formations

The use of membranes for CO_2 capture has gained relevance due to advantages like lower energy requirements, compactness and ease of operation. Dense membranes, used for this purpose, may be classified as either organic or inorganic based on their material composition. In this regard, organic membranes, composed of polymeric materials, emerged as particularly promising due to their versatility and processability [2]. CO_2 transportation is typically achieved by means of ships or pipelines, depending on external factors, such as the distances to be covered. In any case, CO_2 should be transported in the so-called dense phase (i.e. supercritical conditions or near the triple point) in order to get higher transportation efficiency [3,4]. In such severe conditions, characterized by high pressure, CO_2 may interact with the polymeric components that,

thanks to their high corrosion resistance, are often used as liners, gaskets, or sealings along transportation infrastructures.

The activity carried out in my PhD project is focused on the first two stages of CCUS: CO_2 capture and transport. Hence, the research involves the use of thermodynamic tools, flow characteristics, and non-equilibrium phenomena. By employing a combination of experimental and modeling approaches, the project aims to gain a comprehensive understanding of mechanisms involved in CCUS to develop effective climate change mitigation strategies.

Experimental

The experimental section focuses on the development of polymeric membranes and mixed polymeric membranes to be used in CCUS. Polymeric materials have gained relevance in membrane separation processes due to their versatility, ease of processing, and low cost. However, their main drawback is the inability to simultaneously achieve high permeability and high selectivity (i.e., high productivity and separation efficiency). Such feature is depicted in Robeson's upper bound and drives a relevant portion of the field research to develop systems that can overcome that limitation [5,6].

One promising strategy is about mixed-matrix membranes, where nanomaterials are typically dispersed in the polymer matrix to combine advantages of polymers with the sieving capacity of nanofillers [7,8]. For instance, graphene and graphene derivative emerged as rising stars in the field of nanomaterials, due to their minimal thickness (less than 1 nm) guaranteeing high membrane permeance, and highly selective character [9,10].

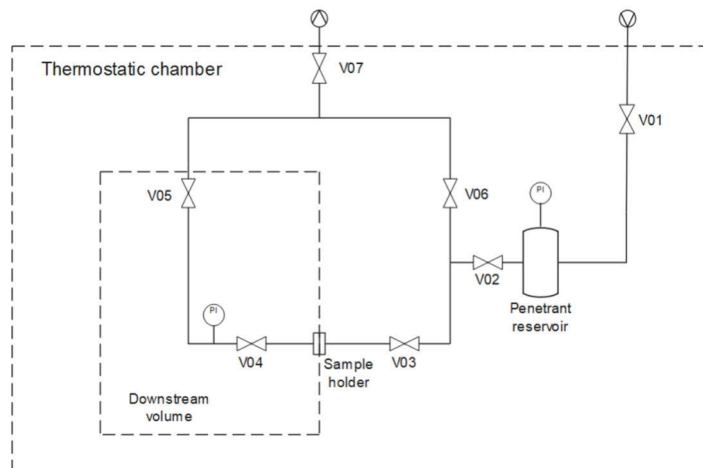The aim is to develop ultra-thin composite systems with the addition of nanomaterials.

Figure 1, Layout of the permeometer apparatus

Dense thin films made up of Matrimid polyimide (provided in powder by Huntsman) have been produced by means of doctor blade solvent casting on top of a porous polymeric support. These films are coated with a graphene oxide multilayer, serving as the actual active layer for the separation process.

Permeation tests on these polymer-based systems are performed using a manometric apparatus, whose layout is illustrated in Fig. 1, developed in house according to ASTM D1434-82 (2015)e1 [11].

The effect of CO_2 uptake in diverse polymeric materials will be studied in high-pressure conditions after setting up of new experimental apparatuses, including pressure decays. Additionally, CO_2 induced variation of polymeric structure and properties will be investigated through the use of Differential Scanning Calorimetry and X-Rays Diffraction techniques.

Modeling

Thermodynamic modelling is applied to investigate the sorption and transport properties (i.e., diffusion and permeability) of polymers exposed to CO_2, under high pressure or supercritical conditions.
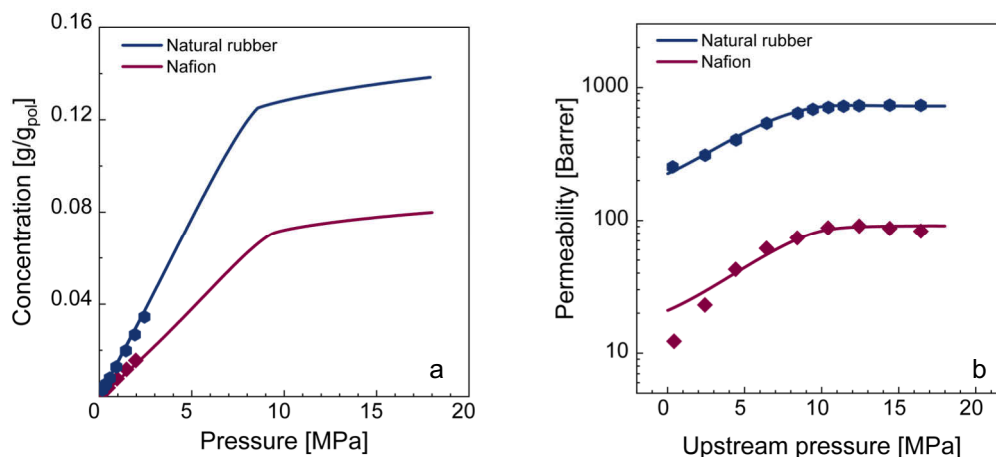
Figure 2, Sorption and permeability of CO_2 in Natural rubber and Nafion. Experimental data are from: (a)[12,13] (b) [14]. Curves are from (a) EoS and (b) ST calculations.

The sorption of CO_2 (and more in general gases) in polymers is effectively described using the Sanchez-Lacombe equation of state, and its rearrangement, Non Equilibrium Thermodynamics for Glassy Polymers (NET-GP), for nonequilibrium conditions [15–17]. At the equilibrium, the chemical potential may be written as follows:

$$\mu_i^s(T, p, \rho_{pol}, \omega_i) = \mu_i^g(T, p) \qquad (1)$$

In rubbers, equilibrium conditions allow to univocally determine the polymeric density on the basis of temperature T, pressure p, and composition ω.

$$\rho_{pol} = \rho_{pol}^{eq}(T, p, \omega) \tag{2}$$

On the other hand, when dealing with glassy systems the previous equation does not hold true, and the polymeric density should be corrected with the swelling coefficient k_{sw}, considering that the polymer swells with a linear trend with pressure [18].

$$\frac{1}{\rho_{pol}} = \frac{1}{\rho_{pol}^0}(1 + k_{sw}p) \tag{3}$$

Where ρ_{pol}^0 is the density of the polymer in the dry state.

Permeability is then estimated, by using the Standard Transport Model (STM), considering that the diffusive mass flux across the membrane can be written as follows:

$$J_1 = -\rho L \omega_i \nabla \left(\frac{\mu_i}{RT}\right)_{T,P} \tag{4}$$

Where L is a kinetic factor that depends on CO_2 concentration in the polymer. Coupling equation 4 with the definition of permeability, it is possible to write [19]:

$$P_i = \frac{1}{p_i^u - p_i^d} \int_{p_i^d}^{p_i^u} L_0 e^{\beta \omega_i} S_i z_i dp_i \tag{5}$$

$p_i^u - p_i^d$ is the partial pressure difference between the upstream and the downstream of the polymer, S_i is penetrant solubility in the polymer, while z_i is the compressibility factor of i in the pure gas state. The only two adjustable parameters are the infinite dilution mobility coefficient L_0, that is linked to the polymer fractional free volume, and β, the plasticization factor that accounts for polymer swelling induced by the gas penetrant.
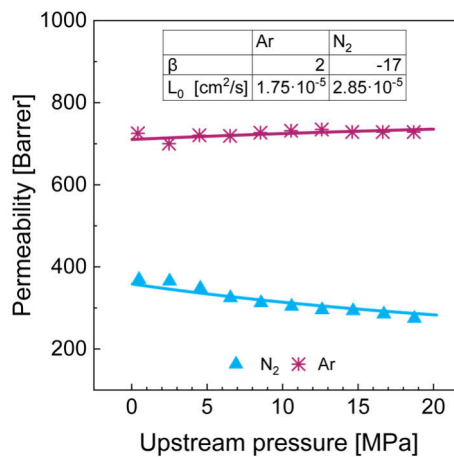

Figure 3, Permeability of N_2 and Ar in PDMS at 45°C. Experimental data from [14,20]. Curves are from STM calculations.

The modeling framework is effective in predicting solubility, diffusivity and permeability behavior of different penetrant gases (i.e., CO_2, N_2 and Ar) in various polymeric systems: P84/Matrimid polyimide blends, Nafion, Natural Rubber (NR), Silicon Rubber (PDMS) and fluorine rubber (FKM). Additionally, this combination of EoS and STM provides interesting insights in high-pressure and supercritical conditions, helping to reduce the extent of the experimental campaign.

Summary

This project investigates CO_2 transport in polymers, focusing on both pure components or in gaseous mixtures, to optimize carbon capture and transport processes. A high-pressure setup will be developed for permeation and sorption testing, allowing for in-depth analysis of these phenomena. Mixed matrix membranes will be the primary platform for developing of CO_2 capture systems. The project will also evaluate the effects of supercritical CO_2 on polymers, comparing the observed experimental behavior with modeled predictions. Such comprehensive approach will be useful to achieve a deeper understanding of all the relevant phenomena for gas transport in polymeric materials.

Acknowledgment

References

[1] R. Nataly Echevarria Huaman, T. Xiu Jun, Energy related CO2 emissions and the progress on CCS projects: A review, Renewable and Sustainable Energy Reviews 31 (2014) 368–385. https://doi.org/10.1016/j.rser.2013.12.002.

[2] Y. Yampolskii, I. Pinnau, B. Freeman, eds., Materials Science of Membranes for Gas and Vapor Separation, 1st ed., Wiley, 2006. https://doi.org/10.1002/047002903X.

[3]   L. Ansaloni, B. Alcock, T.A. Peters, Effects of CO2 on polymeric materials in the CO2 transport chain: A review, International Journal of Greenhouse Gas Control 94 (2020) 102930. https://doi.org/10.1016/j.ijggc.2019.102930.

[4]   U. Berge, M. Gjerset, B. Kristoffersen, M. Lindberg, T. Palm, T. Risberg, C.S. Skriung, CARBON CAPTURE AND STORAGE, (n.d.).

[5]   L.M. Robeson, Correlation of separation factor versus permeability for polymeric membranes, Journal of Membrane Science 62 (1991) 165–185. https://doi.org/10.1016/0376-7388(91)80060-J.

[6]   L.M. Robeson, The upper bound revisited, Journal of Membrane Science (2008).

[7]   A. Arabi Shamsabadi, H. Riazi, M. Soroush, Mixed Matrix Membranes for CO2 Separations, in: Current Trends and Future Developments on (Bio-) Membranes, Elsevier, 2018: pp. 103–153. https://doi.org/10.1016/B978-0-12-813645-4.00004-0.

[8]   F.N. Al-Rowaili, M. Khaled, A. Jamal, U. Zahid, Mixed matrix membranes for H2/CO2 gas separation- a critical review, Fuel 333 (2023) 126285. https://doi.org/10.1016/j.fuel.2022.126285.

[9]   U.K. Sur, Graphene: A Rising Star on the Horizon of Materials Science, International Journal of Electrochemistry 2012 (2012) 1–12. https://doi.org/10.1155/2012/237689.

[10] H.W. Yoon, Y.H. Cho, H.B. Park, Graphene-based membranes: status and prospects, Phil. Trans. R. Soc. A. 374 (2016) 20150024. https://doi.org/10.1098/rsta.2015.0024.

[11] ASTM-D1434-82-2015-e1, (2015).

[12] R.C. Reis Nunes, M. López-González, E. Riande, Basic studies on gas solubility in natural rubber–cellulose composites, J Polym Sci B Polym Phys 43 (2005) 2131–2140. https://doi.org/10.1002/polb.20507.

[13] M. Mukaddam, E. Litwiller, I. Pinnau, Gas Sorption, Diffusion, and Permeation in Nafion, Macromolecules 49 (2016) 280–286. https://doi.org/10.1021/acs.macromol.5b02578.

[14] A. Shamu, M. Dunnewold, H. Miedema, Z. Borneman, K. Nijmeijer, Permeation of supercritical CO2 through dense polymeric membranes, The Journal of Supercritical Fluids 144 (2019) 63–70. https://doi.org/10.1016/j.supflu.2018.10.009.

[15] I.C. Sanchez, R.H. Lacombe, Statistical Thermodynamics of Polymer Solutions, 11 (1978).

[16] I.C. Sanchez, R.H. Lacombe, An elementary molecular theory of classical fluids. Pure fluids, J. Phys. Chem. 80 (1976) 2352–2362. https://doi.org/10.1021/j100562a008.

[17] F. Doghieri, G.C. Sarti, Nonequilibrium Lattice Fluids: A Predictive Model for the Solubility in Glassy Polymers, Macromolecules 29 (1996) 7885–7896. https://doi.org/10.1021/ma951366c.

[18] M.G. De Angelis, G.C. Sarti, Solubility of Gases and Liquids in Glassy Polymers, Annu. Rev. Chem. Biomol. Eng. 2 (2011) 97–120. https://doi.org/10.1146/annurev-chembioeng-061010-114247.

[19] M. Minelli, G.C. Sarti, Permeability and diffusivity of CO2 in glassy polymers with and without plasticization, Journal of Membrane Science 435 (2013) 176–185. https://doi.org/10.1016/j.memsci.2013.02.013.

[20] A. Shamu, H. Miedema, K. Nijmeijer, Z. Borneman, The effect of supercritical CO2 on the permeation of dissolved water through PDMS membranes, Journal of CO2 Utilization 35 (2020) 145–152. https://doi.org/10.1016/j.jcou.2019.09.011.

Catalytic Carbon Dioxide Reduction

Fernando Caballero Rojo

Departament of Chemical Engineering and Environmental Technology,

University of Valladolid, fernando.caballero@uva.es

Introduction

In recent years, climate change is one of the main topics of concern around the world. The high concentrations of greenhouse gases, among which carbon dioxide stands out. Within this framework, all institutions are working to reduce CO_2 emissions, and thereby reduce the temperature of the planet. The Paris Agreement aims to limit global warming to less than 2 C above the temperature in pre-industrial times (del Río et al., 2021).

In this framework, institutional recommendations promote the use of renewable energies, but the need to continue using fossil fuels makes the use of carbon dioxide capture and storage technologies of vital importance for the future. This is where the importance of this project arises, in which we will work with a technology based on amines to achieve the capture and storage of CO_2, and to study the reduction of emissions(Andérez-Fernández et al., 2018).

In this way, we will work with a hydrothermal conversion process of carbon dioxide through capture with amines. It is a known and studied process, which provides great advantages to the conversion of CO_2. The objective of the project is to create a kinetic model of the catalytic reaction through which the conversion of CO_2 occurs.

Experimental

Materials

The products used in the process are:

- Palladium in carbon as a catalyst, from the Aldrich brand,
- 3-amino-1-propanol amine, 99% pure, also from the Aldrich brand.

Regarding the team:

- Non-stirred reactor, Parr, Model 4791, volume 25 mL, T316 stainless steel.
- Aggregated Parr reactor, with a volume of 50 mL

Amine charge

For the preparation, an aqueous solution of this amine is made and CO_2 is loaded into it. Once the solution has been made in the fume hood, it is transferred to a bottle with a stopper containing holes. The carbon dioxide is pumped through one of the holes. The CO_2 bottles are also in a separate booth, and once opened, the tube is introduced into the solution, so that the carbon dioxide begins to load into the solution. This process is carried out with low pressures in the CO_2 line, controlling the pressure at all times so that the pipes do not freeze, and ensuring that no problems occur in them. The CO_2 loading process is maintained for half an hour. Once the amine has been loaded, it is subjected to a total organic carbon analysis in a TOC device to determine the amount of carbon in the amine.

Reactions

For the experiments, it is shown with a batch reaction system, in which the reagents and catalyst are loaded, and once connected to the piping system, can be introduced into the gas. In the laboratory of the University of Valladolid, we work with a two-reactor system, which follows the diagram shown in Figure 1. This system allows us to work both with a single reactor and with the two batch reactors at the same time. The reactors are reactors prepared to work under high pressure conditions and also withstand high temperatures, to which they are subjected when heated.

Fig. 1.: Process flow diagram

As can be seen in the diagram, there are two lines for the gas feed to the reactors, one for the nitrogen feed and one for the hydrogen feed. In the case of our laboratory, the hydrogen is contained in a bottle in a small hut outside the laboratory for safety reasons. Each time the hydrogen is to be filled, the bottle and several intermediate valves along the entire line have to be opened. As soon as all the venting has been done and the reactor has been loaded with hydrogen, all the lines containing nitrogen are vented again and the cylinder is closed to ensure safety.

The nitrogen bottle is located in the same room as the reactors and, like the hydrogen bottle, has a valve to control the pressure. In both reactors, there is a nitrogen valve on the inlet line and another one on the outlet line, the first one for feeding the reactors, and the second one so that, when venting the hydrogen from the reactor, it is diluted in nitrogen and does not release hydrogen only through the vent. In addition, there is a vent valve on the outlet of each of the reactors, to vent the reactor, and another on the inlet line, which serves to vent this line.

Fig. 2.: Image of the 25 mL reactor

Palladium in carbon is being used as a catalyst. As it is a batch process, the reactor must be loaded first with the amine and the catalyst. In one of the reactors, we work with a volume of amine of 20 mL, in which, in the case of palladium in carbon, 0.1 grams of catalyst must be added. With the rest of the catalysts, the amount that needs to be added depends on the catalyst. In the other reactor, whose volume is half, 10 mL of amine must be added, and the amount of catalyst is also half.

The larger volume reactor has a mechanical stirring system using a stirrer located on the reactor lid, which is subsequently connected to a mechanical motor that rotates it. In the case of the smaller volume reactor, the stirring is magnetic, so when loading the reagents, a stirring magnet must be added, which will then rotate thanks to this magnetic stirring.

Once the reactors have been filled, they are closed with the lid by placing a clamp system that is tightened with screws, which guarantees the correct closure of the reactor and that there are no leaks. With this, the reactor pipes are joined with those of the plant, incorporating the reactor into the system. The first step prior to the reaction is venting with nitrogen, to eliminate any air that may remain. This venting is carried out four times, passing nitrogen through the reactor, at a pressure similar to that at which the hydrogen will be introduced. After this, the reactor is vented with hydrogen, passing it three times, to eliminate any nitrogen that may remain present. Whenever hydrogen is vented, the nitrogen valve on the outlet line must remain open, as undiluted hydrogen cannot be vented for safety reasons.

Fig. 2.: Image of the 50 mL reactor

Once all the venting has been carried out, the reactor is filled with hydrogen to operating pressure. The heating of the reactor is carried out by means of a heating jacket, which covers the entire reactor, and which electrically heats the reactor to the indicated temperature. Before starting the reaction, a jacket of insulating material is placed to cover

both the heating system and the reactor, and the upper part is also covered with insulating material to guarantee correct cooling. In the case of the reactor where the agitation is given by a motor, there is a water cooling system in the part where the agitation is, to avoid overheating in that area. As already said, the hydrogen detector is passed at all times during the reaction, and if a leak is detected, the reaction is stopped.

Experiments are being carried out at three different temperatures, three different pressures and three different catalyst concentrations. Once the reaction has concluded, the heating system is removed and the reactor is placed in a bath of cold water with ice, to accelerate cooling. When the temperature has decreased, the hydrogen is emptied from the reactor, and it is vented up to three times with nitrogen to eliminate all the hydrogen. When everything is depressurized, the reactor is removed from the system and the reactor is opened.

Samples analysis

The contents of the reactor are filtered by vacuum filtration, so that the liquid sample is prepared for analysis, and the solid catalyst is taken to the corresponding drying system for subsequent recovery. Liquid sample analysis is performed on a liquid chromatography column. The HPLC equipment (Waters, Alliance separation module e2695) has an IR detector (Waters, model 2414) and an Aminex HPX-87H column to analyse the samples. The mobile phase used is a solution of sulfuric acid that circulates with a flow of 0.6 mL/min, for half an hour for each sample. The column temperature is 60ºC and the detector temperature is 30ºC.

Safety system

In addition, high safety measures are in place at all times when hydrogen is used. In the room where the reactors are located, there is a detector that detects hydrogen from 4000 parts per million, 10% of the explosive limit. As soon as it detects this, the system automatically closes the hydrogen line. In addition, there is a manual hydrogen detector that detects hydrogen from 40 ppm. This detector is being passed around the reactor while it is being loaded with hydrogen, and during the reaction it is passed every few seconds to ensure that there are no leaks. If it detects any hydrogen in the environment, the reaction is stopped and the reactor and the line are vented.

Summary

In summary, various catalysts are being tested in CO_2 reduction processes in reactions with amines, previously loaded with carbon dioxide, for the determination of the kinetic model of the reaction. These reactions are carried out in batch reactors, pressurized with hydrogen, at a certain temperature and with stirring. With the results obtained from all the reactions, the reaction model will be determined methodically, which is the objective of the project.

Acknowledgements

References

Andérez-Fernández, M., Pérez, E., Martín, A., & Bermejo, M. D. (2018). Hydrothermal CO_2 reduction using biomass derivatives as reductants. *The Journal of Supercritical Fluids*, *133*, 658–664. https://doi.org/10.1016/J.SUPFLU.2017.10.010

del Río, J. I., Pérez, E., León, D., Martín, Á., & Bermejo, M. D. (2021). Catalytic hydrothermal conversion of CO_2 captured by ammonia into formate using aluminum-sourced hydrogen at mild reaction conditions. *Journal of Industrial and Engineering Chemistry*, *97*, 539–548. https://doi.org/10.1016/j.jiec.2021.03.015

Development of Oxygen Carriers for Chemical Looping Combustion Process

Rafal Lysowski, Ewelina Ksepko

Department of Engineering and Technology of Chemical Processes,

Wrocław University of Science and Technology

rafal.lysowski@pwr.edu.pl

Introduction

Chemical Looping combustion (CLC) is a novel technology of flameless fuel combustion that could become an alternative, more environmentally friendly to traditional combustion techniques[1]. This technology could be applied to gaseous, liquid, and solid fuels such as coal or biomass[2,3]. In CLC technology, usually, a system of two fluidized bed reactors is used: fuel and air reactor. In an air reactor (AR), the spent oxygen carrier is regenerated to the oxidized form. In the fuel reactor (FR) process of combustion occurs due to contact between fuel and a material called oxygen carrier (OC). Such approach prevents contact between atmospheric air and fuel, therefore flue gas stream is composed mostly of carbon dioxide and water vapor [1]. Therefore, further process of carbon dioxide capture is much more simplified, in comparison to traditional combustion technologies.[4]. Moreover, with CLC technology coupled with an efficient CO_2 capture system, it is possible to achieve negative carbon dioxide net-emission when biomass is used as a fuel. [5] It is also possible for certain classes of oxygen carriers to release gaseous oxygen in reaction to changes in temperature or partial pressure of O_2 in the reaction environment. That second approach is referred as Chemical Looping with Oxygen Uncoupling (CLOU) and oxygen carriers that exhibit such property are called CLOU capable. In this case, oxygen released from OC is used for fuel combustion. CLOU capable OCs are particularly valuable for the combustion of solid fuels, as combustion in this case can occur three to five times faster than in the traditional CLC process [6].

As it was mentioned before, oxygen carrier is a crucial element in this technology. Since the cost of oxygen carrier can represent a large proportion of the total operating costs of CLC installation it is important for OC to be characterized by not only high oxygen transport capacity measured as a mass percent of the oxygen that OC can release during contact with fuel, but also with relatively low price[1] and since OCs are operating inside fluidized bed reactors – with high mechanical durability [7]. Moreover, since CLC is considered an

environmentally friendly technology, materials of which oxygen carriers are made, suppose to be relatively non-toxic. As a material for oxygen carriers usually naturally occurring ores [8] or transition metal oxides such as Fe_2O_3, Mn_3O_4, or CuO are used often supported with inert material like Al_2O_3 or ZrO_2 to increase their mechanical properties [9]. Another approach is to use perovskite [10] or spinel-based materials [11].

One of the promising spinel-based materials for OCs is cuprospinel ($CuFe_2O_4$), characterized by a high CLOU effect (>3 wt.%), however, it has been reported that this class of material can undergo deactivation during the reactions with certain fuels [12].

In this work, research into the improvement of properties such as stability and mechanical durability of $CuFe_2O_4$, by using magnesium as a dopant was presented.

Experimental

Five different spinel-based oxygen carriers with overall $Cu_{1-x}Mg_xFe_2O_4$, formula with x = 0,0.25,0.5,0.75;1, were synthesized using the solid-state method, form metal oxide precursors, ground and sieved to obtain 120-180 μm fraction. CLOU capacity and reactivity toward biomass as a fuel were measured on thermogravimetric equipment (TGA). CLOU effect was measured in five different temperatures (800, 850,900,950, 1000 °C) by observing sample mass change in oxidizing (air) and neutral (nitrogen) atmosphere

For calculation of the CLOU effect following equation (1) was applied

$$CLOU\ (\%) = \frac{M_{ox} - M_{red}}{M_{ox}} * 100\% \qquad (1)$$

Where CLOU(%) is a CLOU effect measured in wt.%, M_{ox} is a mass of oxidized oxygen carrier, M_{red} is a mass of reduced oxygen carrier

Tests with biomass fuel (wood chips) were conducted on TGA equipment coupled with a quadrupole mass spectrometer(QMS) as follows: 50mg of OC and biomass mixture (ratio 6:1) were heated up in a neutral (argon) atmosphere inside TGA device to three different temperatures. Reaction rates between biomass and OCs were determined in a following way (2)

$$r = \frac{dm}{dt} \qquad (2)$$

Where r is a reaction rate measured in wt.%/min, m – a mass of the measured as a percentage of the initial mass of, t – time (min).

Conversion of fuel was determined by registering on QMS ions with a mass corresponding to carbon dioxide (m/z:44) as follows (3):

$$Conv = \left(\frac{\int_0^{t_{comb}} I_{CO_2}(t)dt}{\int_0^{t_{exp}} I_{CO_2}(t)dt} \right) \cdot 100\% \qquad (3)$$

Where: Conv is a fuel conversion measured in percent, t – total time of the experiment, t_{comb} – time of combustion segment, I_{CO2} – Ion current registered for CO_2.

Moreover, since mechanical durability is an important property of OC, crushing resistance was measured for both fresh and reacted OC granules. For each OC, 30 granules were tested on a digital force gauge meter.

Summary

The tested oxygen were CLOU capable (with $MgFe_2O_4$ as an exception). High conversion of solid fuels was achieved (>90 %). The addition magnesium as a dopant for $CuFe_2O_4$ spinel-based oxygen carrier can increase both mechanical durability (over 50% of increased crushing strength resistance, for magnesium doped samples). However high Mg content has a negative impact on the CLOU effect, which could affect their reactivity toward solid fuels.

Acknowledgment

References

[1] Adánez J, Abad A. Chemical-looping combustion: Status and research needs. Proc Combust Inst 2019;37:4303–17. https://doi.org/10.1016/J.PROCI.2018.09.002.

[2] Adánez J, Abad A, Mendiara T, Gayán P, de Diego LF, García-Labiano F. Chemical looping combustion of solid fuels. Prog Energy Combust Sci 2018;65:6–66. https://doi.org/10.1016/J.PECS.2017.07.005.

[3] Pérez-Vega R, Abad A, García-Labiano F, Gayán P, de Diego LF, Izquierdo MT, et al. Chemical Looping Combustion of gaseous and solid fuels with manganese-iron

mixed oxide as oxygen carrier. Energy Convers Manag 2018;159:221–31. https://doi.org/10.1016/J.ENCONMAN.2018.01.007.

[4]   Narindri B, Winayu R, Tseng T-K, Chu H. Chemical Looping Strategy in Various Types of Carbon Capture Technologies. Process 2023, Vol 11, Page 3164 2023;11:3164. https://doi.org/10.3390/PR11113164.

[5]   Rydén M, Lyngfelt A, Langørgen O, Larring Y, Brink A, Teir S, et al. Negative CO2 Emissions with Chemical-Looping Combustion of Biomass – A Nordic Energy Research Flagship Project. Energy Procedia 2017;114:6074–82. https://doi.org/10.1016/J.EGYPRO.2017.03.1744.

[6]   Leion H, Mattisson T, Lyngfelt A. Using chemical-looping with oxygen uncoupling (CLOU) for combustion of six different solid fuels. Energy Procedia 2009;1:447–53. https://doi.org/10.1016/J.EGYPRO.2009.01.060.

[7]   Rydén M, Moldenhauer P, Lindqvist S, Mattisson T, Lyngfelt A. Measuring attrition resistance of oxygen carrier particles for chemical looping combustion with a customized jet cup. Powder Technol 2014;256:75–86. https://doi.org/10.1016/J.POWTEC.2014.01.085.

[8]   Cuadrat A, Abad A, Adánez J, De Diego LF, García-Labiano F, Gayán P. Behavior of ilmenite as oxygen carrier in chemical-looping combustion. Fuel Process Technol 2012;94:101–12. https://doi.org/10.1016/J.FUPROC.2011.10.020.

[9]   Ksepko E, Siriwardane R V., Tian H, Simonyi T, Sciazko M. Effect of H2S on Chemical Looping Combustion of Coal-Derived Synthesis Gas over Fe–Mn Oxides Supported on Sepiolite, ZrO2, and Al2O3. Energy and Fuels 2012;26:2461–72. https://doi.org/10.1021/EF201441K.

[10]   Ksepko E. Perovskite-type Sr(Mn1−xNix)O3 materials and their chemical-looping oxygen transfer properties. Int J Hydrogen Energy 2014;39:8126–37. https://doi.org/10.1016/J.IJHYDENE.2014.03.093.

[11]   Azad A-M, Hedayati A, Rydén M, Leion H, Mattisson T. Examining the Cu-Mn-O Spinel System as an Oxygen Carrier in Chemical Looping Combustion. Energy Technol 2013;1:59–69. https://doi.org/10.1002/ENTE.201200009.

[12]   Wang B, Wang W, Ma Q, Lu J, Zhao H, Zheng C. In-Depth Investigation of Chemical Looping Combustion of a Chinese Bituminous Coal with CuFe2O4 Combined Oxygen Carrier. Energy and Fuels 2016;30:2285–94. https://doi.org/10.1021/ACS.ENERGYFUELS.5B02605.

Photonic Nanosensor Receptors Based on Functionalized SiO₂-Nanoparticles for Detection of Stress Biomarkers

Valeriia Sliesarenko[a,b], Urban Bren[a,b,c], Aleksandra Lobnik[a,d]

[a]Institute for Environmental Protection and Sensors, Maribor, Slovenia

[b]University of Maribor, Faculty of Chemistry and Chemical Engineering, Maribor, Slovenia

[c]University of Primorska, Faculty of Mathematics, Natural Sciences and Information Technologies, Koper, Slovenia

[d]University of Maribor, Faculty of Mechanical Engineering, Maribor, Slovenia

valeriia.sliesarenko@ios.si

In the modern world, stress has become an integral part of human life. During stress, the body is subjected to significant pressure from within, as it produces hormones and neurotransmitters to protect against danger through the fight, flight, or freeze mechanism [1]. However, such a tactic is not always applicable, and addressing life problems requires attention and thoughtful analysis, which is generally impossible in a state of stress. Nevertheless, the human body continues to instinctively react in this way, depriving the ability to make rational decisions and exacerbating the negative consequences of stress. Chronic stress can lead to conditions such as neurosis, depression, stroke, or heart attack [2].

Since some hormones and neurotransmitters are responsible for the state of rest or stress, their concentrations in the human body serve as an objective indicator of mental condition and are called stress biomarkers [3]. Stress biomarkers include cortisol, dopamine, norepinephrine, serotonin, and others [3]. The study of stress biomarker concentrations and their combined effects is actively researched. For example, it is known that concentrations of dopamine and serotonin decrease in states of depression [4] and stress [5]. Cortisol levels significantly increase when a person is reacting to a stress factor [6]. A high level of dopamine along with a low level of serotonin provides impulsivity in reaction [7].

Monitoring stress biomarkers allows preventing pathological conditions and taking precautionary measures in a timely manner by seeking medical help [8]. Additionally, monitoring stress biomarkers enables tracking the effectiveness of treatment, as well as the impact of diet and physical activity on the body.

Measuring concentrations of stress biomarkers in human fluids is only possible in specialized facilities with specialized equipment and trained personnel. Portable sensors for monitoring stress biomarkers are not available in the mass market, despite extensive scientific advancements in various optical and electrochemical biosensors. This is due to the complexity of production, toxicity, high cost, and other factors [9].

The aim of my scientific research is to develop photon-based nanosensor receptors for detecting stress biomarkers. These photon-based nanosensor receptors must adhere to the following principles: environmental friendliness, non-toxicity, and ease of use, for further integration into specialized portable devices for numerical assessment.

To create photon-based nanosensor receptors, two components are necessary: the presence of photon molecules capable of optical effects resulting from interaction with stress biomarkers, and a carrier ensuring the efficiency of photon molecules' operation.

Photon molecules can be substances that change their optical properties, such as color or fluorescence, upon interaction with stress biomarkers. The intensity of the change in optical properties depends on the concentration of the stress biomarker, allowing for the identification of patterns and concentration calculations [10]. Attaching photon molecules to the surface of silicon or other carriers has several advantages:

- Increased Sensitivity: The high surface area of the carrier can enhance the contact between stress biomarkers and photon molecules, leading to an increase in signal and, consequently, improving the sensitivity of the methodology.
- Enhanced Stability: Photon molecules attached to the surface can be more stable and less susceptible to external influences, such as changes in pH or temperature.
- Regeneration Capability: Attaching photon molecules to carriers provides the opportunity for regeneration and reuse, reducing reagent costs.
- Improved Selectivity: Carriers can facilitate selective interaction between photon molecules and target stress biomarkers, excluding interaction with other components in the environment.

Various materials can be used as carriers for photon molecules, including metallic nanoparticles, polymers, and silicon dioxide (silica) [11]. Silica is of particular interest for addressing this task because it possesses several qualities that make it an excellent candidate for carrying photon molecules:

- Abundant Availability: Silica is widely available and cost-effective, making it accessible for large-scale production.
- Biocompatibility: Silica is biocompatible and non-toxic, making it suitable for biomedical applications and reducing potential health risks.
- Tailorable Surface Chemistry: The surface of silica can be modified to control its interaction with photon molecules and stress biomarkers, allowing for enhanced sensitivity and selectivity.
- Stability: Silica is chemically inert and stable under various environmental conditions, ensuring the longevity and reliability of the sensor.
- Ease of Functionalization: Silica nanoparticles can be easily functionalized with various functional groups or coatings to improve their performance and versatility in detecting stress biomarkers.
- Optical Properties: Amorphous silica particles exhibit a high isotropic refractive index and excellent optical transparency, making them suitable for optical applications.
- Utilization of Sol-Gel Technology: Silica-based materials can be synthesized using sol-gel technology to create various forms such as films, xerogels, mesoporous silica, and microspheres. This versatility allows for the tailored design of carriers for photon molecules, enhancing their performance in stress biomarker detection.

The sol-gel synthesis method offers broad opportunities for manipulating the parameters of silica [12]. Sol-gel synthesis can produce silica nanoparticles on a nanometer scale (Stöber method), which possess unique properties compared to bulk silica. Sol-gel synthesis can be used to incorporate organic molecules or polymers into the silica network, resulting in hybrid silica materials with enhanced properties. These materials combine the advantages of both organic and inorganic components. The use of surfactants as templates allows for the control of pore structure and morphology, yielding ordered mesoporous structures (template method) [13].

Silica surfaces can be functionalized with various functional groups, such as amino, thiol, or epoxy groups, during the sol-gel process or through post-synthetic modification.

For the effective immobilization of photon molecules, doping is a preferred method due to several advantages, including simplicity, nonspecificity, and low cost. In this case, photon molecules are directly mixed into the initial sol-gel solution, including sol-gel precursors (e.g., TEOS, MTriEOS, p-TriMOS, ph-TriMOS), solvent (e.g., ethanol), and catalyst (NH_4OH).

Additionally, an alternative approach to immobilizing photon molecules is the use of a covalent method, which also ensures reliable fixation of photon molecules. In the covalent method, photon molecules first form covalent bonds with a precursor, after which they are introduced either into a sol-gel solution with subsequent silica formation or undergo post-synthetic modification. This process allows for the creation of stable bonds between photon molecules and the silica matrix, ensuring their reliable immobilization. Thus, the choice between doping and the covalent method depends on the specific requirements and characteristics of the investigated photon-molecular system.

To understand the main factors and effects on the synthesis of photon nanosensor receptors, the following investigations will be conducted:

- The composition of the silica carrier will be regulated by using different precursors (TEOS, MTriEOS, p-TriMOS, Ph-TriMOS) and varying their ratios.
- The parameters of the silica structure will be adjusted by changing process parameters such as: (i) TEOS concentration, (ii) catalyst concentration, (iii) water concentration, (iv) type of solvent.
- Silica surfaces will be functionalized to enable covalent immobilization or to facilitate sample concentration by adsorbing stress biomarkers from human fluids in case of insufficient sensitivity of the photon sensor receptor.
- Photon nanosensors will be further evaluated for their sensory responses (detection limits, response time, reversibility, stability, concentration range, interference, etc.), as well as mechanical and other stability properties (stability, leaching, etc.).

Based on the general characteristics, we can understand the mechanisms and effectiveness of immobilizing photon molecules into SiO_2 particles. Optimization of the synthesis of photon nanosensors will be implemented to ensure maximum sensor sensitivity and temperature stability.

Exploring in this direction will yield a product that offers advantages for potential realistic applications, while also contributing to a better understanding of synthetic pathways for

preparing photon nanosensors, thus providing new fundamental knowledge in the field of nanomaterials and nanotechnologies.

The research results will contribute to enriching both fundamental knowledge (the relationship between structure, morphology, texture, functionality) and applied knowledge (synthesis optimization for obtaining larger quantities of sensor receptors, implementation of new technologies, quality control of synthesized materials).

References

1. K. Roelofs, Freeze for action: neurobiological mechanisms in animal and human freezing, Phil. Trans. R. Soc. B 372: 20160206 (2017) DOI:10.1098/rstb.2016.0206

2. T. Dar, A. Radfar, S. Abohashem, R.K. Pitman, A. Tawakol, M.T. Osborne, Psychosocial Stress and Cardiovascular Disease, Curr Treat Options Cardiovasc Med; 21(5): 23. DOI:10.1007/s11936-019-0724-5

3. A.J. Steckl, P. Ray, Stress Biomarkers in Biological Fluids and Their Point-of-Use Detection, ACS Sens. 3 (2018) 2025−2044 DOI:10.1021/acssensors.8b00726

4. C.S. Wijaya, J.J.Z. Lee, S.F. Husain, C.S.H. Ho, R.S. McIntyre, W.W. Tam, R.C.M. Ho, Differentiating Medicated Patients Suffering from Major Depressive Disorder from Healthy Controls by Spot Urine Measurement of Monoamines and Steroid Hormones, Int. J. Environ. Res. Public Health (2018) 15, 865; DOI:10.3390/ijerph15050865

5. K. Tanabe, A. Yokota, Mental stress objective screening for workers using urinary neurotransmitters, DOI:10.1371/journal.pone.0287613

6. M. Cay, C. Ucar, D. Senol, F. Cevirgen, D. Ozbag, Z. Altay, S. Yildiz, Effect of increase in cortisol level due to stress in healthy young individuals on dynamic and static balance scores, North Clin Istanb. 2018; 5(4): 295–301. DOI:10.14744/nci.2017.42103

7. J. Hennig, P. Netter, A.J.L. Munk, Interaction between serotonin and dopamine and impulsivity: A gene×gene-interaction approach, Personality and Individual Differences 169 (2021) 110014 DOI:10.1016/j.paid.2020.110014

8. D.T. Marc, J.W. Ailts, D.C. Ailts Campeau, M.J. Bull, K.L. Olson, Neurotransmitters excreted in the urine as biomarkers of nervous system activity: Validity and clinical

applicability, Neuroscience and Biobehavioral, Reviews 35 (2011) 635–644 DOI:10.1016/j.neubiorev.2010.07.007

9. C. Ravariu, From Enzymatic Dopamine Biosensors to OECT Biosensors of Dopamine, Biosensors (2023) 13, 806. DOI:10.3390/bios13080806

10. V. Sliesarenko, U. Bren, A. Lobnik, Fluorescence based dopamine detection, Sensors and Actuators Reports Volume 7, June 2024, 100199 DOI:10.1016/j.snr.2024.100199

11. A. Lobnik, M. Turel, S. Korent Urek, A. Kosak, Nanostructured Materials Use in Sensors: Their Benefits and Drawbacks, Carbon and Oxide Nanostructures (2010) pp.307-354 DOI:10.1007/8611_2010_21

12. A. Lobnik, M. Turel, S. Korent Urek, Optical Chemical Sensors:Design and Applications, Advances in Chemical Sensors (2012) DOI:10.5772/31534

13. S. Korent Urek, N. Franlil, M. Turel, A. Lobnik, Sensing Heavy Metals Using Mesoporous-Based Optical Chemical Sensors, Hindawi Journal of Nanomaterials (2013) DOI:10.1155/2013/501320

Sampling Device for High-Pressure Polymerization Systems

Patryk Sewruk, Markus Busch*

Ernst-Berl-Institute of Technical and Macromolecular Chemistry, Technical University of Darmstadt, 64287 Darmstadt/Germany, *e-mail: markus.busch@pre.tu-darmstadt.de

Introduction

The production of low-density polyethylene (LDPE) is conducted at conditions of up to 330 °C and 3500 bar.[1] This increases the complexity of sample-taking from reaction mixtures. Sampling and analysing are important parts of the chemical industry since it is used for process and quality control, identification, and regulatory assessment.[2] By obtaining representative samples at selected stages during the process, valuable information about the polymer properties and composition can be gained. This lead to an unchanging product while ensuring consistent product quality.[3] Additionally, sampling is the step with the highest error potential to falsely represent the reaction composition.[4]

This works aims to design and build a sampling device for a continuous high-pressure LDPE mini-plant to enable the fulfilment of the mass balance by the determination of the reaction mixture with a low concentration threshold. Up to this work, it has been only possible to analyse the produced polymer leaving the reactor and the exhaust, which is purged with nitrogen to prevent the formation of an explosive atmosphere. The sampling is supposed to take place during process conditions. The setup can then be implemented into the current lab-scale plant and incorporated into the operator interface.

Experimental

For this, a bypass system using pneumatic valves has been implemented into the continuous high-pressure polymerization system for LDPE on a lab scale. The bypass can be purged with the reactor mixture and then shut off from the main process while not endangering the continuous process. The setup is displayed in Fig. 1 and works in the following way: The feed is continuously pressurized and fed into the continuously stirred tank reactor (CSTR). During the experimental procedure, the reaction mixture leaves the reactor through the opened PV-2, while PV-3 and PV-4 are closed. The product stream is depressurized to atmospheric pressure into the separator S-1 through PV-1 and purged with nitrogen to prevent the formation of an explosive atmosphere. Upon reaching a

stationary state the valves PV-3 and PV-5 can be opened. The valve PV-5 remains closed. The additional closing of valve PV-2 leads to the redirection of the process mixture through the bypass. The bypass can then be closed off with valves PV-3 and PV-4, with simultaneous opening of valve PV-2 to ensure the pressure release of the continuous process. The valves V-1 to V-3 are used to evacuate the sample-container (S-CN) to ensure no contamination. After closing valve V-3, valve PV-5 can be opened to depressurize the content of the bypass into the evacuated sample-container. The pressure-reduction quenches the reaction, and the sample can be used for various analytical methods of choice. After this, the container can be sealed with the use of valve V-2. The container including the valve V-2 can then be detached for sample analysis and a new sample-container can be connected.
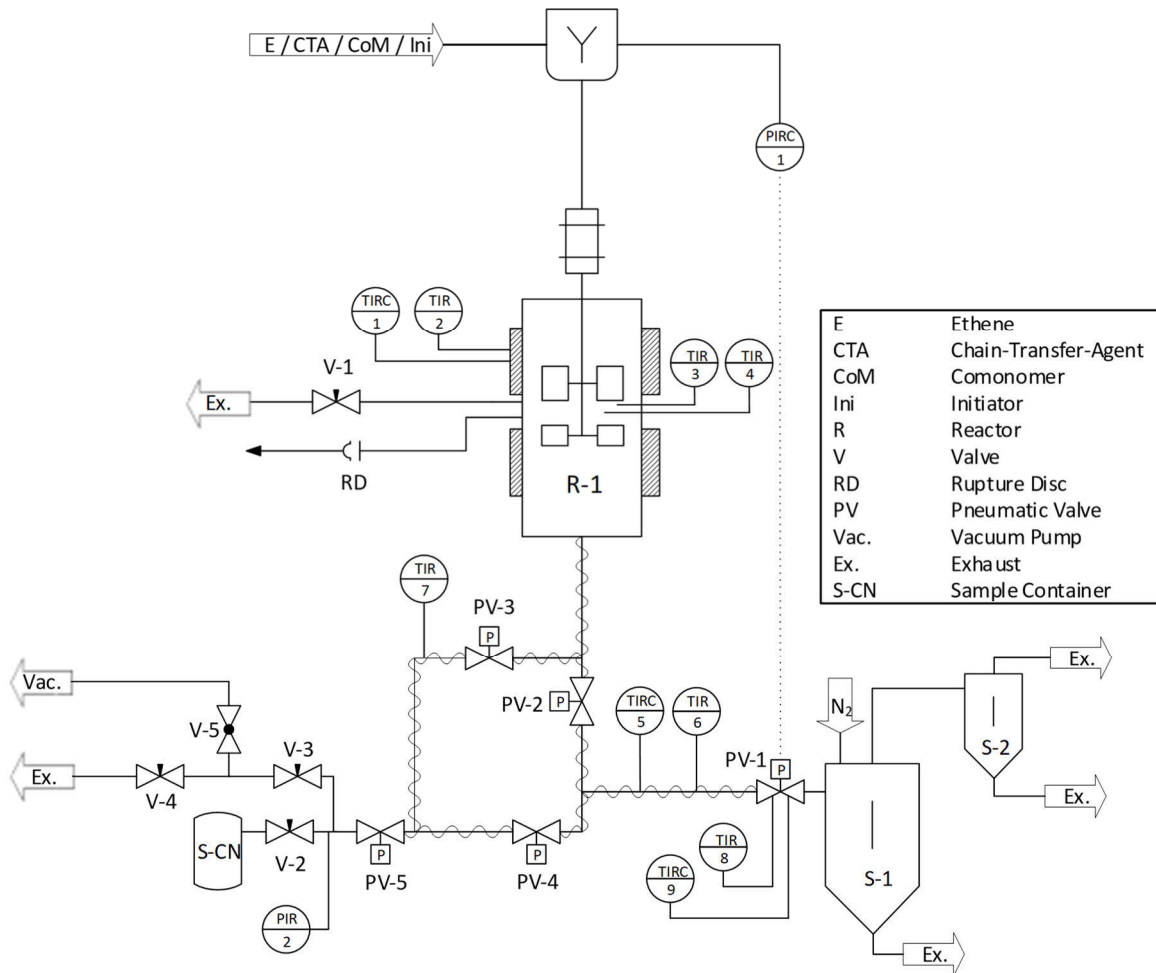

Fig. 1: Flowsheet of the reactor R-1 with its safety peripherals and the connected gas sampling apparatus. The pneumatic valves PV-2 to PV-5 are used to take samples using the bypass. The valves V-2 to V-4 are used to evacuate and depressurize the sample-container S-CN, while PV-1 relieves the product stream into the separators S-1 and S-2.

The following Fig. 2 shows a CAD drawing of the mini-plant setup with the presented bypass device. The autoclave is shown in the upper part, the sampling container is the one-meter-long high-pressure tube in the bottom, and the exhaust valve PV-1, which is connected to the sample barrel, is on the left side.

Fig. 2: CAD-drawing of the bypass setup connected to the autoclave and sample barrel.

To describe the reactor, the ideal CSTR-model can be used as an approximation.[5] During the process, the feed stream is converted into a product stream. It contains the mass flow of polymer and unreacted educt. In this case, the system has been investigated using a gaseous feed composition, which results in a product stream that is divided into a gas and polymer phase. The streams are visualized in Fig. 3.
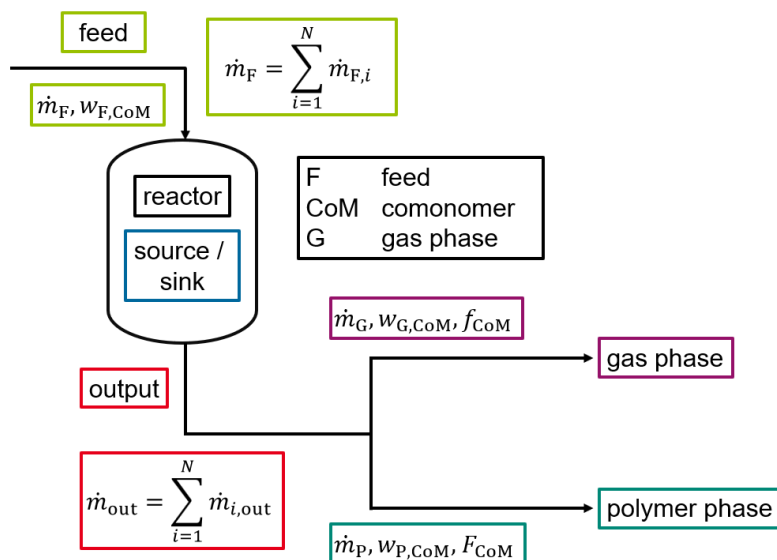

Fig. 3: Schematic visualization of the mass balance of a CSTR with the input and output streams. In this setup, the output stream can be divided into a gas phase (purple) and a polymer phase (dark green) mass flow stream.

During the polymerization comonomers are incorporated in the polymer, which can be described after the terminal model by MAYO and LEWIS.[6] Depending on the concentration in the reaction mixture of one monomer and its reactivity ratio, it is incorporated preferably into the polymer. Therefore, the composition of the exhaust gas phase changes compared to the feed. Both product streams can be analysed, for example, using gas chromatography, and for the polymer phase the nuclear magnetic resonance (NMR) spectroscopy. The aim is to fulfil the mass balance of the entire autoclave and determine the incorporation of different components in the polymer phase without analysing the polymer itself. Additionally, volatile byproducts in the gas phase of the process can be determined.

The setup was first put into operation with ethene as the main monomer and propene as the comonomer. It was polymerized at different feed compositions and varying conversions. The gas phase was then analysed using gas chromatography and the polymer phase was analysed using ^{13}C-NMR-spectroscopy. The gas phase composition was then used to calculate the incorporation of propene into the polymer and is compared to the determined propene ratio using NMR in the following Fig. 4. As can be seen, the comparison between both analytical methods shows a decent agreement in the incorporated amount. The deviation could be caused by the error and sensitivity of both methods, as it is for example reported that ^{13}C-NMR spectroscopy of LDPE can have a deviation of up to 32 %.[7]
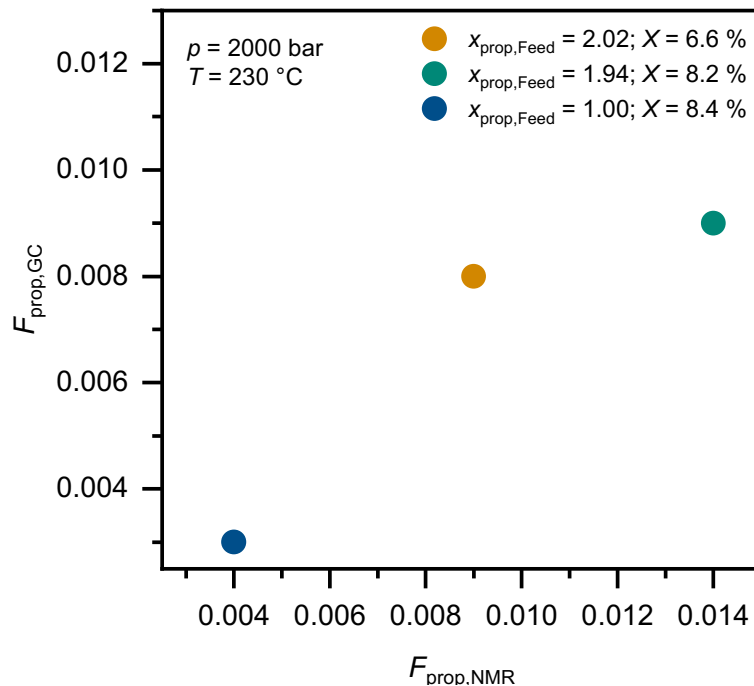

Fig. 4: Plot of the determined propene content in the polymer using the exhaust stream and mass balance against using the ^{13}C-NMR-spectroscopy.

Summary

The presented device has been implemented into the high-pressure polymerization mini-plant at TU Darmstadt and has been used to investigate the ethene/propene copolymerization at different feeds and varying conversions. With the introduction of a sampling system at high-pressure conditions, it is possible to sample the reaction mixture without contaminations. This enables the fulfilment of the mass balance of the process and allows the determination of volatile byproducts. It has been shown that the setup is capable of sampling the reaction mixture and that the taken samples reflect the composition inside the autoclave within the error of analytical methods. The analysis of the gas phase provides a possibility to backtrace the polymer composition with the calculation of the mass balance and assuming an ideal CSTR-behaviour of the autoclave. In this way, the analysis of polymer can be bypassed by a certain degree and long NMR measurement times can be reduced.

References

[1] G. Luft, *Chemie Ingenieur Technik* **1979**, *51*, 960–969.

[2] S. Peper, R. Dohrn, *The Journal of Supercritical Fluids* **2012**, *66*, 2–15.

[3] D. Muhammad, Z. Ahmad, N. Aziz, *IOP Conference Series: Materials Science and Engineering* **2020**, *736*, 42014.

[4] G. Schwedt, *Analytische Chemie. Grundlagen, Methoden und Praxis*, Thieme **1995**.

[5] M. Baerns, A. Behr, A. Brehm, J. Gmehling, H. Hofmann, *Technische Chemie*, Wiley & Sons, Limited, John **2013**.

[6] F. R. Mayo, F. M. Lewis, *Journal of the American Chemical Society* **1944**, *66*, 1594–1601.

[7] I. Neuhaus, *Dissertation*, TU Darmstadt **2014**.

Sustainable Supercritical Fluid Processing of Vegetable Oils

Azemina Bajramova

Lund University, Department of Chemistry, Centre for Analysis and Synthesis, Lund, Sweden

AAK AB, Skrivaregatan 9, S-215 32 Malmö, Sweden

azemina.bajramova@chem.lu.se or azemina.bajramova@aak.com

Introduction

Vegetable oils have been used by humans for millennia and are still extensively used today, in different applications such as culinary, personal care products, cosmetics, pet food additives, and biofuel. Isolation of the oil from the plant seed or kernel is commonly performed in two stages; mechanical pressing followed by solvent extraction [1]. The most widely used extraction solvent is hexane, with a global annual demand of about 2 Mt whereof 650 Kt is used for vegetable oil extraction [2]. Hexane has been used in the vegetable oil industry for over a century due to some of its benefits such as its complete miscibility with oil, low boiling point (55-70 °C for technical hexane), easy recyclability, and low cost. However, studies suggest that hexane can affect health negatively by, for instance, acting as a neurotoxic substance, damaging fertility, and being an environmental hazard. Furthermore, hexane is derived from non-renewable resources (naphtha) and is an occupational hazard due to being flammable [1, 2].

Despite the negative associations with hexane, the maximum residue limit of hexane in vegetable oils for food consumption is 1 mg/kg with current legislation, and traces of hexane do not need to be declared due to hexane being classified as a processing aid [2, 3]. However, due to the increasing evidence and consumer awareness of the negative health and environmental impacts of hexane, attention has been shifted towards limiting the use of hexane and other non-renewable and toxic solvents. A possible result could be a complete ban of the use of hexane, for instance due to the European Green Deal and the Chemicals Strategy for Sustainability [2]. This emphasizes why efforts need to be put towards finding alternatives to hexane. One such alternative is supercritical carbon dioxide (scCO$_2$) which is carbon dioxide at pressures and temperatures above its critical point (see Fig. 1.).
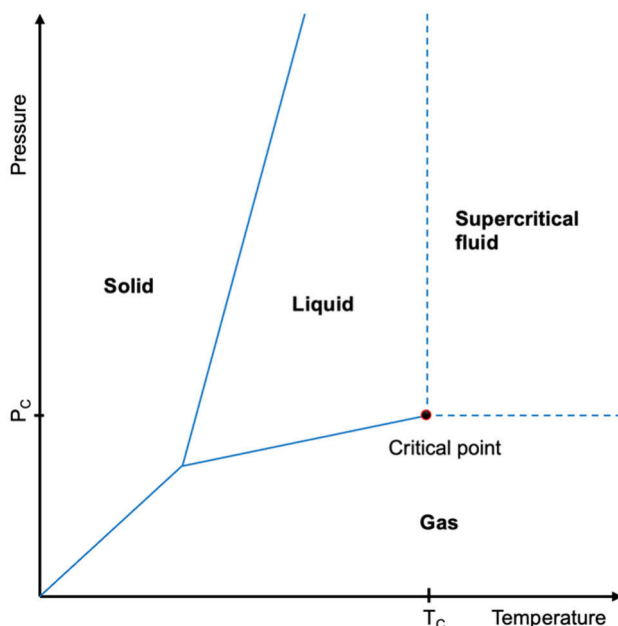
Fig. 1.: Hypothetical phase diagram illustrating that the supercritical fluid state can be reached by raising the pressure and temperature above the critical pressure and temperature (P_C and T_C, respectively).

The critical point of carbon dioxide is 31 °C and 74 bar [4]. $scCO_2$, and supercritical fluids in general, have properties in between liquids and gases: they have liquid-like density and gas-like viscosity and diffusivity. The liquid-like density causes the supercritical fluid to demonstrate solvation properties similar to liquids. Unlike liquids, the density of a supercritical fluid is compressible, which entails that a small change in pressure and temperature can lead to a big change in density and volume, especially close to the critical point. Consequently, the solubility of an analyte in a supercritical fluid can be tuned by changing the density of the fluid. The gas-like viscosity of a supercritical fluid causes higher diffusion constants, which entails faster mass transfer processes and that higher flow rates can be reached with acceptable back pressures. Furthermore, the surface tension of a supercritical fluid is zero. These properties of a supercritical fluid have importance in both extraction and separation processes.

Unlike hexane, $scCO_2$ is also considered to be a "green" solvent due to being derived from renewable sources, being non-flammable, nontoxic, and easy to remove from the extract and recycle due to being a gas at room temperature and pressure [4]. However, in most applications, high pressure equipment is needed which require a lot of electricity and, due to the high vapor pressure of CO_2, gas tight systems with proper ventilation should be

used. Consequently, the feasibility and cost of a process based on $scCO_2$ depends on the specific application.

Furthermore, the polarity of $scCO_2$ resembles that of hexane which entails that it can solubilise mainly non-polar compounds and that the extraction of more polar compounds require the addition of organic modifiers such as ethanol or ethyl acetate [4]. The properties of a solvent mixture consisting of a supercritical fluid and an organic modifier differs from that of a supercritical fluid. One of the differences is that the critical point of the solvent mixture will be increased to higher pressures and temperatures depending on the exact composition of the mixtures. As a consequence, during normal operation ranges, the solvent mixture is not in its supercritical state. In these cases, it would be more appropriate to use the terms subcritical fluid at low molar fraction of organic modifier or carbon dioxide expanded liquid at high molar fraction of organic modifier.

Considering the composition of vegetable oils, which usually consist of primarily nonpolar compounds such as triglycerides and smaller levels of diglycerides, monoglycerides, free fatty acids, and the unsaponifiable fraction (hydrocarbons, sterols, terpenoids, tocopherols, etc), it is likely that high-density $scCO_2$ can give high extraction yields of the oily plants, as has been previously observed for some oils such as from peach seeds [5], linseeds [6, 7], moringa seeds [8], and berry seeds [9]. Furthermore, the use of $scCO_2$ extraction allows for the option to fractionate the extract by sequential release of the pressure, precipitating the less soluble compounds in separate collection vials.

The aim of the research project is to investigate the possibilities of developing an extraction, fractionation, and/or refining process targeting nonpolar compounds in different plant kernels/seeds and vegetable oils utilising $scCO_2$ as a solvent rather than hexane. Possible vegetable oils could be based on palm, rapeseed, coconut, or shea. Compositional and physiochemical properties of the $scCO_2$ extracted oils will be compared with the traditionally hexane-extracted oils. Life cycle assessment will shed some light on the process environmental performance in comparison to current petroleum-based ones. The results should pave the way towards hexane-free vegetable oil production, which enables both a safe and sustainable work environment and food products without hexane residues. This project is a collaboration between Lund University in Sweden and AAK AB in Denmark/Sweden.

Experimental

Vegetable oil extracts will be produced using supercritical fluid extraction based on neat scCO$_2$, where the extractability and selectivity of the extraction process will be investigated using design of experiment with temperature, pressure, flow rate, and extraction time as variables. The extracts will be analysed using supercritical fluid chromatography coupled to charged aerosol detection and ion-mobility high-resolution mass spectrometry. Selectivity will be further investigated by introducing solvent composition as a fifth variable in the design of experiment after the initial trials. Life cycle assessment and physiochemical characteristics will be evaluated and compared with the vegetable oils extracted with hexane.

Summary

Vegetable oils, often extracted with the toxic and fossil-based solvent hexane, are staple products in many homes and industries. Efforts need to be put towards finding alternative solvents for the extraction of vegetable oils that enable safe and sustainable work environment and food products without hexane residues. The aim of this research project is to investigate the possibilities of using scCO$_2$ as a solvent rather than hexane for the extraction, fractionation and/or refinement of vegetable oils. The influence of pressure, temperature, flow rate, extraction time, and solvent composition will be investigated, and the extract composition and yield will be compared with that of the hexane-extracted vegetable oils. Life cycle assessment will be performed to investigate the process environmental performance in comparison to current petroleum-based ones.

Acknowledgment

References

[1]   A. Thomas, "Fats and Fatty Oils," in *Ullmann's Encyclopedia of Industrial Chemistry*, Wiley, 2000. doi: 10.1002/14356007.a10_173.

[2]   C. Cravotto *et al.*, "Towards Substitution of Hexane as Extraction Solvent of Food Products and Ingredients with No Regrets," *Foods*, vol. 11, no. 21, p. 3412, Oct. 2022, doi: 10.3390/foods11213412.

[3]   Directive 2009/32/EC of the European Parliament and of the Council of 23 April 2009 on the Approximation of the Laws of the Member States on Extraction Solvents Used in the Production of Foodstuffs and Food ingredients (Recast) (Text with EEA Relevance)," Volume 141.

        Available online: http://data.europa.eu/eli/dir/2009/32/oj/eng (accessed 20240520).

[4]   L. P. Cunico and C. Turner, "Supercritical Fluids and Gas-Expanded Liquids," in *The Application of Green Solvents in Separation Processes*, Elsevier, 2017, pp. 155–214. doi: 10.1016/B978-0-12-805297-6.00007-3.

[5]   M. S. Ekinci and M. Gürü, "Extraction of oil and β-sitosterol from peach (Prunus persica) seeds using supercritical carbon dioxide," *J Supercrit Fluids*, vol. 92, pp. 319–323, Aug. 2014, doi: 10.1016/j.supflu.2014.06.004.

[6]   V. Abrahamsson, N. Andersson, B. Nilsson, and C. Turner, "Method development in inverse modeling applied to supercritical fluid extraction of lipids," *J Supercrit Fluids*, vol. 111, pp. 14–27, May 2016, doi: 10.1016/j.supflu.2016.01.006.

[7]   V. Abrahamsson, I. Rodriguez-Meizoso, and C. Turner, "Supercritical fluid extraction of lipids from linseed with on-line evaporative light scattering detection," *Anal Chim Acta*, vol. 853, pp. 320–327, Jan. 2015, doi: 10.1016/j.aca.2014.09.052.

[8]   Y. N. Belo, S. Al-Hamimi, L. Chimuka, and C. Turner, "Ultrahigh-pressure supercritical fluid extraction and chromatography of Moringa oleifera and Moringa peregrina seed lipids," *Anal Bioanal Chem*, vol. 411, no. 16, pp. 3685–3693, Jun. 2019, doi: 10.1007/s00216-019-01850-x.

[9]   S. Al-Hamimi and C. Turner, "A Fast and Green Extraction Method for Berry Seed Lipid Extraction Using CO2 Expanded Ethanol Combined with Sonication," *European Journal of Lipid Science and Technology*, vol. 122, no. 4, Apr. 2020, doi: 10.1002/ejlt.201900283.

Synthesis and Characterization of PVDF Aerogels

Razmehr Sahraeian

Institute of Technical Chemistry, Technical University of Clausthal,

razmehr.sahraeian@tu-clausthal.de

Introduction

Due to constantly advancing modern technology and efficiency, it is necessary to develop new and more efficient high-performance materials that meet the increasing requirements. Aerogels are a promising approach for such modern materials. Aerogels are the lightest processed solids on earth with the largest proportion of voids in their structure. The nanostructure is the reason why these materials have interesting properties such as a very low density (0.0001 to 0.2 g/cm^3), high specific surface area (>200 m^2/g) porosity larger than 90% with predominance of open pores in the mesoscale (2–50 nm).[1,2] Aerogels therefore have very good applications in sound insulation, catalysis and thermal insulation.[3] The production of these versatile, ultra-light and porous materials, which are first synthesized using traditional low-temperature sol-gel chemistry and then treated using special drying techniques.[4] The structure of the network and thus the properties of the aerogel can be modified by the chemicals used, the synthesis and the subsequent drying process. Aerogels can be made from a wide variety of materials, e.g. inorganic silica[4] or carbon[3], organic resorcinol-formaldehyde polymer or biopolymers such as cellulose[5] or alginate.[6]

One potential candidate would be poly(vinylidene fluoride) (PVDF) aerogels, which not only have excellent physical properties but are also inert to chemicals. PVDF is a semi-crystalline polymer with the repeating unit $(CH_2CF_2)_n$. VDF is polymerized to PVDF by radical polymerization in water under controlled pressure and temperature conditions using an initiator and emulsifier. The degree of crystallinity of PVDF ranges from 35% to 70%, whereby the crystallization of PVDF is controlled by several variables: Molecular weight, molecular weight distribution, polymerization process, thermal history and cooling rates. PVDF aerogels have the potential to be used in a wide range of applications by combining the properties of fluorine-containing polymers and highly porous aerogels.[7] Some examples are oil-water separation,[8] thermal insulation[9] and hybrid insulating membrane.[10] Despite its wide range of possible applications, this type of PVDF aerogel has not yet been researched in detail. For this reason, PVDF synthesis parameters were systematically varied to provide access to PVDF with widely varying properties. These

materials will be used to prepare PVDF aerogels and to correlate the properties of polymer and aerogel. In addition, it will be studied which properties are required for specific applications.

Experimental

First, PVDF was synthesized in an emulsion polymerization in a semi-batch process. For this, deionized water was added to the temperature-controlled reactor. VDF was then added. For this purpose, the corresponding quantities of emulsifier and, if necessary, transfer reagent are weighed out, placed in the airlock and conveyed into the reactor by means of a nitrogen overpressure. Before the initiator dissolved in water is added to the reactor in the same way. The reaction was controlled with the aid of DLS. The polymerization is terminated when the desired conversion is reached. To break up the emulsion, it is frozen overnight. The next day, the PVDF is filtered off and washed with water. Finally, the moist polymer is dried in a vacuum drying oven at 70 °C.
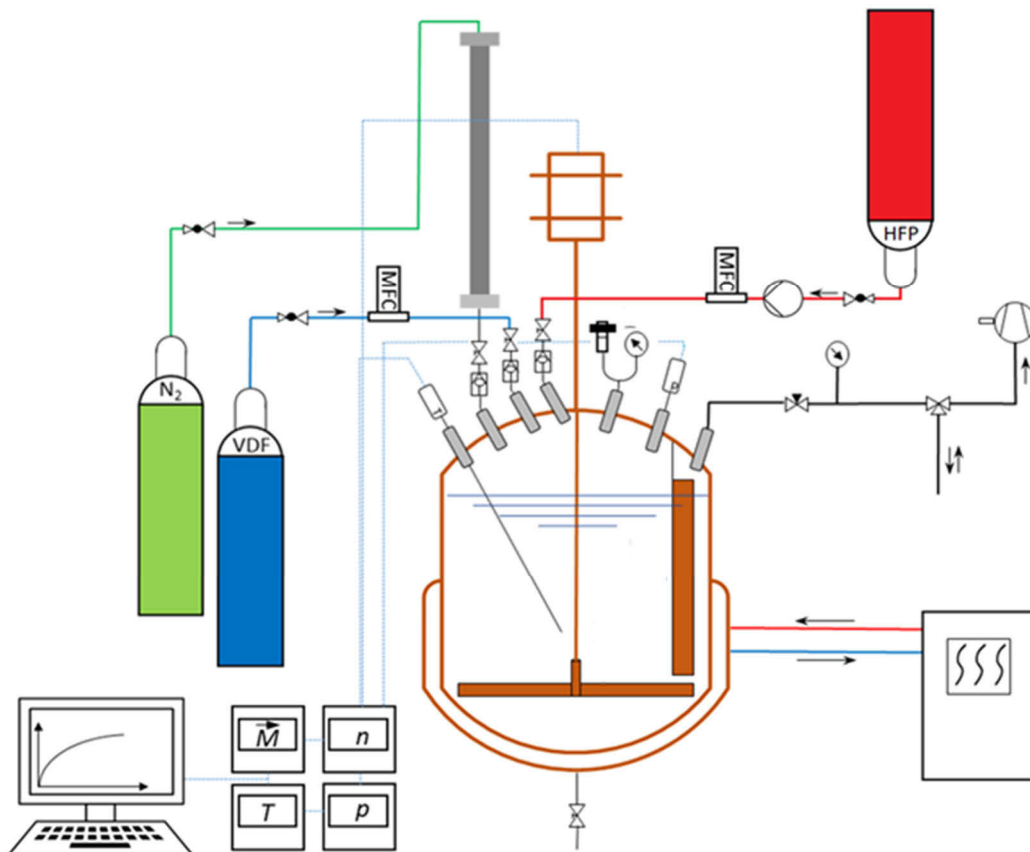

Fig. 1: Reactor setup for homopolymerization of VDF and for copolymerization with HFP.[7]

The production of the PVDF aerogel via the vapor-induced phase separation (VIPS) process requires precise control of the conditions for polymer solution preparation. The polymer solution consists of PVDF and DMSO as a solvent. The open vessel containing

PVDF dissolved in DMSO was placed in a second vessel containing non-solvent. The ensuing transfer of solvent and nonsolvent leads to phase inversion and the formation of a three-dimensional porous polymer network. The fractional solvent exchange was then continued until the solvent was completely replaced by ethanol. Finally, the gel was dried with supercritical CO_2.

Summary

As part of my work, radical emulsion polymerizations of vinylidene fluoride were carried out in a semi-batch process. Iodine transfer polymerizations were also investigated to obtain control over the molecular weight distributions of the product PVDF. In addition, the effect of the transfer reagent on the polymerization rate and the molar mass control of the product PVDF was evaluated.

In the second part of this thesis, the synthesis and characterization of aerogels based on poly(vinylidene fluoride) and their properties will be investigated. For this purpose, aerogels based on PVDF were produced. During the synthesis, various parameters such as solvent, dissolution temperature and molecular weight of PVDF were varied and the influence of these parameters on the properties of the aerogel was investigated.

References

[1] A. Du, B. Zhou, Z. Zhang, J. Shen, *Materials* **2013**, *6*, 941–968.

[2] A. Zaman, F. Huang, M. Jiang, W. Wei, Z. Zhou, *Energy Built Environ.* **2020**, *1*, 60–76.

[3] Y. Zhang, J.-B. Huo, J.-C. E. Yang, M.-L. Fu, *Mater. Lett.* **2019**, *240*, 88–91.

[4] Y. Pan, X. Cheng, T. zhou, L. Gong, H. Zhang, *Mater. Lett.* **2018**, *229*, 265–268.

[5] T. Zhang, Y. Zhang, X. Wang, S. Liu, Y. Yao, *Mater. Lett.* **2018**, *229*, 103–106.

[6] C. A. García-González, A. Sosnik, J. Kalmár, I. D. Marco, C. Erkey, A. Concheiro, C. Alvarez-Lorenzo, *J. Controlled Release* **2021**, *332*, 40–63.

[7] F. Brandl, S. Beuermann, *Chem. Ing. Tech.* **2018**, *90*, 372–379.

[8] D. Zang, F. Liu, M. Zhang, X. Niu, Z. Gao, C. Wang, *Chem. Eng. J.* **2015**, *262*, 210–216.

[9] F. Yang, X. Zhao, T. Xue, S. Yuan, Y. Huang, W. Fan, T. Liu, *Sci. China Mater.* **2021**, *64*, 1267–1277.

[10]   K. Li, K. Wang, Y. Zhang, H. Liu, J. Wang, *J. Membr. Sci.* **2020**, *597*, 117632.

Investigation of the Single- and Two-Phase Flow in High-Pressure Relief Scenarios

Daniel Dyck, Markus Busch*

Ernst-Berl-Institute of Technical and Macromolecular Chemistry, Technical University of Darmstadt, 64287 Darmstadt/Germany, *e-mail: markus.busch@pre.tu-darmstadt.de

Introduction

The demand of polymers is still increasing with polyethylene being produced in a scale of hundreds of mega tons per year. The production of low-density polyethylene (LDPE) via radical polymerization is conducted at temperatures of up to 330 °C and pressures of up to 3500 bar.[1] In a worst-case scenario, these harsh conditions can lead to an endanger of the people at the plant and in the immediate vicinity. To ensure a safe operation of the polymerization plant, a valid safety concept consisting of inherent and passive safety measures is needed. The inherent safety measures include the knowledge of the maximum permissible process variables like the decay limits or maximum pressures. Passive safety measures include the implementation of passive safety devices like rupture discs and safety valves, which provide a relief of the system to safe operation conditions. Today, relief systems are mostly sized by the usage of empirical methods.[2] Their calculations use the discharge coefficient K_d, a parameter describing the deviation of the calculated mass flow from the experimental one. It is often determined by the valve manufactures with nitrogen under normal conditions. Since the sizing of the safety devices play a decisive role for its proper functioning, a sound knowledge of the relief process inside the devices and further down the vent line under process conditions allows to optimize the sizing process of safety valves.

The aim of this work was to investigate the influence of various process parameters like starting temperature, pressure, gas type on the relief process and to develop a model for the transient description of a two-phase flow.

Experimental

The investigation of the flow during the relief process is done with a 200 mL shrunk-constructed autoclave designed for temperatures up to 300 °C and pressures up to 3000 bar, in which several modified thermocouples and pressure sensors are positioned to allow a fast measuring and recording of the temperature and pressure

(Figure 1). The gases are fed compromised into the reactor using a piston compressor from *Andreas Hofer GmbH*, while the dosing of the liquid components is done with a piston pump from *FINK*. The relief of the mixtures is initiated by the opening of a pneumatically controlled valve from *SITEC*.
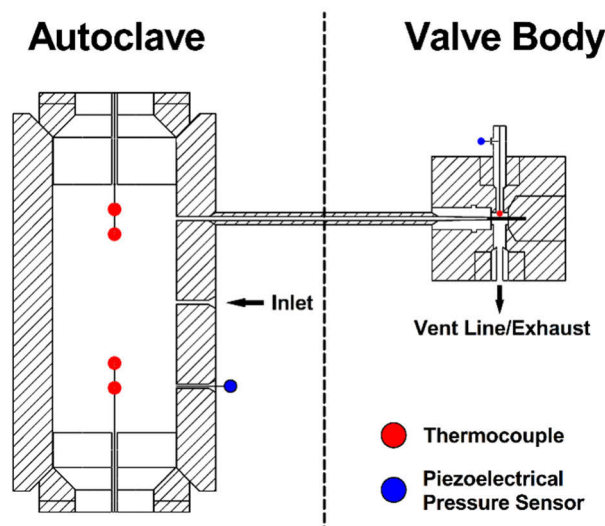

Fig. 1.: Schematic overview of the experimental setup and positions of the thermocouples and pressure sensors for the relief experiments.

The transient reproduction of the experimental pressure drop curves is done with a *VBA*-script[3] based on the isentropic nozzle model by J. Schmidt[4], which for the description of the two-phase flow is combined with a script based on the HNE-DS[5,6] model. The script uses the PC-SAFT EOS[7] and the PVT-program *Multiflash* by *KBC* for its calculations. The adjustment of the calculated pressure drop curves on the experimental ones allows the determination of the discharge coefficients. Figure 2 shows the experimental pressure drop curves in dependency of the starting temperature (left) and investigated gas type (right). The pressure drop rate during the relief increases with a decreasing starting temperature since the compressibility of the gases increases. In contrast to that, the discharge coefficients increase with the temperature. This trend is to be expected due to a decrease of the density, sound velocity and viscosity of the system with a smaller temperature leading to more frictional pressure losses during the flow. The investigation of the influence of the gas type shows a large influence, as the pressure drop rate for methane is quite higher than the one for nitrogen and ethene. This dependency is also visible in the discharge coefficients, which vary from 0.765 to 0.81.
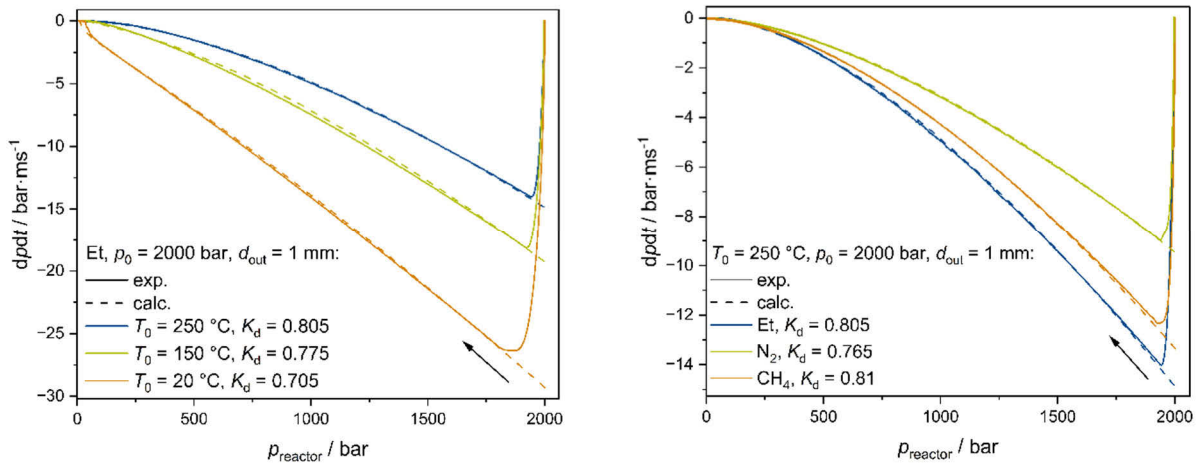
Fig. 2.: Left: Plot of the pressure drop rate curves of ethene in dependency of the starting temperature. Right: Plot of the pressure drop rate curves in dependency of the gas type.

For the investigation of the two-phase flow, relief experiments of a mixture of ethene and vinyl acetate are carried out (Figure 3). Here, the *VBA*-script changes from the one-phase to two-phase model ones the simulation expects a phase change of the mixture into the two-phase regime. The addition of the vinyl acetate leads to a decrease in the pressure drop rate compared to the ethene ones. Around a reactor pressure under 80 bar, which is more visible on the right side of Figure 3, a change of the curvature behavior from left-curved to right-curved is visible, which is contributed to the change of the flow from single- to two-phase flow. The liquefied parts of the two-phase flow lead to a reduced mass outcome from the nozzle of the valve and therefore to a further reduction of the pressure drop rate.
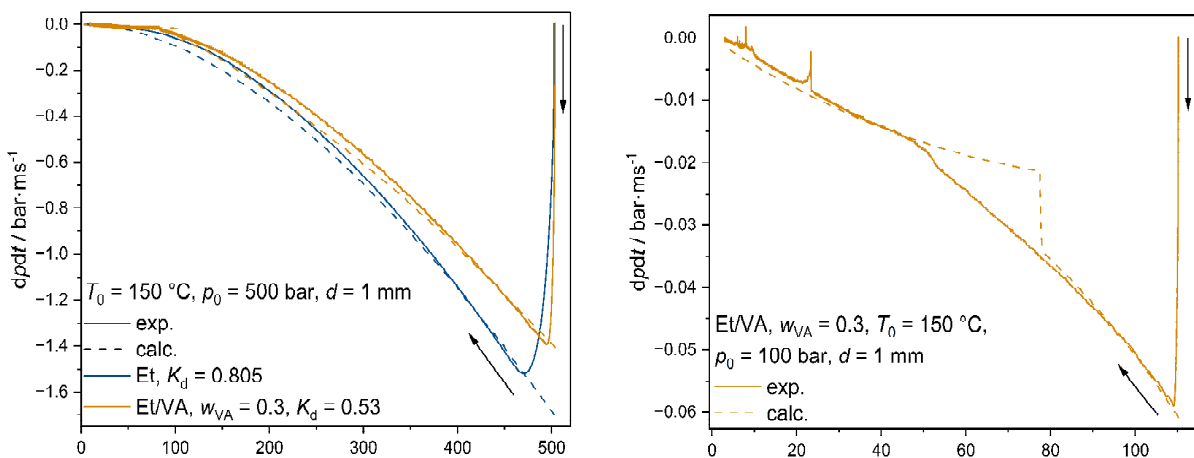

Fig. 3.: Left: Plot of the pressure drop rate of a 0.3 wt% ethene/vinyl acetate mixture compared to the one of ethene at 500 bar. Right: Plot of the pressure drop rate of a 0.3 wt% ethene/vinyl acetate mixture at 100 bar.

By combining both the single- and two-phase flow model, the experimental curve can be reproduced (dashed line). For the discharge coefficients the trend of a decreasing value for higher mass fractions of vinyl acetate is visible, which is consistent with the results from Ö. DELIBALTA[8] for higher starting pressures (Figure 4). The added vinyl acetate results in a phase separation occurring at the narrowest point of the valve during the relief, which reduces the valve seat cross-section and therefore reduces the experimental outflow compared to the calculated one leading to smaller values for the discharge coefficient.
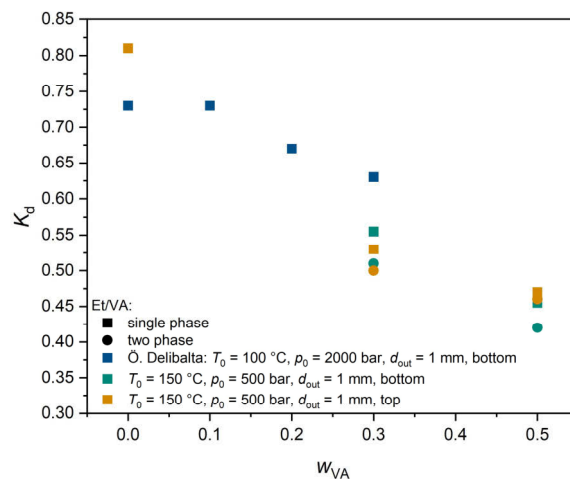

Fig. 4.: Plot of the discharge coefficients in dependency of the mass fraction of vinyl acetate w_{VA} in the mixture. The blue points represent the results from the work of Ö. DELIBALTA[8].

Summary

The investigation of the relief scenario in dependence of several input parameters like gas type and starting temperature has shown a strong influence of these parameters on the pressure drop rates as well as the discharge coefficients. Therefore, the determination of those values at normal conditions for the sizing calculation of valves is not ideal for such harsh conditions occurring in a LDPE plant. Those influences can also be seen by the addition of comonomers like vinyl acetate. A combination of both the isentropic nozzle model and the HNE-DS model has been able to reproduce the experimental pressure drop curve with its phase transition from single- to two-phase flow.

References

[1] G. Luft, *Chem. Unserer Zeit* **2000**, *34*, 190.

[2] R. Darby, *Process. Saf. Prog.* **2006**, *25*, 130.

[3] D. Zink, *Sicherheitstechnische Untersuchungen im Bereich der LDPE-Hochdrucksynthese*. Dissertation, Shaker, Düren, **2023**.

[4] J. Schmidt, W. Peschel, A. Beune, *Forsch. Ingenieurwes.* **2009**, *73*, 105.

[5] J. Schmidt, S. Claramunt, *J. Loss. Prev. Process. Ind.* **2016**, *41*, 419.

[6] J. Schmidt, *Forsch. Ingenieurwes.* **2007**, *71*, 47.

[7] J. Gross, G. Sadowski, *Ind. Eng. Chem. Res.* **2001**, *40*, 1244.

[8] Ö. F. Delibalta, *Safety Assessment of Decomposition and Pressure Relief Scenarios in High-Pressure LDPE Process*, Shaker, Düren, **2023**.

Supercritical Fluid Extraction from Cornelian Cherry (*Cornus mas* L.) Seeds

Dušan Đurić, Marko Stamenić

Department of Organic Chemical Technology, Faculty of Technology and Metallurgy,

University of Belgrade

E-mail: 20224017@estudent.tmf.bg.ac.rs

Introduction

Cornelian Cherry (*Cornus mas* L.) is a species of the genus *Cornus L.* which belongs to the *Cornaceae Link* family, comprising 2 genera (*Alangium Lam.* and *Cornus*) with about 85 species that mostly grow in temperate climate and subtropical parts of both hemispheres [1]. The fruit of the Cornelian Cherry is of spherical or elliptical shape, with an average length of 1.5–2 cm and weight of 1.6–9 g, depending on the species. The fruits of the Cornelian Cherry are juicy, with a tart-sour taste, and ripen gradually in late summer and early autumn. The Cornelian Cherry fruit is a proven rich source of compounds such as polyphenols (anthocyanins, flavonols, and phenolic acids), iridoids, terpenoids (ursolic acid), and vitamin C [2].

The seed of the Cornelian Cherry accounts for 8.0–15.9% [3] or 5.7–11.0% [4] of the total weight of the fruit and is considered waste material in the processing of the fruit [5]. The chemical composition of Cornelian Cherry seeds shows that in terms of polyphenol content, Cornelian Cherry seeds contain 90% of the total polyphenol content of the fruit, just like the fruit skin. When it comes to fatty acids, six fatty acids are identified in the oil fraction of the seed and, importantly, about 90% are unsaturated fatty acids [6]. The highest fatty acid content, ranging from 64.8–75.0%, was observed for linoleic acid, followed by 15.0–22.9% for oleic acid and 1.3–2.1% for linolenic acid. The remaining fatty acids were stearic, palmitic, and arachidic acids. It has also been found that the seed contains mineral compounds such as calcium, potassium, magnesium, boron, copper, manganese, sodium, nickel, lead, and strontium [7].

The use of Cornelian Cherry and its by-products is various, as it can be used in manufacturing jams, compotes, liqueur, juices, and other food products [8]. Also, it has been found that the Cornelian Cherry has therapeutic properties, so in traditional medicine, all parts of the Cornelian Cherry are used for the treatment of diseases of the digestive organs, inflammation, and infections [2]. Fatty acids and alcohol extract of the Cornelian Cherry seed have shown strong antimicrobial effects on bacteria such as *S. Aureus, E. Coli,* and *Pseudomonas aeruginosa* [9]. The analyses carried out by Ahmetović et al. [10]

showed that the oil obtained from Cornelian Cherry seeds is of high quality and is similar to other vegetable oils such as sunflower oil, corn oil, etc. Additionally, this oil has resistance to oxidative deterioration due to the presence of components that have an antioxidant effect [10]. The seeds can also be a substitute for coffee or represent an aromatic and bioactive addition to cereal coffee [11]. Additionally, the seed of Cornelian Cherry can also be used to obtain biofuels from hydrothermal liquefaction [12].

Supercritical fluid extraction (SFE) has been classified among emerging extraction techniques that can be used for obtaining substances with potential applications in a variety of industries. It uses the specific characteristics of supercritical fluids that offer several advantages over the conventional extraction methods [13]. A supercritical fluid (SCF) is any substance at temperature and pressure above the critical values of these parameters. A substance in at supercritical state possesses a combination of liquid-like and gas-like properties. For example, the density of SCFs is relatively high, similar to liquid density, so they can be used as solvents. On the other hand, SCFs viscosity is comparable with viscosity of gasses, so they can easily diffuse through solid matrices [14]. Various fluids have been investigated for potential use in the supercritical state, such as carbon dioxide, water, ethane, propane, butane, ethanol, etc., with carbon dioxide being the dominant choice [15].

The use of carbon dioxide is desirable because of its non-toxic, non-flammable, and non-polluting properties, in addition to being inexpensive. Its critical properties (T_c = 31.1°C; P_c = 73.8 bar) make it an excellent solvent for extracting heat-sensitive bioactive compounds, such as antioxidants, pigments, flavors, odors, fatty acids, and essential oils [16]. Additionally, the use of supercritical carbon dioxide (scCO$_2$) leads to the absence of chemical residues in the extract because carbon dioxide is a gas at room temperature and atmospheric pressure, and therefore is easily removed at the end of extraction [15]. Carbon dioxide is a nonpolar compound so the solubility of highly polar compounds in scCO$_2$ is fairly low. However, it is possible to alter the selectivity and solubility of these compounds in scCO$_2$ by adding polar cosolvents, such as ethanol, which is mostly used for this purpose [17]. During SFE different parameters, such as temperature, pressure, co-solvent addition, and plant material particle size can be optimized to improve the extraction yield of target compounds because the solubility and mass transfer resistance of raw materials are related to those variables [18].

Various studies have shown numerous advantages of SFE including its fast processing time, suitability for extracting volatile and thermolabile compounds, higher productivity in terms of increased yields, reduced solvent use, and environmental

protection using safe solvents. It plays a vital role in various fields such as food, pharmacy, agriculture, and cosmetics [19]. As stated, today SFE is not only applied in laboratories for research purposes, but its application has been commercially developed on an industrial scale, for the production of natural food ingredients (hops, flavors, spices, dyes, vitamin-rich extracts, specific lipids), nutraceuticals, pharmaceuticals, and more [20].

Experimental

For the experiments, Cornelian Cherry seeds from two areas of the Western Balkans, namely Bosnia and Montenegro, were used. Prior to the experiments the seeds were dried, ground, and sifted, after which 10 g of a fraction with a medium diameter of 0.4 µm was used in each experiment. As it was expected that there were fatty acids in the seeds, experiments were performed at a pressure of 30 MPa and temperatures of 40 and 60°C. For comparison, an additional experiment was performed with seeds from Bosnia at the pressure of 10 MPa and a temperature of 40°C. Additionally, classic (Soxhlet) extractions were performed with seeds from Bosnia, using hexane and ethanol as solvents. In Figure 1. the apparatus used for the SFE is shown.

C – cryostat
P – pump
E - extractor
S – separator
PI – pressure indicator
TI – temperature indicator
HJ – heating jacket
V -valves
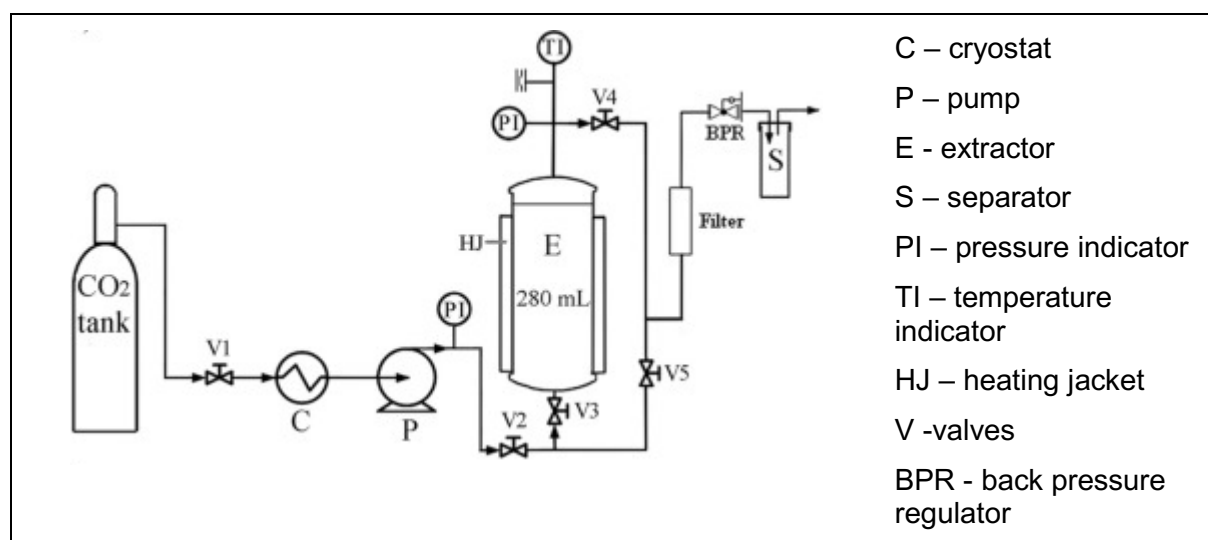BPR - back pressure regulator

Fig. 1. Scheme of the SFE apparatus.

The results from SFE experiments, shown in Figure 2., show that the kinetics of the extraction are practically the same at 30 MPa for seeds from both locations. The extraction rate is higher at higher temperature, but the overall yield is substantially higher at lower temperature in both samples. This result indicates that the composition of the extracts should be quite dependent on the temperature, which is expected to be confirmed with qualitative analysis. Expectedly, the yield obtained from the additional experiment at 10

MPa and 40°C was lower compared to the one obtained at the same temperature and higher pressure. The yields of the Soxhlet extractions were 6.57% and 23.65% with hexane and ethanol, respectively, indicating that the extract constituents are mainly polar compounds.
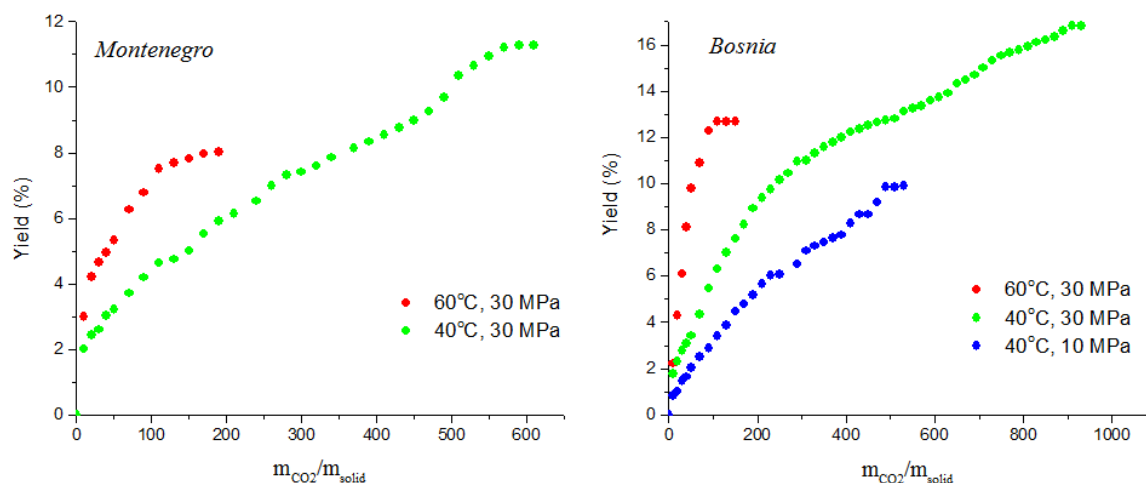

Fig. 2. Results of SFEs from seeds of Cornelian Cherry

Summary

Cornelian Cherry seed extracts can potentially be used in industry to obtain various products for many applications. The results from this investigation showed that the overall yield of the scCO2 extraction from Cornelian Cherry seeds from two locations was higher at lower temperature at a pressure of 30 MPa. What could be done in the future is analysis of the obtained extracts using gas chromatography-mass spectroscopy (GC-MS) and high-performance liquid chromatography (HPLC) in order to analyze the composition of the obtained extracts and, subsequently, optimize the SFE conditions for extraction of selected components or group of components.

References

[1] M. Christenhusz and J. W. Byng, "The number of known plants species in the world and its annual increase," *Phytotaxa,* vol. 261, no. 3, pp. 201-217, 2016.

[2] B. Dinda, A. Kyriakopoulos, S. Dinda, V. Zoumpourlis, N. M. Thomaidis, A. Velegraki, C. Markopoulos and M. Dinda, "Cornus mas L. (cornelian cherry), an important European and Asian traditional food and medicine: Ethnomedicine, phytochemistry and pharmacology for its commercial utilization in drug industry," *Journal of Ethnopharmacology,* vol. 193, pp. 670-690, December 2016.

[3] A. Z. Kucharska, A. Sokol-Letowska and N. Piórecki, "Morphological, physical and chemical, and antioxidant profiles of polish varieties of cornelian cherry fruit (Cornus mas L.)," 2011.

[4] O. M. Szczepaniak, J. Kobus-Cisowska, W. Kusek and M. Przeor, "Functional properties of Cornelian cherry (Cornus mas L.): a comprehensive review," *European Food Research and Technology,* vol. 245, no. 10, pp. 2071-2087, Jun 2019.

[5]   D. Przybylska, A. Z. Kucharska, I. Cybulska, T. Sozański, N. Piórecki and I. Fecka, "Cornus mas L. Stones: A Valuable by-Product as an Ellagitannin Source with High Antioxidant Potential," *Molecules,* vol. 25, no. 20, October 2020.

[6]   D. Przybylska, A. Z. Kucharska, I. Cybulska, T. Sozański, N. Piórecki and I. Fecka, "Cornus mas L. Stones: A Valuable by-Product as an Ellagitannin Source with High Antioxidant Potential," *Molecules,* vol. 25, no. 20, p. 4646, October 2020.

[7]   I. Juranović-Cindrić, M. Zeiner, M. Krpetić and G. Stingeder, "ICP-AES determination of minor and major elements in Cornelian cherry (Cornus mas L.) after microwave assisted digestion," *Microchemical Journal,* vol. 105, pp. 72-76, 2012.

[8]   P. Brindza, J. Brindza, D. Tóth, S. V. Klimenko, and O. Grigorieva, "Slovakian Cornelian Cherry (Cornus mas L.): Potential for Cultivation," *Acta Horticulturae,* no. 760, pp. 433-437, July 2007.

[9]   H. M. Bayram and S. A. Ozturkcan, "Bioactive components and biological properties of cornelian cherry (Cornus mas L.): A comprehensive review," *Journal of Functional Foods,* vol. 75, October 2020.

[10] M. Ahmetović, E. Trumić, J. Bajraktarević, H. Keran and I. Šestan, "Examination the Quality of Oil Obtained from Cornelian Cherry (Cornus mas L.) Seeds as an Additive in the Production of Cosmetic Preparations and Food Supplements," *International Journal for Research in Applied Sciences and Biotechnology,* vol. 8, no. 1, pp. 1-6, January 2021.

[11] R. Spychaj, A. Z. Kucharska, A. Szumny, D. Przybylska, E. Pejcz and N. Piórecki, "Potential valorization of Cornelian cherry (Cornus mas L.) stones: Roasting and extraction of bioactive and volatile compounds," *Food Chemistry,* vol. 358, 2021.

[12] M. Akalin, K. Tekin and S. Karagöz, "Hydrothermal liquefaction of cornelian cherry stones for bio-oil production," *Bioresource technology,* vol. 110, 2012.

[13] P. A. Uwineza and A. Waśkiewicz, "Recent Advances in Supercritical Fluid Extraction of Natural Bioactive Compounds from Natural Plant Materials," *Molecules,* vol. 25, no. 17, August 2020.

[14] L. Padrela, M. A. Rodrigues, S. P. Velaga, H. A. Matos and E. G. de Azevedo, "Formation of indomethacin–saccharin cocrystals using supercritical fluid technology," *European Journal of Pharmaceutical Sciences,* vol. 38, no. 1, pp. 9-17, 2009.

[15] H. Ahangari, J. W. King, A. Ehsani and M. Yousefi, "Supercritical fluid extraction of seed oils – A short review of current trends," *Trends in Food Science & Technology,* vol. 111, pp. 249-260, 2021.

[16] N. Budisa and D. Schulze-Makuch, "Supercritical Carbon Dioxide and Its Potential as a Life-Sustaining Solvent in a Planetary Environment," *Life,* vol. 4, no. 3, pp. 331-340, 2014.

[17] K. Tyśkiewicz, M. Konkol and E. Rój, "The Application of Supercritical Fluid Extraction in Phenolic Compounds Isolation from Natural Plant Materials," *Molecules,* vol. 23, no. 10, 2018.

[18] R. P. F. F. da Silva, T. A. P. Rocha-Santos and A. C. Duarte, "Supercritical fluid extraction of bioactive compounds," *TrAC Trends in Analytical Chemistry,* vol. 76, pp. 40-51, 2016.

[19] C. G. Pereira and M. A. A. Meireles, "Supercritical Fluid Extraction of Bioactive Compounds: Fundamentals, Applications and Economic Perspectives," *Food and Bioprocess Technology,* vol. 3, no. 3, pp. 340-372, 2009.

[20] M. Cvjetko Bubalo, S. Vidović, I. Radojčić Redovniković and S. Jokić, "New perspective in extraction of plant biologically active compounds by green solvents," *Food and Bioproducts Processing,* vol. 109, pp. 52-73, 2018.

[21] J. Jovanović, Flora of SR Serbia, J. M., Ed., Belgrade: Serbian Academy of Sciece and Arts, 1973, pp. 175-179.

[22] R. Vidrih, Ž. Čejić and J. Hribar, "Content of certain food components in flesh and stones of the cornelian cherry (Cornus mas L.) genotypes," *Croatian Journal of Food Science and Technology,* vol. 4, 2012.

[23] G. Brunner, "Supercritical fluids: technology and application to food processing," *Journal of Food Engineering,* vol. 67, no. 1-2, pp. 21-33, 2005.

[24] O. M. Szczepaniak, J. Kobus-Cisowska, W. Kusek and M. Przeor, "Functional properties of Cornelian cherry (Cornus mas L.): a comprehensive review," *European Food Research and Technology,* vol. 245, no. 10, pp. 2071-2087, Jun 2019.

Recycling of Ti6Al4V Chips from the Aerospace Industry (RECoTiA)

Gauthier Grejois

IMT Mines Albi / RAPSODEE gauthier.grejois@mines-albi.fr

Keywords: aerospace metal chips, cutting oil, Ti6Al4V recycling, supercritical processes

Introduction

Titanium is widely used in the aerospace industry because of its mechanical and physical-chemical properties. It accounts for 0.6% of the earth's crust, making it the fourth most abundant metal on earth after iron, aluminium and magnesium [1]. Since 2020, the European Union has classified titanium as a "Critical Metal" [2]. This category groups together metals that are essential to the economy, but which can sometimes be difficult to access. During the manufacture of a part for the aerospace industry (such as landing gear), it is estimated that almost 90% of the initial material is eliminated and ends up in the form of scrap and shavings [3]. Interesting properties such as light weight, high mechanical properties and corrosion resistance make Ti6Al4V an alloy of choice for certain aeronautical parts, such as engine pylons, landing gear and structural parts [4]. It is the most widely used titanium alloy in the world, accounting for more than 50% of the aerospace market [5]. Machining this alloy produces waste in the form of swarf, polluted by cutting oils. Machining Ti6Al4V also leads to surface oxidation of the alloy because it is a metal with a very high affinity for oxygen, up to 33% at atomic level [6]. This explains why, in the United States, only 40-60% of these chips are recycled in the aerospace industry, due to the high oxygen content [7]. Cutting oils contaminating the swarf can be recovered using solvents such as ethanol and acetone in ultrasonic baths [8]. This thesis work is part of the RECULITI project (Recycling and covalorisation of critical metals (lithium, titanium) from Li-ion batteries and machining chips from the aerospace industry). Its aim is to explore new approaches to the recycling of critical lithium and titanium metals, based on innovative technologies and the co-use of recovered metals.

RECULITI focuses on recycling titanium alloy waste using alternative methods to those currently on the market, with a view to reintroducing it into the aerospace industry.

However, if the material recycled in this way does not meet the requirements of the aerospace sector, new recovery routes are envisaged, such as the production of battery electrode materials or catalysts supported on titanium dioxide (TiO_2).
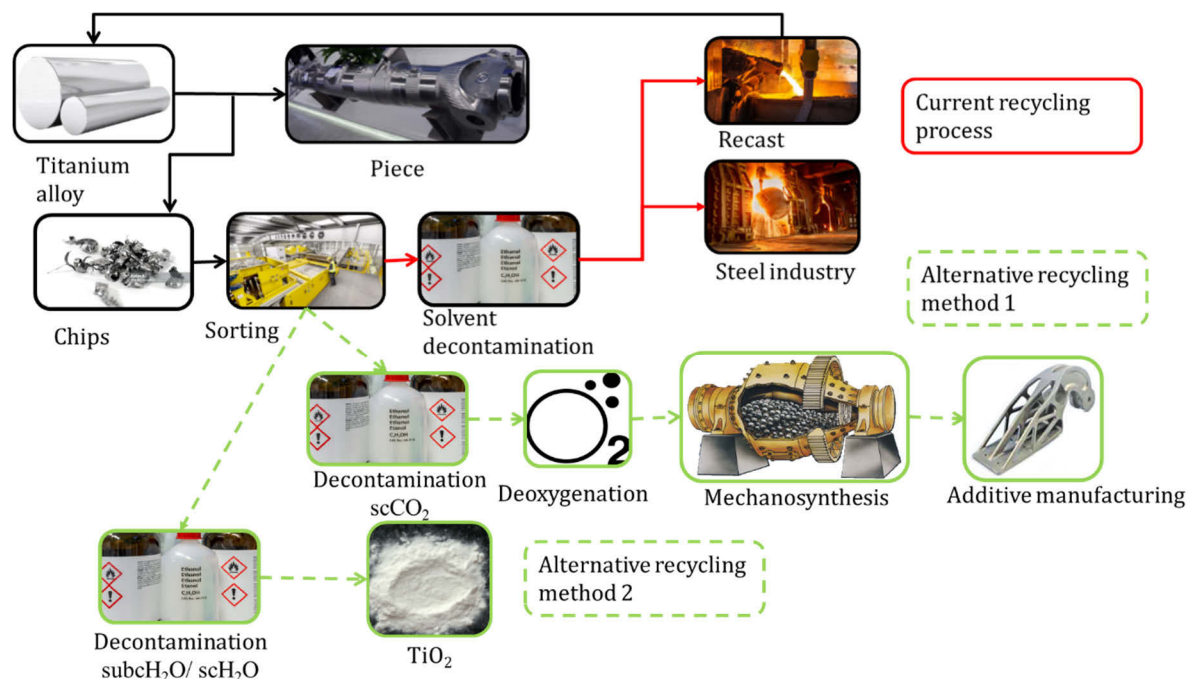

Fig.1 Current and alternative ways of recycling titanium

This project has two main objectives (Fig. 1). The first objective is to propose innovative methods for decontaminating Ti6Al4V machining chips from the aerospace industry. The first recycling route envisaged involves decontaminating the swarf by solubilising the cutting oils in supercritical CO_2 (CO_2sc). This step will extract the cutting oils and recover them once the gas has been decompressed. Next, deoxygenation is used to reduce the oxygen content of the alloy. Finally, the material will be powdered using a mechanosynthesis process, with the aim of using additive manufacturing to produce the final parts from recycled Ti6Al4V. The second objective is to find alternative recycling routes for these chips by combining them with another metal (Li). For example, for applications such as catalysis or batteries. The methods envisaged should be less energy-intensive and less harmful to the environment. The use of sub- and super-critical hydrothermal processes (H_2Osub/H_2Osc) is envisaged to destroy cutting oils and promote oxidation of titanium (TiO_2).

As part of the collaboration between the RAPSODEE laboratory and the ICA in Toulouse, preliminary experiments were carried out at both sites. At RAPSODEE, characterisations were carried out, including thermogravimetric analyses to study the titanium chips and determine the quantity of organic oil on their surface. The cutting oil was also characterised, using gas chromatography coupled with a mass spectroscopy detector to determine the composition of the cutting oil (not available on the safety data sheet) and to monitor its evolution during the recycling processes. Next, CO_2sc, H_2Osub and H_2Osc treatments are planned for the chips in order to separate or degrade the cutting oil present on the surface of the Ti6Al4V chips. In addition, ICP-OES will be used to determine the composition of the chips. The ICA site focuses on industrialisation and part design. The raw materials and additive manufacturing will be carried out in their laboratory. The aim of this multi-disciplinary process engineering and recycling project is to ensure rapid transfer and valorisation at the end of the work. We hope to increase our technological maturity and be in a position to initiate scientific value-added partnerships with industrial partners.

Acknowledgements

References

[1] G. Lütjering et J. C. Williams, Éd., « Introduction Titane », in *Titanium*, in Engineering Materials, Processes. , Berlin, Heidelberg: Springer, 2007, p. 1☐14. doi: 10.1007/978-3-540-73036-1_1.

[2] E. Commission, E. Directorate-General for Internal Market Industry, SMEs, M. Grohol, et C. Veeh, *Study on the critical raw materials for the EU 2023 – Final report*. Publications Office of the European Union, 2023. doi: doi/10.2873/725585.

[3] O. Takeda et T. H. Okabe, « Recycling of Ti », in *Extractive Metallurgy of Titanium*, vol. Chapitre 16, Elsevier, 2020, p. 363☐387. doi: 10.1016/B978-0-12-817200-1.00016-8.

[4] J. Delfosse, « Titane et alliages de Titane Airbus », 2016.

[5] World Intellectual Property Organization., *Production of Titanium and Titanium Dioxide from Ilmenite and Related Applications.* in Wipo. Unknown, 2023. doi: 10.34667/TIND.47029.

[6] Y. Zhang, Z. Z. Fang, P. Sun, Y. Xia, H. D. Lefler, et S. Zheng, « Chapter 10 - Deoxygenation of Ti metal », in *Extractive Metallurgy of Titanium*, Z. Z. Fang, F. H. Froes, et Y. Zhang, Éd., Elsevier, 2020, p. 181☐223. doi: 10.1016/B978-0-12-817200-1.00010-7.

[7] P.-F. Louvigné, « Etude de veille sur le marché du titane 2018 – 2020 », 2018.

[8] E. Teke, M. Sütçü, Y. Baskurt, et Ö. Seydibeyoglu, « Recovery of pressed titanium alloy machining chip via vacuum induction melting », *Scientific Research Communications*, vol. 2, nᵒ 1, janv. 2022, doi: 10.52460/src.2022.001.

Novel Aerogels from Alginic Acid: Kinetic Studies and Structural Transitions in the Fabrication Process

Preethi Aranala Gurumoorthi

Institute of Thermal Separation Processes, Hamburg University of Technology,

preethi.aranala@tuhh.de

Introduction

In the last few decades, biopolymer aerogels have gained importance due to their high porosity, high specific surface area, and low density. Alginates – polysaccharides obtained from brown seaweeds – represent an important class of model systems for the large-scale fabrication of biopolymer-based aerogels.

Conventional processing of alginate aerogels starts with calcium-induced gelation in an aqueous medium to form hydrogels. Supercritical drying using sc-CO_2 is then performed to remove the solvent from the hydrogel to obtain the aerogel. Since water has a large miscibility gap with CO_2, the hydrogels must be solvent-exchanged with a suitable solvent prior to be sc-dried. The solvent exchange yields so-called lyogels. The transformation from hydrogel to lyogel results in a certain stiffening of the gel matrix. The solvent exchange and supercritical drying steps cause considerable gel shrinkage, which results in reduced porosity and specific surface area. Although, from a practical perspective, the shrinkage must be minimized [1], its origin is still poorly understood.

The goal of this work is to systematically study the evolution of both mechanical properties and shrinkage on the way from hydrogel to aerogel. Based on both experimental results and simulations, a plausible mechanism of shrinkage will be proposed. As a model system, employing novel acid-induced alginate hydrogels is suggested, as they are cross-linker-free and represent a simpler system compared to calcium-alginate gels. The fabrication of this novel class of aerogels will also be discussed in this work.

Experimental

(a) Fabrication of gels

There are well-established methods to form gels of alginic acid. This research work focuses on gelation through the diffusion setting method. The precursor aqueous solution

of alginate is prepared in five different concentrations, ranging from 1 to 5 wt%. They are placed in an ultrasonic bath for 4 hours to remove the air bubbles that were trapped during the preparation of the precursor solutions. The solutions are filled in dialysis bags from Carl Roth with a flat width of 25 mm and a molecular weight cut-off of 14 kDa. The dialysis bags are then immersed in a 5 wt% sulfuric acid solution in the upright position. The gelation of alginate in sulfuric acid is fast, but to reach equilibrium, the dialysis bags are left in the acid bath for 24 hours. The hydrogels are then removed from the dialysis bags, sliced into small cylinders, and washed in water to remove the excess acid.
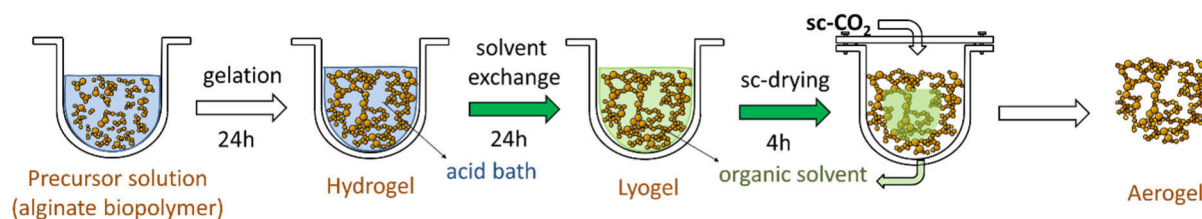

Figure 1: The schematic diagram for the fabrication of aerogels.

The hydrogels are then solvent-exchanged in an organic non-solvent (*i.e.* it does not dissolve the gel) to remove water, as the latter cannot be extracted with supercritical CO_2 due to poor miscibility under reasonable operating conditions. Ethanol is a suitable non-solvent that possesses complete miscibility with supercritical CO_2 as well as with water in the hydrogels. For the solvent exchange, two approaches are employed. The first approach is direct solvent exchange (DSE), where the hydrogels are exposed to pure ethanol. The non-solvent is replaced after 24 hours with fresh non-solvent. This is done until the concentration of the non-solvent at least 97%. The second approach is stepwise solvent exchange (SSE), where the hydrogels are slowly exposed to increasing concentrations of ethanol, from 20 wt% to 40, 60, 80 wt% and finally water-free ethanol. The hydrogels and alcogels (*i.e.* solvent-exchanged with ethanol) are characterized using a texture analyzer at the Institute of Solids Process Engineering and Particle Technology, Hamburg University of Technology, to study the mechanical properties of the gels (uniaxial compression tests).

(b) Kinetics of gelation

This work also involves the study of gelation kinetics in mineral and organic acids. 1 g of 5 wt% alginate solution is dropped on to a glass slide. A circular or square cover slip is placed above this drop and pressed gently to create a circular sandwich of alginate

solution between the two glass layers. This setup is then placed in a petri dish with the acid bath. The setup is shown in Figure 2.
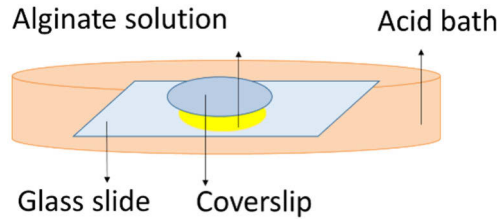

Figure 2: The schematic representation of the kinetics experiment.

The periphery of the alginate solution is in contact with the acid bath. The gelation starts from the periphery and progresses to the centre. The experiment is repeated for different acids and images are taken in regular intervals to capture the progress of the gelation.

Summary

(a) Shrinkage

The diameter of the hydrogels and alcogels are measured during the course of the experiment, such as after washing, and after every step of solvent exchange. Figure 3 shows the shrinkage of hydrogels and alcogels that were prepared using sulfuric acid.
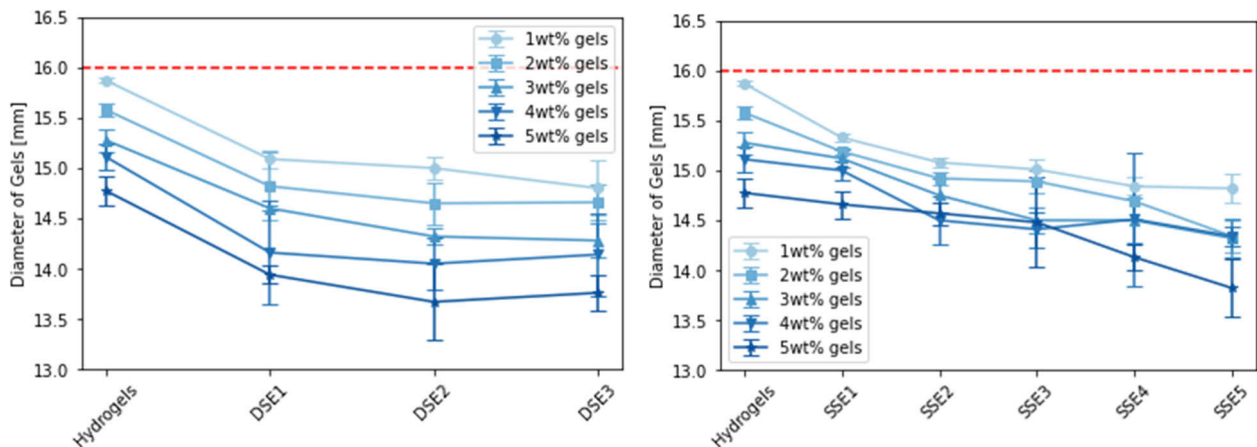

Figure 3: The shrinkage of hydrogels and alcogels in direct solvent exchange (DSE) on the left and step-wise solvent exchange (SSE) on the right, for alginate gels of concentration 1 to 5 wt%.

The step-wise solvent exchange is generally considered better for the gels as they are slowly exposed to the increasing concentrations of ethanol in the successive steps. From Figure 3, it is clear that as soon as the hydrogels are exposed to the pure ethanol in the

direct solvent exchange, they shrink considerably. In the end, the step-wise solvent exchanged gels also reach similar shrinkage as the direct solvent exchanged gels. This shows that the primary fibres of the gel demonstrate a certain aggregation as the solvent becomes enriched with ethanol, and the gels shrink.

(b) Mechanical properties

The mechanical properties of the hydrogels and alcogels are measured from the uniaxial compression test. The force vs. displacement data are obtained from the texture analyser, from which the elastic modulus of the gels are calculated.
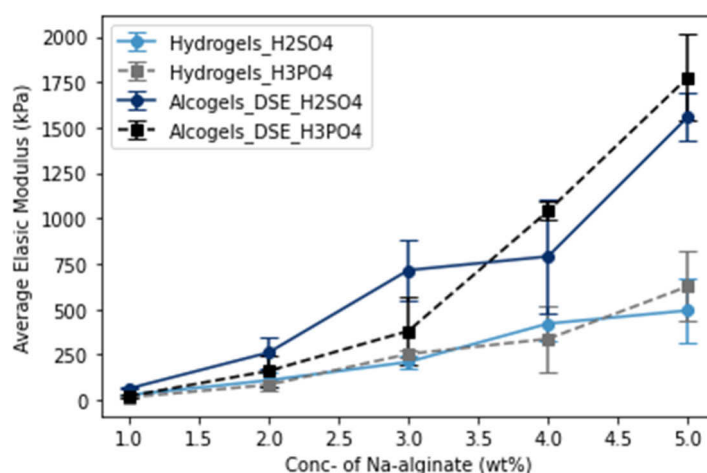

Figure 4: Comparison of elastic modulus of hydrogels and alcogels prepared using sulfuric and phosphoric acids with a compression velocity of 1 mm/s.

It is clear from Figure *4* that 5 wt% gels become stiffer when processed in the solvent exchange. This may be explained by two factors: (i) the volume fraction of alginate increases when gels shrink, causing an increase of the elastic modulus; (ii) structural reorganization of the solvent-exchanged gels result in a stiffer gel. The role of each factor is the subject of our ongoing work.

(c) Kinetics

From Figure 5, it can be seen that the gelation is complete in 70 min in case of sulfuric acid. Sulfuric acid is strong and yields a large concentration of H^+ ions when compared to organic acids taken in the same concentration. Influence of the nature of the gelation acid is part of our ongoing work.
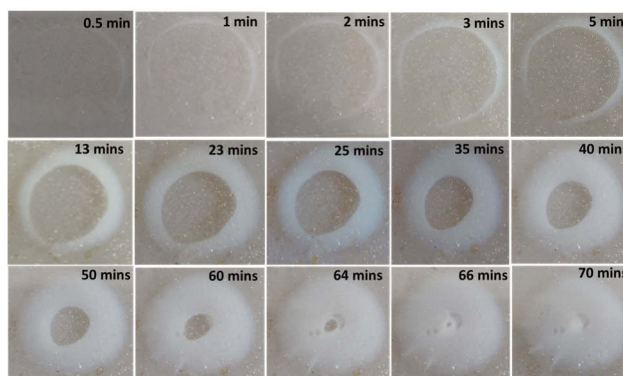
Figure 5: Gelation kinetics of 5 wt% alginate in sulfuric acid.

When gel from Figure 5 is observed under light microscope, the rings of gelation are clearly visible, which shows a clear separation of pregel layer from gel at a given time. The nature of the rings and their role in the overall gelation kinetics remains an open question.
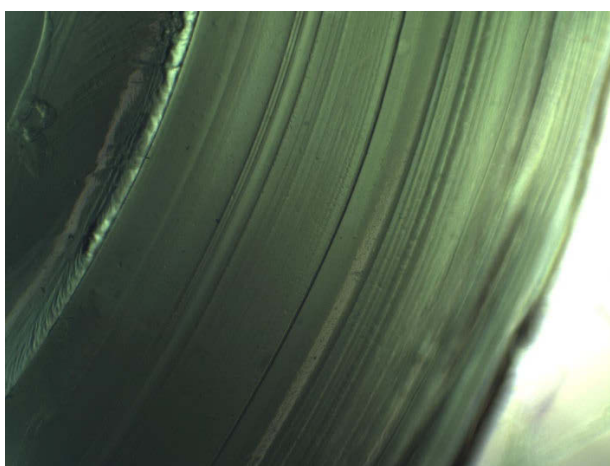

Figure 6: 5 wt% alginate gel observed under light microscope.

Outlook

The kinetic studies and mechanical properties of hydrogels and alcogels prepared with the organic acids have to be studied and compared with the mineral acids. The hydrogels and alcogels are to be characterized using Small Angle X-ray Scattering to observe the association of solvent and non-solvent in the primary fibres.

Acknowledgment

References

[1]   P. Gurikov, R. S. P., J. S. Griffin, S. A. Steiner, and I. Smirnova, "110th Anniversary: Solvent Exchange in the Processing of Biopolymer Aerogels: Current Status and Open Questions," Ind. Eng. Chem. Res., vol. 58, no. 40, pp. 18590–18600, Oct. 2019, doi: https://doi.org/10.1021/acs.iecr.9b02967.

Manufacturing and Analytics of Lipid Nanoparticles – Enabled by Monolithic Chromatography

Tristan Kovačič

Faculty of Chemistry and Chemical Engineering, University of Maribor / Sartorius BIA Separations, tristan.kovacic@biaseparations.com

Introduction

Lipid nanoparticle (LNP)-based therapeutics and vaccines have been on the forefront of non-viral delivery since SARS-CoV-2 vaccines rolled out and proved their worth.[1][2] Lipid nanoparticles enable a high degree of modularity depending on your desired outcomes. Lipids and/or manufacturing process can be tuned. Manufacturing of LNPs carries a major advantage over established viral vector therapies, by being easily scalable and much faster.[3]

All that modularity then leads to large diversity of LNP properties and heterogeneity within the samples. Formulation development needs a lot of time and energy to optimize those formulations to a desirable outcome.[4] The analytical tools for comprehensive analyses of LNPs are few and far between. Thus, prediction of in vivo LNP activity and immunogenicity is a very poor. Better, faster and more insightful analytical methods are needed to better predict LNP effectiveness, safety and stability, so that development can be accelerated and money saved.[5]

In the world of chromatography, monolithic columns are uniquely suitable for LNPs as they are made from one piece with large pores that cause no shear stress to the nanoparticles and can thus keep particles intact. Numerous diverse surface modifications can be made to achieve the desired binding and selectivity. Particles can thus be separated based on their size, charge, hydrophobicity, hydrophilicity, hydrogen bonding or a combination of those. These unique selectivities give a powerful insight into the particle composition and structure.

Especially problematic with LNPs are also off-target effects, undesired organ distribution and high immunogenicity. Thus, safety profile is a critical attribute that must be addressed during development.[6] A lot of those safety issues can stem from the heterogeneity of the sample, impurities present, empty particle present, fused/aggregated particles present.[7]

Those can be addressed by utilizing monolithic chromatography with the above described ways. This can be done both analytically and preperatively.

Preparatively, monolithic columns enable also a great alternative to TFF/dialysis.[8] Membrane adhesion and fouling is a large problem when scaling up. Monolithic columns provide an alternative by having no membranes. They can achieve all the same processes, like concentration, buffer exchange, while at the same time also being able to separate away non-encapsulated payload and undesired particle formations.

Experimental

SM-102, cholesterol, DSPC and PEG-DMG-2000 lipids were used in molar ratios 46.3:42.7:8.9:1.6. They were added to a glass vial and diluted with absolute ethanol to a final total lipid concentration of 12.5 mmol/L. A solution of mRNA mFIX4 (4 kb, Sartorius BIA Separations d.o.o.) was added to an Eppendorf tube and diluted to a final concentration of 105 µg/mL. A sodium citrate buffer solution (25 mM, pH 3.5) was used for dilution for formulation purposes. The two solutions were mixed with a flow rate ratio of 3:1 (cargo acidic solution: lipid solution) using NanoAssembler from Precision NanoSystem (Vancouver, British Columbia, Canada), based on microfluidic mixing, at a total flow rate of 10 ml/min. The resulting particles were diluted immediately to 1x PBS, pH 7.4 and either buffer exchanged and concentrated into 1xPBS+9% sucrose using Amicon 30 kDa 0.5 mL centrifugal filters or buffer exchanged, concentrated and purified using a CIMmac HIC column (Sartorius BIA Separations d.o.o.) under hydrophobic interaction chromatographic conditions. mRNA was quantified using a chromatographic approach to quantify mRNA within the particles. Size of particles was measured using Videodrop® (Myriade) or NTA (Malvern, NanoSight 3000).
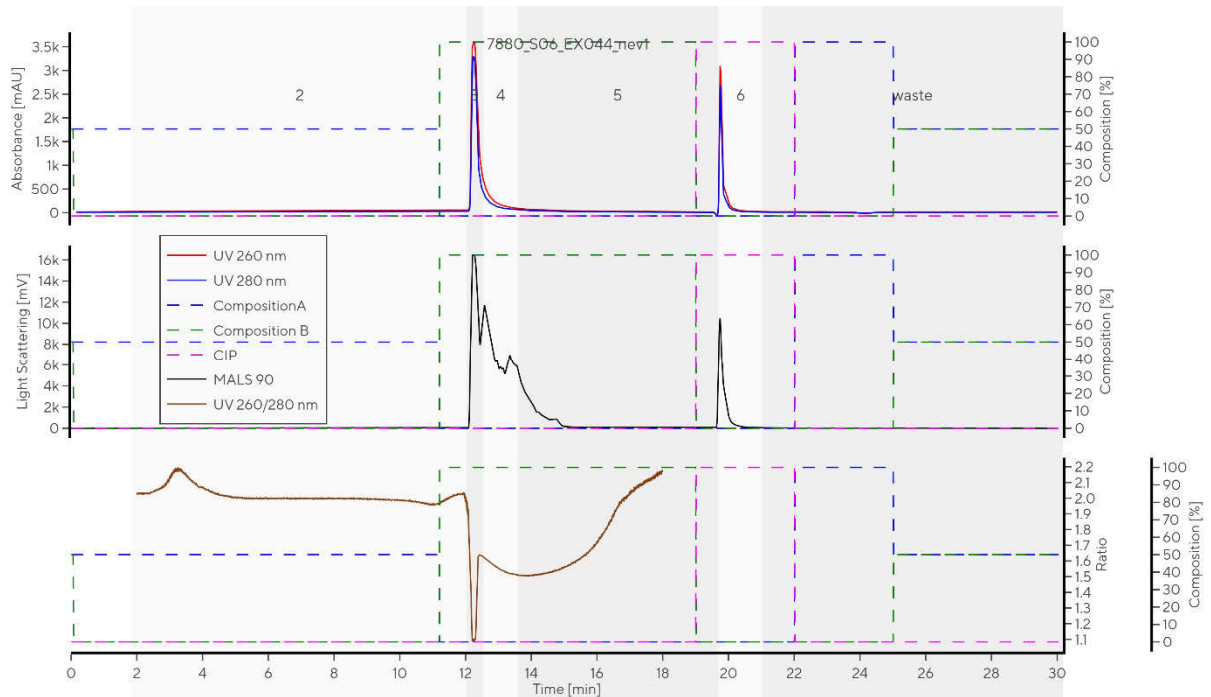
Fig. 1.: Chromatogram representing HIC monolithic chromatography of LNPs. It shows good binding of LNPs under these conditions, and efficient elution.
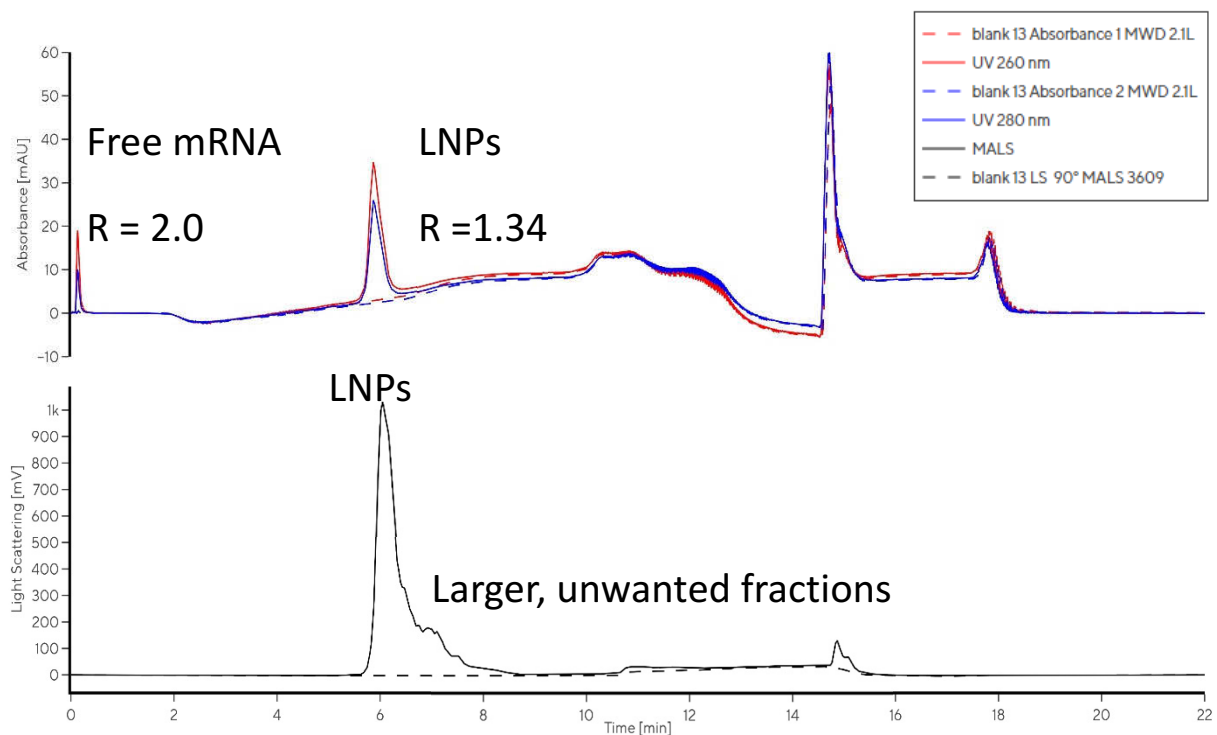

Fig. 2.: A chromatogram showing the separations allowed by HIC chromatography of LNPs.

Tab. 1.: Results of LNPs pre and post monolithic HIC.

	Enc. Eff. (Chromatographic)	Mean size (VideoDrop)	Concentration (Videodrop)
1	85%	107 nm	3,06E+10 particles/mL
3	97%	114 nm	2,98E+11 particles/mL

Summary

Utilising monolithic columns as the go to choice for chromatography of large biomolecules, applications for LNPs are showcased. There is a plethora of analytical techniques missing to be able to comprehensively characterize LNPs. Monolithic chromatography offers a helping hand. Hydrophobic interaction chromatography enables determining heterogeneity of sample, quantifying mRNA and separating free mRNA from LNPs. Scaling-up from analytics, it also allows for efficient capture and elution and thus subsequent concentration of LNPs, offering an alternative to established processes.

Acknowledgment

References

▪ 1   R. Tenchov, R. Bird, A. E. Curtze and Q. Zhou, *ACS Nano*, 2021, **15**, 16982–17015.

▪ 2   X. Hou, T. Zaks, R. Langer and Y. Dong, *Nature Reviews Materials 2021 6:12*, 2021, **6**, 1078–1094.

- 3   J. P. Bost, H. Barriga, M. N. Holme, A. Gallud, M. Maugeri, D. Gupta, T. Lehto, H. Valadi, E. K. Esbjörner, M. M. Stevens and S. El-Andaloussi, *ACS Nano*, 2021, **15**, 13993–14021.

- 4   E. Kon, U. Elia and D. Peer, *Curr Opin Biotechnol*, 2022, **73**, 329–336.

- 5   M. Kamiya, M. Matsumoto, K. Yamashita, T. Izumi, M. Kawaguchi, S. Mizukami, M. Tsurumaru, H. Mukai and S. Kawakami, *Pharmaceutics 2022, Vol. 14, Page 2357*, 2022, **14**, 2357.

- 6   G. S. Naidu, S. B. Yong, S. Ramishetti, R. Rampado, P. Sharma, A. Ezra, M. Goldsmith, I. Hazan-Halevy, S. Chatterjee, A. Aitha and D. Peer, *Adv Sci (Weinh)*, , DOI:10.1002/ADVS.202301929.

- 7   S. Li, Y. Hu, A. Li, J. Lin, K. Hsieh, Z. Schneiderman, P. Zhang, Y. Zhu, C. Qiu, E. Kokkoli, T. H. Wang and H. Q. Mao, *Nature Communications 2022 13:1*, 2022, **13**, 1–13.

- 8   R. Vargas, M. Romero, T. Berasategui, D. A. Narváez-Narváez, P. Ramirez, A. Nardi-Ricart, E. García-Montoya, P. Pérez-Lozano, J. M. Suñe-Negre, C. Moreno-Castro, C. Hernández-Munain, C. Suñe and M. Suñe-Pou, *Colloid Interface Sci Commun*, 2023, **54**, 100709.

Lecturers ERASMUS+ BIP ESS-HPT 2024

	University / Company	Name	Email
AT	Graz	Prof. Thomas Gamse	thomas.gamse@tugraz.at
AT	NATEX	DI Martin Sova	m.sova@natex.at
AT	NATEX	Dr. Eduard Lack	e.lack@natex.at
AT	INNOWELD	Maximilian Schrittwieser	m.schittwieser@innoweld.at
CZ	Prague	Dr. Helena Sovova	helsov@seznam.cz
DE	Bochum	Prof. Marcus Petermann	petermann@fvt.ruhr-uni-bochum.de
DE	Bochum	Prof. Thomas Müller	thomas.mueller@ls-csc.ruhr-uni-bochum.de
DE	Darmstadt	Prof. Markus Busch	markus.busch@pre.tu-darmstadt.de
DE	Erlangen	Prof. Eberhard Schlücker	eberhard.schluecker@fau.de
DE	Freising	Prof. Sabine Grüner-Lempart	sabine.gruener-lempart@hswt.de
DE	Hamburg	Dr. Carsten Zetzl	zetzl@tu-harburg.de
DE	Hamburg	Dr. Pavel Gurikov	pavel.gurikov@tuhh.de
ES	Valladolid	Prof. Angel Martin	angel.martin.martinez@uva.es
ES	Valladolid	Prof. Maria Jose Cocero	mariajose.cocero.alonso@uva.es
FR	Albi	Prof. Martial Sauceau	martial.sauceau@mines-albi.fr
HU	Budapest	Prof. Edit Szekely	edit.szekely@edu.bme.hu
HU	Budapest	Prof. Erika Vagi	vagierikamaria@gmail.com
PL	Wroclaw	Prof. Irena Zizovic	irena.zizovic@pwr.edu.pl
PT	Lisbon	Dr. Ana V.M. Nunes	avn07929@fct.unl.pt
RS	Belgrade	Prof. Marko Stamenic	stamena@tmf.bg.ac.rs
SI	Maribor	Prof. Urban Bren	urban.bren@um.si
SI	Maribor	Dr. Amra Perva	amra.perva@um.si
SI	Maribor	Dr. Maša Knez-Marevci	masa.knez@um.si
SI	Maribor	Prof. Zeljko Knez	zeljko.knez@um.si

Participants ERASMUS+ BIP ESS-HPT 2024

	University / Company	First Name	Family Name	Sex	Nationality
AT	NATEX	Thomas	Steinlechner	m	Austria
CZ	Ostrava	Ivana	Troppová	f	Czech Republic
DE	Bochum	Daniel	Terhorst	m	Germany
DE	Clausthal	Razmehr	Sahraeian	m	Germany
DE	Darmstadt	Alina	Weber	f	Germany
DE	Darmstadt	Christoph	Weigel	m	Germany
DE	Darmstadt	Daniel	Dyck	m	Germany
DE	Darmstadt	Laura	Dietrich	f	Germany
DE	Darmstadt	Patryk	Sewruk	m	Poland
DE	Darmstadt	Phillip	Weigmann	m	Germany
DE	Hamburg	Preethi	Aranala Gurumoorthi	f	India
ES	Valladolid	Andrea	Arribas Sanchidrián	f	Spain
ES	Valladolid	Elizabeth	González Cortés	f	Cuba
ES	Valladolid	Esther	García García	f	Spain
ES	Valladolid	Fernando	Caballero Rojo	m	Spain
ES	Valladolid	Irene	Magdaleno De La Fuente	f	Spain
ES	Valladolid	Sara	Pahino Villardón	f	Spain
FR	Albi	Adeline	Leluc	f	France
FR	Albi	Gauthier	Grejois	m	France
FR	Albi	Mustafa	Altinisik	m	France
IT	Bologna	Roberta	di Carlo	f	Italy
IT	Bologna	Zahra	Maghazeh	f	Iran
NO	SINTEF	Filippo	Bisotti	m	Italy
NO	SINTEF	Matteo	Gilardi	m	Italy
PL	Wroclaw	Rafal	Łysowski	m	Poland
RS	Belgrade	Bojana	Mihajlović	f	Serbia
RS	Belgrade	Dusan	Duric	m	Serbia
SE	Chalmers	Nils	Zachmann	m	Germany
SE	Lund	Azemina	Bajramova	f	Sweden
SI	Maribor	Mihael	Irgolič	m	Slovenia
SI	Maribor	Nika	Atelšek Hozjan	f	Slovenia
SI	Maribor	Tjaša	Skarlovnik	f	Slovenia
SI	Maribor	Tristan	Kovačič	m	Slovenia
SI	Maribor	Valeriia	Sliesarenko	f	Ukraine
SK	Bratislava	Martin	Štosel	m	Slovakia